Coordination Chemistry Reviews 441 (2021) 213984

Contents lists available at ScienceDirect

Coordination Chemistry Reviews

journal homepage: www.elsevier.com/locate/ccr

Review

Single-Molecule Magnets: From Mn12-ac to dysprosium metallocenes, a travel in time

Andoni Zabala-Lekuona [a,*], José Manuel Seco [a,*], Enrique Colacio [b,*]

[a] Departamento de Química Aplicada, Facultad de Química, Universidad del País Vasco/Euskal Herriko Unibertsitatea UPV/EHU, Paseo Manuel Lardizabal, n°3, 20018 Donostia, Spain
[b] Departamento de Química Inorgánica, Facultad de Ciencias, Universidad de Granada, Av. Fuentenueva S/N, 18071 Granada, Spain

ARTICLE INFO

Article history:
Received 12 February 2021
Accepted 13 April 2021
Available online 7 May 2021

Keywords:
Molecular magnetism
Transition metals
Lanthanides
Single-Molecule Magnet
Multifunctionality
Hybrid systems

ABSTRACT

The discovery of the first Single-Molecule Magnet, Mn12-ac, in 1993 changed the perspective of how information can be stored. The current bit, occupying few hundreds of nanometers in present devices, would be minimized to tens of angstroms at molecular level. However, until a couple of years these materials could only operate at temperatures near to the absolute zero. From 1993 to date, the field of Single-Molecule Magnets (SMMs) has continuously evolved thanks to the close collaboration of chemists and physicists obtaining materials already operating above the liquid nitrogen temperature. This long journey, however, has involved the study of many different routes towards high performance SMMs, being each of them essential in order to deeply understand the quantum dynamics behind these molecules. An era of high spin 3d metal clusters was the beginning of everything, but it went through highly anisotropic low coordinate 3d compounds, lanthanide based magnets, radical bridged compounds and 3d-4f mixed systems, among others, to end up in the current state of the art dysprosium metallocenes. Furthermore, after the magnetic studies in bulk, SMM based hybrid systems are emerging for future application devices, which also involve very interesting multifunctionalities. All in all, this work aims to explain how these materials work and show the trajectory and some of the major advances that have been made during recent years in this field.

Contents

* Correspnding authors.
E-mail addresses: andoni.zabala@ehu.eus (A. Zabala-Lekuona), josemanuel.seco@ehu.es (J.M. Seco), ecolacio@ugr.es (E. Colacio).

https://doi.org/10.1016/j.ccr.2021.213984
0010-8545/

1. Introduction

We currently live in an era where mostly all of the information is electronically stored. Relatively few years ago books, notes, documents, photos, newspapers and so on where typically printed and paper based. Nowadays, however, all these data could be digitally found. It is worth mentioning, though, that this new technology has evolved along few decades involving huge and fast changes. Indeed, the first data storage devices were launched during the 70 s, which were known as floppy disks. Despite their big dimensions, around 8 in., they could barely store the information corresponding to a simple pdf. Around five decades later, USB flash drives no bigger than our thumbs are able to accumulate films, thousands of photographs and millions of documents. The evolution has been colossal.

In order to be able to save all these data, the devices employ the binary language: combinations of 1 and 0, which represent the *bit* information unit. For instance, the nuclei of hard drives are constituted by nanoscopic (few tens of nanometers) ferro- or ferrimagnetic (they behave as magnets below the Cure temperature, T_C) alloy particles that form individual magnetic domains, where each of them contains a significant number of magnetic moments. Below the Curie temperature, T_C, all the magnetic moments inside a nanoparticle are aligned giving rise to a resultant magnetic moment, M_S. Similarly to common paramagnets, all the M_S are randomly oriented due to the thermal energy, but since magnetic moments are much higher than for a single atom, this phenomenon is named *superparamagnetism* (Fig. 1).

In the presence of a magnetic field, these nanoparticles could be easily magnetized in a determined direction (easy axis of magnetization) due to the presence of an axial anisotropy, which depends on intrinsic factors, such as the type of metallic ions and the shape

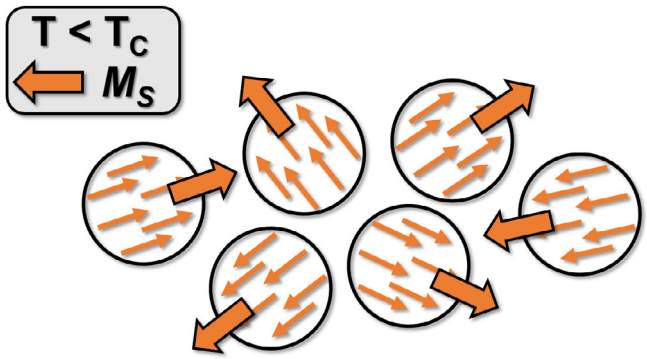

Fig. 1. -Superparamagnetic material.

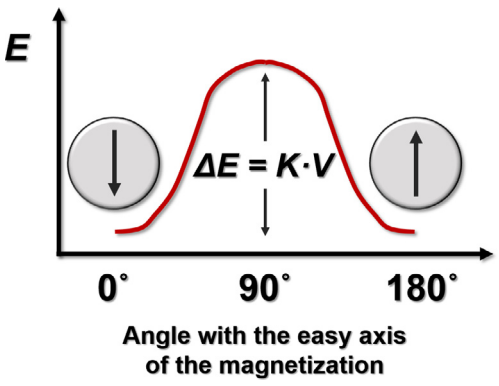

Fig. 2. -Energy of the orientation of the magnetization considering the easy axis of magnetization.

of the nanoparticles. When a magnetic field is applied, the nanoparticles tend to point out their magnetic moments collinear to the field, obtaining the highest magnetic moment (M_S). If the magnetic field is removed ($H = 0$) and the temperature of the system is below a certain temperature, known as blocking temperature T_B, the magnetic moment remains blocked in the same direction. Hence, the system behaves as a magnet, a hysteresis loop could be observed and, therefore, it has memory effect. This occurs due to the existence of an activation barrier, ΔE that prevents the reorientation of the magnetization, which depends on the anisotropy, K, and the volume of the nanoparticle, V (Fig. 2). Below T_B, the thermal energy, E_T, is not big enough to overcome the energy barrier ($E_T < \Delta E$) and thus the magnetic moment becomes blocked. Above T_B, in contrast, the system possesses enough energy to surpass the barrier ($E_T > \Delta E$) and an equilibrium between the two orientations (positive and negative) is obtained, where the material shows a superparamagnetic behavior and no hysteresis could be observed. Thus, if the system is maintained below T_B, the orientation of the magnetization in one direction will represent the information corresponding to 1, while in the opposite direction will represent 0. In consequence, the lower the dimensions of the nanoparticle, the higher the information density within the device.

Nonetheless, this "up-down" strategy towards information storage devices presents some limitations. As an example, it is not possible to reduce the size of the nanoparticle as much as desired, since this inherently reduces the anisotropy value and hence the thermal activation barrier. Indeed, the critical size of the nanoparticle is known to be around 10 nm, and below it the hysteretic behavior disappears and therefore is not possible to store information (Fig. 3). Moreover, it is a hard task to obtain monodisperse particles and normally nanoparticles that differ in size and shape are obtained, which means that the anisotropy values will be different, as well as their activation barriers.

In this context, Single Molecule Magnets, SMMs, emerged in 1993 when Sessoli and co-workers observed that the coordination compound named as Mn12-ac (compound **1**, Fig. 4) was able to store information at a molecular level [1]. Thus, the smallest material unit with memory effect was heavily reduced in size from few hundreds of nanometers to few angstroms.

1.1. How do single molecule magnets work?

As it can be deducted from the name, Mn12-ac is a coordination compound containing 12 metallic centers, four Mn^{IV} and eight Mn^{III} ions. The antiferromagnetic interaction between metallic centers that possess different oxidation state gives rise to a ground state with a spin value of $S = 10$, which is 21-fold degenerate ($M_S = 2S + 1$). However, due to the zero field splitting (ZFS), which fundamentally depends on the axial anisotropy of the ground state, the 21 sublevels are separated by the energy that follows the expression: $E(M_S) = M_S^2 \cdot D$ (where D is the axial anisotropy parameter, see Fig. 5).

When $D < 0$, the low lying energy levels are the ones with highest $|M_S|$ value, in this case $M_S = \pm 10$. The magnetization associated to each of the $M_S = \pm 10$ sublevels has its particular orientation along the axial anisotropy axis (as it occurs for superparamagnetic nanoparticles, Fig. 6), thus $M_S = +10$ stands for spin up (or 1 in binary language), whereas $M_S = -10$ stands for spin down (or 0). However, when $D > 0$ the opposite and non-desired situation is given. The sublevels would be inversely oriented so that the ground state would be $M_S = 0$. In this particular situation, there is not any possibility for a bistable ground state and, hence, the system is not valid for information storage. Coming back to the first situation, in order to switch or have an inversion of the magnetization from $M_S = +10$ to $M_S = -10$ (or the other way round), the system needs to overcome an energy barrier, U, as it occurs for superparamagnetic

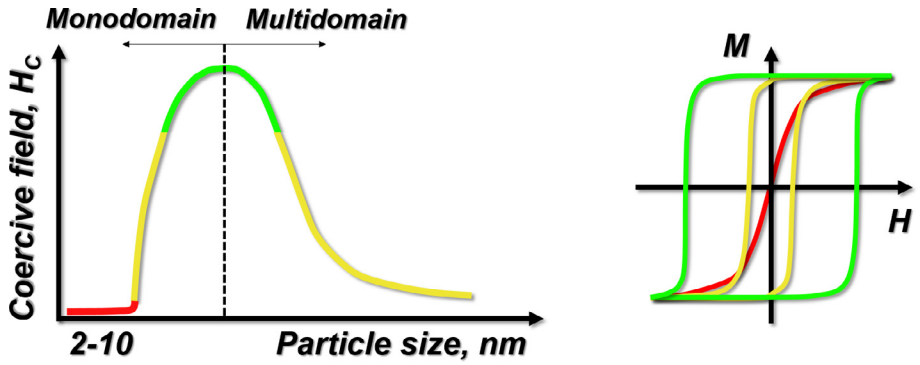

Fig. 3. -Evolution of the hysteresis loops considering the particle size.

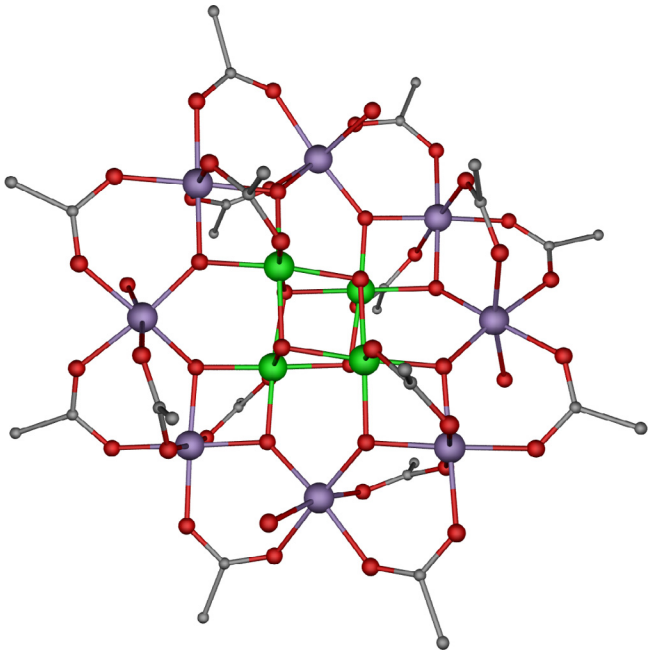

Fig. 4. -Structure of Mn12-ac (**1**) from reference [1]. Color code: Mn^{III}, Mn^{IV}, carbon and oxygen in purple, green, grey and red, respectively. Hydrogen atoms have been omitted for the sake of clarity. The figure has been reproduced from reference [2]. Creative Commons license.

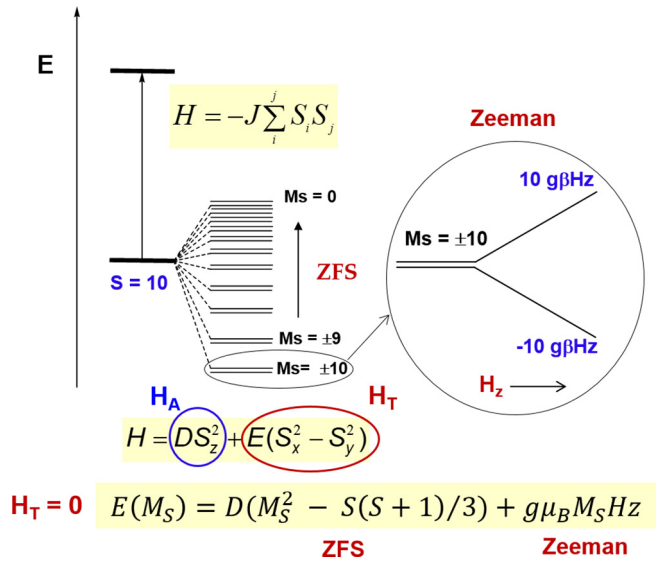

Fig. 5. -Qualitative energy diagram of Mn12-ac displaying the splitting of the ground spin state (S = 10) by an axial zero-field splitting (ZFS) Hamiltonian (H_A), with a transversal Hamiltonian, H_T = 0. The splitting of the ground doublet M_S = ±10 by Zeeman interactions is highlighted in the figure.

materials (Fig. 6). The value of the barrier is the difference between the highest excited state and the ground state. For systems with integer and non-integer spin values it is defined as $U = S^2|D|$ and $U = S^2 - 1/4|D|$, respectively (S being the spin value of the ground state).

Following with the example of compound **1**, in the absence of an external magnetic field the M_S = ±10 sublevels own the same energy, are equally populated and thus the system does not present any magnetization (Fig. 6, left). When an external polarizing magnetic field of enough intensity is applied in a determined direction, one of the M_S sublevels is stabilized in comparison to the other. Therefore, the material suffers a magnetization, since the spin of all the molecules point out in the same direction (Fig. 6, center). When the polarizing magnetic field is removed, the ground state reaches again a doubly degenerate state and if $E_T > U$, the material will tend to achieve the equilibrium between the two orientations (positive and negative) losing magnetization. Nonetheless, if $E_T < U$, which is the situation that occurs when $T < T_B$ (T_B is the blocking temperature), the magnetization will be blocked and that is why SMMs are able to store information. From this fact it is easy to conclude that the larger the energy barrier, the larger will be the temperature at which the magnetization can be retained. However, this is not always (or rather rarely) that way.

1.2. Relaxation processes

If the reorientation or relaxation of the magnetization could occur only by overcoming the energy barrier through all the excited states, any material displaying a $U \sim 298$ K (~207 cm^{-1}) would be valid to implement it in an information storage device. Maintaining the temperature of the mentioned device below 298 K would assure not losing magnetization and thus, would have memory effect. Nevertheless, due to the quantic nature of these materials, the relaxation mechanisms are diverse, complex and extremely sensitive to numerous factors such as temperature, magnetic field, hyperfine (interactions between the electronic and nuclear spins) and intermolecular interactions.

The most common relaxation processes operating in SMMs are the ones that occur through spin-phonon coupling (Orbach, Raman and direct processes) or the ones that occur due to the quantic nature of the materials (Quantum Tunneling of the Magnetization, QTM, and Thermally Assisted QTM, TA-QTM) [3]. Orbach and

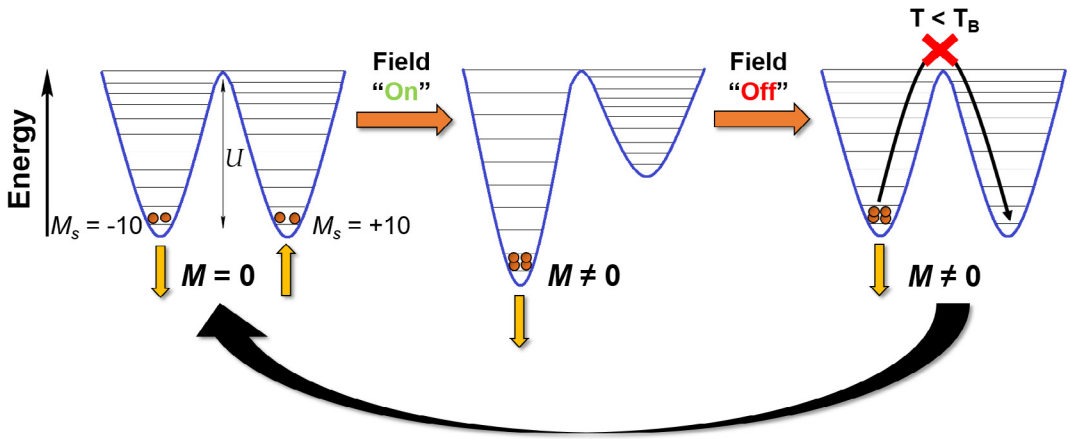

Fig. 6. -Magnetization projections (yellow arrows) in equilibrium in absence of external magnetic field (left), magnetization of the material due to the presence of an external field and subsequent stabilization of M_S < 0 sublevels (center) and blocking of the magnetization in absence of magnetic field for $T < T_B$ (right). Modified from reference [2]. Creative Commons license.

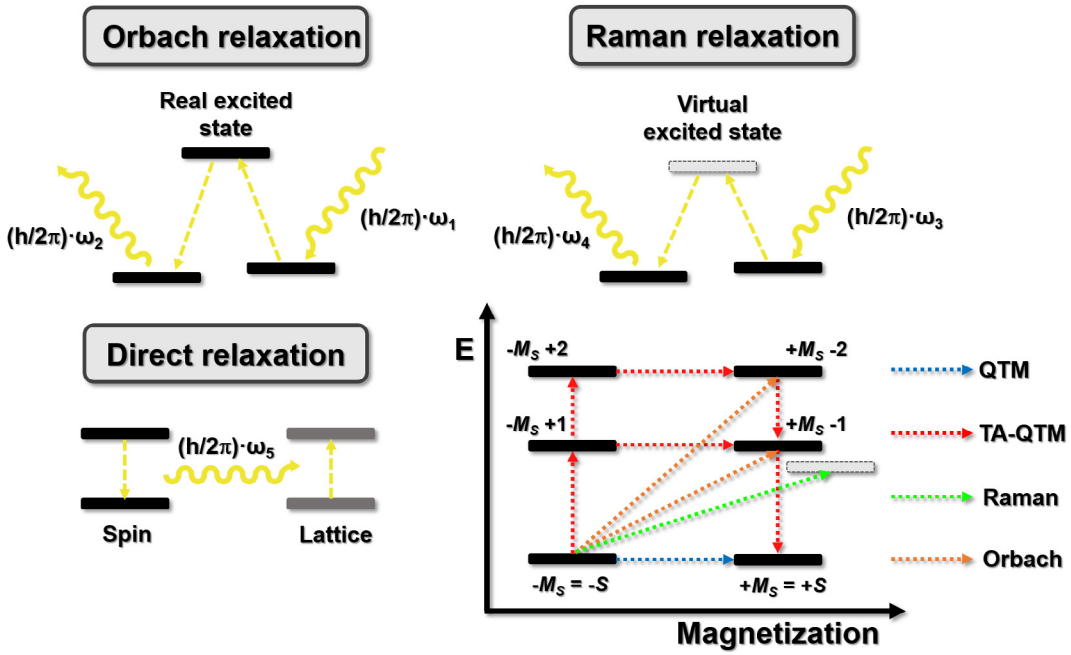

Fig. 7. -Schematic representation of Orbach (top left), Raman (top right) and Direct (bottom left) magnetization relaxation mechanisms. A combination of several relaxation mechanisms, including QTM and TA-QTM, for a part of double-well energy potential (bottom right).

Raman involve two phonons while a single one assists the direct process.

An ideal Orbach relaxation would be the one in which the system overcomes the entire barrier. The system would absorb phonons from the crystal network containing the exact energy ($(h/2\pi)\cdot\omega_1$) to jump from one of the ground sublevels ($M_S = \pm S$) to the highest excited sublevel ($M_S = 0$). From this excited state the system would relax to either of the ground $M_S = \pm S$ state emitting new phonons ($(h/2\ \pi)\cdot\omega_2$, Fig. 7, top left). Noteworthy, in the Figure the energies of the initial and final states are splitted by internal fields caused by dipolar or hyperfine interactions. Thus, the energy difference between the absorbed and emitted phonon corresponds to the energy difference between the $\pm M_S$ sublevels in the ground state. In any case, the Orbach process usually does not happen through the highest excited state and, instead, occurs through the first or second excited state (depending on the axiality of the system, Fig. 7, bottom right). The large phonon energy required for this process to occur is the main reason why it usually operates at highest temperatures.

The energy restrictions related to the Orbach process are not present for Raman, since this mechanism is driven by inelastic dispersion of phonons. The molecule absorbs a phonon $(h/2\ \pi)\cdot\omega_3$, reaches a virtual excited state and emits another phonon $(h/2\ \pi)\cdot\omega_4$ (Fig. 7, top right). Again, the energy difference between the two phonons corresponds to the energy difference between the $\pm M_S$ sublevels in the ground state. Meanwhile, the direct process is a single phonon magnetization relaxation process that directly emits a phonon ($(h/2\ \pi)\cdot\omega_5$) corresponding to the energy difference of the $\pm M_S$ sublevels in the ground state.

All these mechanisms occurring due to spin-phonon interactions require of energy (thermal assistance), but for QTM is different. This process occurs between the $\pm M_S$ sublevels of the doubly degenerate ground state and it is often the primary pathway at low temperatures, where mainly the ground state is populated

(Fig. 7, bottom right). However, the relaxation pathway could be a combination of processes, where the excited states are populated by absorbing phonons and then QTM might occur between M_S states of the same energy (but different sign) followed by relaxation to the ground sublevel. This combined mechanism is known as Thermally Assisted Quantum Tunneling of the Magnetization, TA-QTM (Fig. 7, bottom right). It is noteworthy that processes such as QTM and direct normally operate at low temperatures, Orbach at the highest temperatures and TA-QTM at intermediate ones. Raman, in contrast, could appear in the whole temperature range. Among all of them, QTM and TA-QTM are considered as through barrier shortcuts, since the system relax without overcoming it. Therefore, this causes a diminution on the value of the barrier U giving rise to an effective energy barrier, U_{eff}. This, at the same time, influences the value of the blocking temperature and the relaxation time.

The most common strategies in order to suppress the undesired QTM are: (i) diluting the samples by co-crystallizing the SMM with diamagnetic analogues (usually with Zn^{II} when working with transition metals and Y^{III} or La^{III} when using lanthanides) to avoid intermolecular interactions that enhance QTM, or (ii) applying an external magnetic field that breaks the degeneracy between $M_S = \pm S$ sublevels (or $M_J = \pm J$ usually when referring to lanthanides). Noteworthy, QTM is normally more noticeable for systems with an integer number of S than for non-integer ones (Kramers ions) due to cancellation principle of van Vleck [4]. It indicates that the phonons arising from the network could not induce QTM and direct relaxation processes in Kramers ions in the absence of a magnetic field. Unfortunately, hyperfine interactions, as well as transverse magnetic fields (created by intermolecular interactions) split the Kramers doublets giving rise to new magnetization relaxation channels for QTM and direct mechanisms. Hence, as it will be below discussed, when employing lanthanides, Dy^{III} is used more often than Tb^{III}, which are Kramers and non-Kramers ions, respectively. Moreover, compounds that are based on non-Kramers ions display an intrinsic tunneling gap in the absence of an applied field that favors QTM. In summary, the transverse magnetic fields and the intrinsic tunneling gaps determine the basic relaxation mechanism in metal complexes with SMM properties.

1.3. Detecting SMM behavior

Commonly, two techniques are used to determine whether a material displays slow relaxation of the magnetization or not. The first and the most used one involves carrying out in phase (χ'_M) and out-of-phase (χ''_M) magnetic susceptibility measurements with an alternating magnetic field (ac). These kind of measurements are usually performed above 2 K until 300 K varying the frequency of the alternating current (Fig. 8a). In the example shown in this Fig. 8a, at 20 K and at a frequency of 60 Hz the material does not show any $\chi''_M(T)$ signal. This means that, at this temperature, the material has enough energy to follow the variations of the alternating magnetic field and, thus, the magnetic moment easily follows the change of direction of the magnetic field being in phase (χ'_M) all the time. When diminishing the temperature below 12 K, the out-of-phase signal starts to increase. At this moment, the material possesses lower energy and the magnetic moment of some of the molecules are not able (due to their axial anisotropy and, therefore, to U_{eff}) to follow the flip of the alternating current. In other words, some of the spins are out-of-phase and, hence, an out-of-phase signal appears. When augmenting the frequency of the alternating current, for instance to 10,000 Hz, the reversal of the magnetic field becomes much faster and the signal is detected at higher temperature. In conclusion, detecting frequency dependent peaks in the $\chi''_M(T)$ plots means that the system shows slow relaxation of the magnetization and SMM behavior. Noteworthy, the non-zero going signals, or tails, below the peaks are indicative of QTM. This could also be detected in the $\chi''_M(\upsilon)$ plots when the position of the maxima, which is related to relaxation time, do not shift when increasing temperature (this is in agreement with the temperature independent behavior of this process).

The fact that the magnetization of the molecule is not able to follow the flip of the magnetic field is related to magnetic anisotropy, since every spin projection has its own different energy. When the relaxation time and the period of the alternating current coincide, a maximum appears in both the $\chi''_M(T)$ plot at different frequencies and in the $\chi''_M(\upsilon)$ at different temperatures (Fig. 8a and b). Among both types of graphs, $\chi''_M(\upsilon)$ plots can be fitted to the Debye model with the equation of Casimir-Du Pre [5]. The

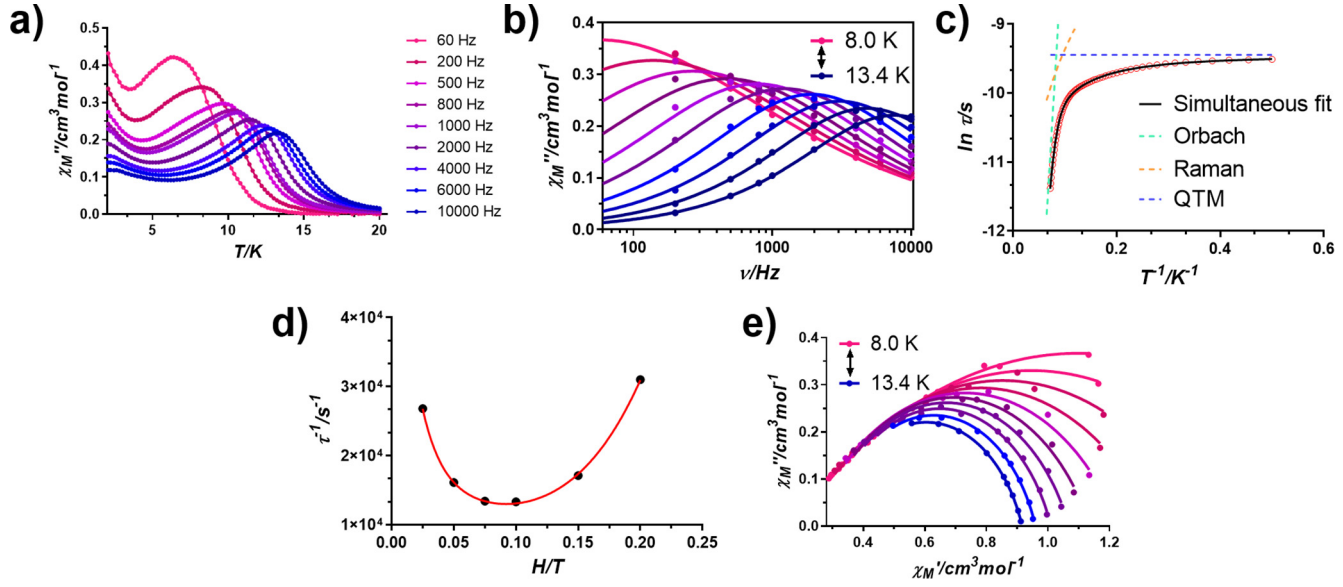

Fig. 8. -For a random Dy^{III} based SMM a) temperature dependence of the out-of-phase magnetic susceptibility (χ''_M) at different frequencies; b) frequency dependence of χ''_M at different temperatures; c) fitting of the relaxation times to simultaneous Orbach, Raman and QTM processes; d) the inverse of the relaxation times obtained at different magnetic fields at a fixed temperature; e) Cole-Cole plot.

curves at different temperatures that show a maximum in the studied frequency range (8.0–13.4 K in Fig. 8b) are fitted to the mentioned model, which allows extracting relaxation times, τ, for each temperature. When the relaxation pathway is purely of Orbach type, the relaxation times follow the linear Arrhenius law (Eq. (1)) and the fitting directly provides the value of the effective energy barrier (U_{eff}). However, this rarely happens and the relaxation of the magnetization usually takes place through diverse mechanisms. In these cases, the equation needs to be completed with new fitting parameters referring to other pathways as exemplified in Eq. (2) (τ_{QTM}^{-1} = QTM; BT^n = Raman and AT = direct). Fig. 8c displays a fitting of the relaxation times considering the simultaneous presence of Orbach, Raman and QTM processes. The dashed lines corroborate the previous statement, which indicates that these processes usually operate at low (QTM), intermediate (Raman) and high (Orbach) temperatures.

$$\tau^{-1} = \tau_0^{-1} exp(-U_{eff}/k_BT) \quad (1)$$

$$\tau^{-1} = \tau_{QTM}^{-1} + AT + BT^n + \tau_0^{-1} exp(-U_{eff}/k_BT) \quad (2)$$

Although relaxation times are commonly fitted to several mechanisms as in the example shown above, sometimes, when too many processes are included in the equation, this might be considered as an overparameterized situation. Including several mechanisms within the model could give us a better fit, but the obtained values for each mechanism will probably lose the physical meaning. In order to overcome this situation, additional experiments can be carried out. By studying the field-dependence of the relaxation times at a fixed temperature, a similar plot to what is shown in Fig. 8d can be obtained. As it can be observed, relaxation times become larger and the relaxation processes slower as the value of the external magnetic field is increased. This occurs up to 0.1 T, the value of the external magnetic field at which the relaxation process becomes the slowest, probably due to the quenching of QTM. Above it, relaxation times start to become faster again, which is probably originated by the enhancement of a direct process. Thus, this curve can be fitted to the following Eq. (3), which accounts for the field-dependency of QTM and direct processes:

$$\tau^{-1} = AH^4T + B_1/\left(1 + B_2H^2\right) + C \quad (3)$$

The first term corresponds to the direct process, which explains why at high fields becomes predominant (depends on H^4). The second term accounts for QTM and the constant term C accounts for field-independent relaxation processes. Hence, studying the field-dependence of the relaxation times could provide us additional information of the relaxation mechanisms. Once the parameters corresponding to direct and QTM mechanisms are obtained from this fit, they can be fixed in Eq. (2) avoiding overparameterization. This will allow us to obtain more reliable parameters for each relaxation mechanism.

Even though the lack of linearity in the Arrhenius plot (Fig. 8c) already indicates that numerous processes are operating, this could be indeed proved by the Cole-Cole plots (Fig. 8e). In these plots, χ''_M vs χ'_M curves display semicircles for each temperature and can be fitted to the generalized Debye model [6]. The fit provides α values between 1 and 0, where α = 0 stands for a single relaxation mechanism, whereas for values nearer 1, the higher is the number of relaxation pathways operating simultaneously. Noteworthy, it is somehow common to find in the literature materials that display two sets of maxima in the $\chi''_M(T)$ plots instead of one (this, at the same time, provokes the presence of two sets of maxima in the $\chi''_M(\upsilon)$ plots and the sum of two semicircles in the Cole-Cole plots) [7–9]. This is associated to the presence of two thermally activated Orbach processes. The origin of this it is not always clear, but several reasons have been postulated and it can differ from one case to another. The presence of two crystallographycally independent compounds in the same structure could be a reason [10], although several compounds have been reported displaying two sets of maxima and with a single paramagnetic ion within the crystal structure [11]. In such cases, the presence of two thermally activated processes has been attributed to direct processes arising from the multi-level system (originated by the presence of an external magnetic field) or intermolecular interactions [12,13]. Anyway, in this special cases the data can be treated by using a sum of two modified Debye functions obtaining relaxation times for each single process. This can be easily done with the software CCFIT that Chilton *et al.* recently developed [14].

The second technique to determine whether a system behaves as SMM or not is the field dependence of the magnetization at different temperatures. When the compound is an SMM, the hysteresis cycles are often open (Fig. 9). Strictly speaking, this is the most relevant feature of an SMM to evaluate its potential. As it will be described during the following sections, even though a considerably large amount of SMMs have been described in the literature with high U_{eff}'s (>500 K), most of them do not display clear open hysteresis loops or these appear at very low temperatures, around 2 K (Fig. 9a). Ideally, the hysteresis loop displayed in Fig. 9b would be the desired one, which even at zero field would maintain all of the magnetization and at room temperature. Nowadays, open hysteresis loops have been reported at up to 80 K (see below) and this has been considered a huge step in the field, because this temperature is higher than the liquid nitrogen temperature.

In contrast to *ac* measurements, this technique allows us to define a very important parameter characterizing SMMs, the blocking temperature (T_B). The most common definition of it stands for the highest temperature at which an open hysteresis cycle can be observed. However, this temperature is largely depending on the

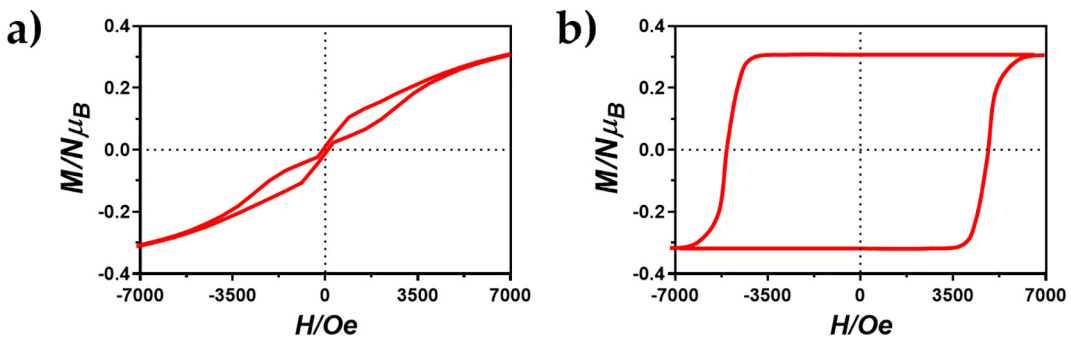

Fig. 9. a) Common hysteresis cycle highly influenced by QTM at 2 K. b) Ideal hysteresis loop at room temperature.

magnetic field sweeping rate and, therefore, when comparing different SMMs using blocking temperature, it is mandatory to be sure that the hysteresis loops were recorded under the same experimental conditions. Noteworthy, there exist some other criteria to determine the T_B: (i) temperature at which τ = 100 s or (ii) temperature at which the FC (Field Cooled) and ZFC (Zero-Field Cooled) magnetic susceptibility curves differ.

2. The beginning: the age of metal clusters

The discovery of Mn12-ac was a milestone in materials science, specifically in the field of molecular magnetism. Indeed, if the temperature at which the SMMs based on transition metal clusters operate (typically below 5 K) was raised over the liquid nitrogen temperature, their application in data storage devices would be really promising. To try to overcome the handicap of the very low working temperature of these systems, it should be kept in mind that the effective energy barrier that prevents the reorientation of the magnetization depends simultaneously on the total value of the spin and anisotropy:

$$U = S^2 \cdot |D|;\ S = integer \quad (4)$$

$$U = \left(S^2 - 1/4\right) \cdot |D|;\ S = non-integer \quad (5)$$

Regarding the quadratic spin dependence of the energy barrier, the most logic and simple way to enhance the energy barrier, and therefore the blocking temperature, would be that of increasing the spin of the ground state. For it, ferromagnetically coupled high nuclearity systems were synthesized. Among them, those containing the Mn^{III} ion were appropriate candidates for exhibiting SMM behavior because twofold: (i) in the high spin configuration possesses up to 4 unpaired electrons, which is positive in terms of enhancing the total value of S and (ii) in an octahedral crystal field (the most common for this metal ion), the Mn^{III} is subjected to Jahn-Teller distortion, leading to zero-field splitting (ZFS) of the ground state and to axial anisotropy, characterized by the D parameter. In addition, numerous theoretical and experimental studies were carried out during these years with the aim of finding out new magneto-structural correlations that enable chemists to deliberately design and synthesize novel transition metal clusters displaying ferromagnetic interactions between metal ions [15–20]. It is worth mentioning that in some cases azide was used as auxiliary ligand because in its end-on bridging mode could lead to ferromagnetic interactions [21,22]. Moreover, apart from the conventional synthetic routes (reactions under atmospheric pressure and at temperatures that were limited to the solvent boiling point), some research groups started to exploit solvothermal techniques, which afforded polynuclear complexes [23]. Synthetic strategies based on all this previous information allowed the successful preparation of a large number of high nuclearity systems with high spin ground state containing not only Mn^{III} ions, but also other transition metal ions. Examples of these type of polynuclear complexes are Mn_9Mo_6 (2), Fe_{19} (3), Mn_{19} (4) and Mn_{25} (5) [24–27]. It is worth highlighting that **4**, which really is a $Mn^{II}_7Mn^{III}_{12}$ complex, exhibited the record spin value of S = 83/2 (Fig. 10). In spite of the large ground state S value found for all these coordination compounds, they exhibited unexpectedly poorer magnetic properties than Mn12-ac in terms of U_{eff} and T_B. Specifically, compound **4** presents a negligible anisotropy and a U_{eff} = 5.8 K (4 cm^{-1}).

Over the course of the time, the problem was more and more evident. Introducing a great number of paramagnetic ions within the system inherently reduced drastically the value of anisotropy. Several studies have proved that the overall anisotropy value is sensitive to the orientation of the Jahn-Teller axis of each single metallic center, diminishing the total anisotropy value when the Jahn-Teller axes are not collinear. Therefore, when including a huge number of metal ions into the cluster it is normal to have a smaller final D value [28]. Indeed, some mathematical expressions have been proposed to calculate the total anisotropy of a cluster considering D and the angle of the Jahn-Teller axis respect to the total anisotropy axis (α) for each ion [29]. In addition, theoretical studies carried out by Neese and co-authors demonstrated that $D \propto 1/S^2$ and, therefore, $U_{eff} = DS^2$ is, in a good approximation, independent of S [30].

All these results lately propitiate a new era for SMMs, in which the coordination compounds with lower nuclearity, but higher magnetic anisotropy became more important.

In order to get very high values of magnetic anisotropy, mainly two options exist: (i) transition metal mononuclear coordination compounds with a very high single-ion magnetic anisotropy and (ii) coordination compounds containing lanthanide ions, which have exceptionally high single-ion anisotropy (with the exception

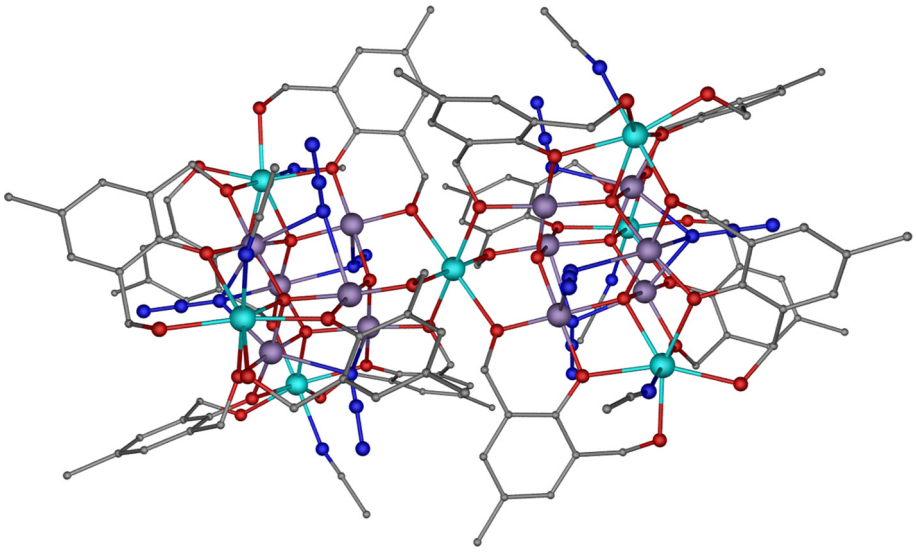

Fig. 10. -Perspective view of compound **4** (Mn_{19}). Color code: Mn^{II}, Mn^{III}, carbon, nitrogen and oxygen in light blue, purple, grey, dark blue and red, respectively. Hydrogen atoms have been omitted for the sake of clarity. Generated from the crystal structure in reference [26].

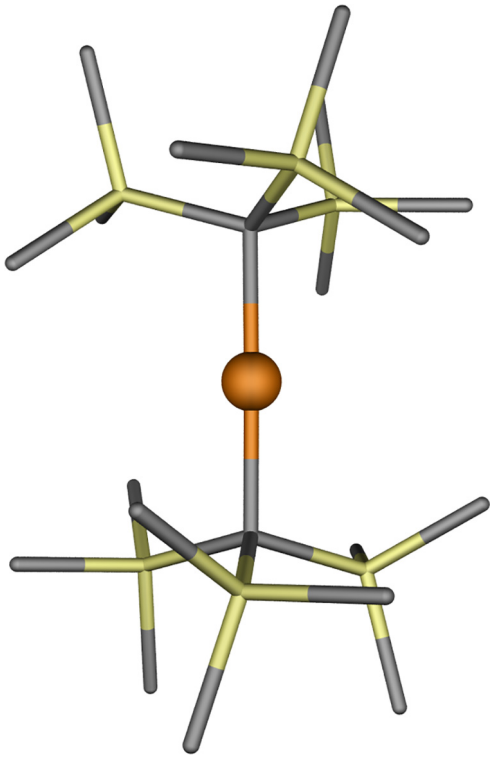

Fig. 11. Perspective view of the anionic structure of compound **6**. Color code: Fe^{I}, carbon and silicon in orange, grey and yellow, respectively. Hydrogen atoms have been omitted for the sake of clarity. Generated from the crystal structure in reference [44].

of the Gd^{III} ion that is isotropic). In the former case, low-coordination complexes lead to weak crystal fields, which favor the presence of orbital angular momentum, spin–orbit coupling and then to high magnetic anisotropy. In the latter case, the inherent large magnetic anisotropy is the result of the combined actions of strong spin–orbit coupling and crystal effects. In addition to this, the geometry plays an essential role in influencing the SMM behavior.

3. Transition-metal based low-coordinated single ion magnets (SIMs)

The idea of substantially enhancing the total *S* value of the compounds was then somehow set aside and the strategy of increasing the anisotropy value became more prominent. In contrast to the valence electrons in lanthanides, where 4f orbitals are spatially 'buried' inside the atom and are shielded from the ligand field (*vide infra*), in first row transition metals the 3d orbitals, even though they are very contracted, are much more exposed to the ligand field. Therefore, the ligand-field splitting can in some cases, depending on the metal ion and symmetry, readily quench the orbital angular momentum, consequently quenching the first order spin–orbit coupling (SOC) [31]. This statement means that the SOC causing magnetic anisotropy often arises from second order SOC derived from the mixing between the excited states with the ground state through the spin–orbit operator [32,33]. However, the first order spin–orbit coupling could be preserved by a rational design of the ligand field, which involves low coordination numbers. Although numerous examples of transition metal complexes with low-coordination number and SIM behavior have been reported to date [34–38], we are going to present here only those having the best SIM properties, which possess linear geometry and contain Kramers metal ions.

Based on these considerations and after the intriguing results observed for linear Fe^{II} systems with $S = 2$ displaying field-induced SMM behavior [39–43], Long and co-workers decided to explore the possibility of achieving large energy barriers for the reversal of the magnetization in the absence of a magnetic field. So as to do that, they smartly took advantage of the Kramers theorem studying a linear Fe^{I} based coordination compound with $S = 3/2$ shown in Fig. 11 and with the general formula [K(crypt-222)][Fe(C(SiMe$_3$)$_3$)$_2$] (6) [44]. Based on the *ab initio* calculations, they demonstrated that the combination of a low coordination number together with the low oxidation state gives rise to a remarkably weak ligand field unable to quench the orbital angular momentum, thus enhancing the total anisotropy of the compound. This leads to a splitting of the ^{4}E ground state into four Kramers doublets (KD) better determined by M_J quantum numbers with $M_J = \pm7/2, \pm5/2, \pm3/2$ and $\pm1/2$. Besides, the energy difference calculated between the ground and first excited state was large, indicative of potential SMM behavior.

Indeed, *ac* measurements carried out at zero *dc* field showed SMM behavior for this compound with an experimentally calculated U_{eff} of 325 K (226(4) cm^{-1}). This value of the effective energy barrier is close to the calculated energy gap between the ground ($M_J = \pm7/2$) and first excited state ($M_J = \pm5/2$), indicating that the relaxation most likely occurs through this first excited state. Even though the relaxation times follow the Arrhenius law in the 20–29 K temperature range, giving rise to the mentioned U_{eff}, the τ values notably deviate from linearity below 20 K indicating that at the lower temperatures a tunneling relaxation that shortcuts the barrier is operative.

As mentioned in the general introduction, another way of determining the blocking temperature (T_B) is performing FC/ZFC measurements. This is because when magnetic blocking is present in a compound, χ_M *vs* *T* curves must be different when the measurement is accomplished in the presence or absence of a magnetic field. In fact, for compound **6** the divergence of both curves was observed at 4.5 K. Since this suggests that hysteresis loops may be observable, they were measured in the 1.8–6.5 K temperature range. The loops showed butterfly shaped or waist-restricted features due to tunneling effect already observed in the *ac* measurements. With the aim of knowing the origin of QTM, they carried out the same magnetic measurements for frozen solutions of **6**, since it is well known that dipolar intermolecular interactions could provoke transverse fields inducing QTM. The data, however, was overall comparable to the one collected for microcrystalline material confirming the molecular origin of such tunneling shortcut. Thus, they attributed this effect to geometric distortions that the C—Fe—C bond could suffer in both solution and solid state (of course, less in the latter) enhancing transverse components that facilitate the shortcut and to vibronic Renner-Teller activity [43].

Apart from the showed example, other researchers also reported on two-coordinated homoleptic compounds based on iron, cobalt or nickel, though not all of them displayed such a good performance due probably to stronger QTM [34,35,38,45,46]. As abovementioned, the vibronic couplings could lead to fast tunneling and this is a clear consequence of the dynamic distortion of the long metal–ligand bonds present in the previous cited examples. To overcome these problems, Atanasov, Neese and co-workers provided a theoretical study analyzing the role of chemical bonding, vibronic coupling and magnetic anisotropy in linear Fe^{II} complexes showing SMM behavior [43]. As a general conclusion, they suggested that metal–ligand bonds with an increased covalency may be the objective towards reducing vibronic coupling and, at the same time, increase magnetic anisotropy.

In the pursuit of obtaining coordination compounds with enhanced covalency, Gao *et al.*, reported on the synthesis and magnetic properties of three Co^{II} based compounds with the general

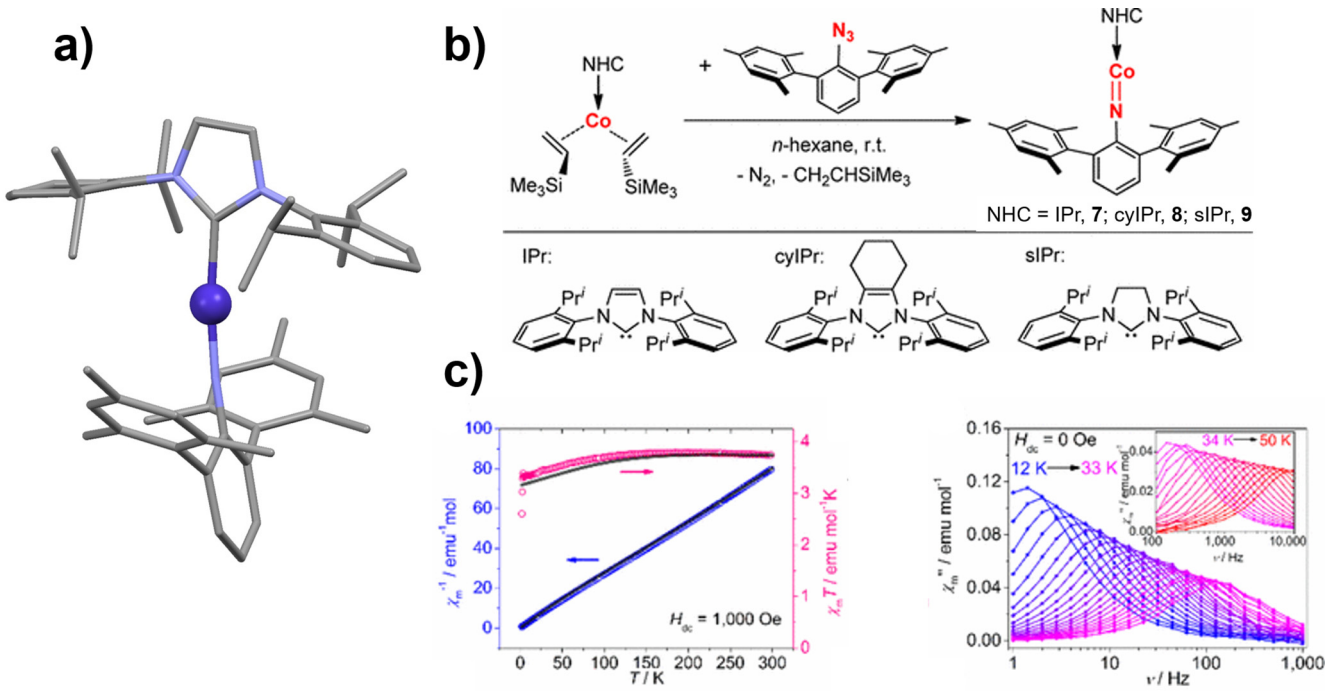

Fig. 12. a) Perspective view of compound **7**. Color code: Co^{II}, carbon and nitrogen in purple, grey and blue, respectively. Hydrogen atoms have been omitted for the sake of clarity. b) Synthetic route to the two-coordinate cobalt imido complexes and the designations for the NHC ligands. c) Temperature dependence of $\chi_M T$ (pink) and χ_M^{-1} (blue) values in the 2–300 K temperature range (left) and frequency dependence of the χ''_M under zero applied *dc* field for **9**. The perspective view of **7** has been generated from the crystal structure in reference [48]. The scheme of the synthetic route and plots of the magnetic properties have been adapted with permission from [47]. Copyright 2017 American Chemical Society.

formula [(NHC)CoNDmp] where Dmp = 2,6-dimesitylphenyl and NHC are different N-heterocyclic carbene ligands as depicted in Fig. 12 (**7**–**9**) [47]. Note that the synthesis, structure and reactivity of compound **7** was previously reported [48]. These two-coordinate cobalt imido compounds showed an almost linear arrangement of the ligands with very short Co-N_{imido} bond distances (1.691(6) Å) in agreement with a formal bond order of two.

The first clear evidence of the retention of first order SOC was already identified from *dc* data (Fig. 12c, left). The very large $\chi_M T$ values (3.86, 3.72 and 3.74 emu·K·mol^{-1} for **7**, **8** and **9**, respectively) at room temperature confirmed the unquenched orbital angular momentum provoked by the weak ligand field. Moreover, for compound **9** an abrupt drop was identified at 3.5 K indicative of a blocking of the magnetic moments, which was then further verified by measuring hysteresis loops. *ac* measurements showed that the three complexes were single molecule magnets under a zero applied *dc* field. Noteworthy, the maxima within the $\chi''_M(\upsilon)$ plots for **9** were found at up to 50 K at the frequency limit of 10,000 Hz (Fig. 12c, right), which gave rise to an effective energy barrier of 594.2 K (413 cm^{-1}), the highest reported until that moment for a 3d based SMM.

With the purpose of shedding some light to explain this extraordinary behavior and make magneto-structural correlations, they performed exhaustive theoretical studies. As expected from the short Co=N bond distance, the simulated variations in terms of this bond length provoked remarkable consequences. In fact, the energy gaps between the ground and excited states, as well as the axiality of the system were dramatically modulated by simply slightly lengthening or shortening the bond, which confirmed its role in determining the total magnetic anisotropy of the complexes. Finally, even though they did not exclude the possibility of considering the simple Co^{II} based mononuclear SMM model, they proposed that the large magnetic anisotropy of the systems arises from the $[CoN]^+$ core featuring a $M_J = \pm 7/2$ ground Kramers doublet with a large Co-N exchange coupling. This model could somehow explain the significant diminution of undesired QTM.

Finally, Long *et al.* recently reported compound **10** (Fig. 13) with general formula $[Co(C(SiMe_2ONaph)_3)_2]$ being Naph = naphthyl [49]. They were motivated by the fact that calculations on the hypothetical $[Co(C(SiMe_3)_3)_2]$ predicted a ground state with $L = 3$ arising from a non-Aufbau 3d-orbital filling [50]. This would somehow mimic what is seen for lanthanides obtaining maximal orbital angular momentum and, thus, very large magnetic anisotropy. However, obtaining the targeted compound was expected to be arduous from the very beginning, since two-coordinate transition metal complexes involving alkyl ligands were only found as $[M(C(SiMe_3)_3)_2]^{0/1-}$, being M = Fe^{II} [51], Fe^{I} [44], Mn^{II} [52] and Mn^{I} [53]. For Co^{II}, instead, other systems such as the above cited ones, as well as $[OCoO]^-$ anions inserted into an apatite's channel [54] and single Co^{II} atoms on MgO surfaces have been described [55].

Prior to obtain the desired linear two-coordinate Co^{II} compound, they had a lot of synthetic challenges such as the strongly reducing nature of the carbanions, bent C—Co—C angles when trying with some other substituents within the ligands and formation of undesired dinuclear systems, among others. Lastly, however, by including —ONaph groups within the structure they crystallized the desired linear compound. Single crystal structure analysis suggested that —C—H··· π interactions may be of relevance in the stabilization of the compound.

As expected from calculations that were previously made, theoretical analysis that was carried out for **10** revealed that the $^4\Phi$ ground state follows a non-Aufbau filling of the d orbitals with a resulting $(d_{x^2-y^2}, d_{xy})^3 (d_{xz},\ d_{yz})^3 (d_{z^2})^1$. The ligand field was so small that a high spin state with a maximized angular momentum was obtained. As a result, a 3d ion based SIM with a record U_{eff} value of 647.5 K (450 cm^{-1}) was obtained, the largest reported so far

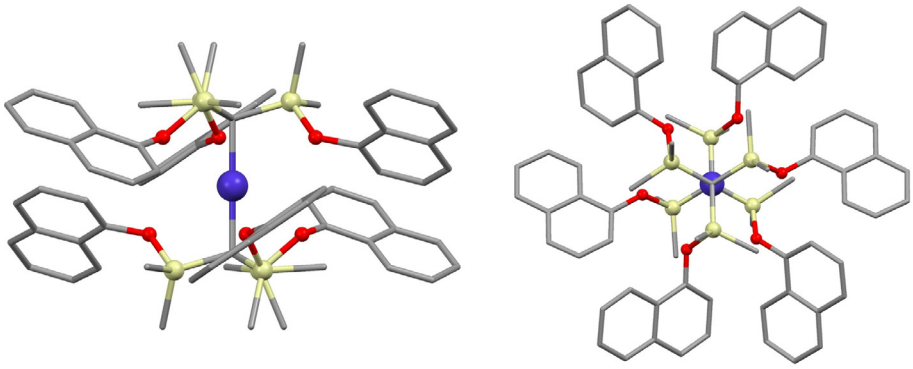

Fig. 13. Perspective view of compound **10** (left). Molecular structure of **10** viewed along the *c* axis (right). Color code: Co^{II}, carbon, oxygen and silicon in purple, grey, red and pale yellow, respectively. Generated from the crystal structure in reference [49].

for a transition metal based SMM. The value of the effective energy barrier represents the energy separation between the ground $M_J = \pm 9/2$ and the first excited $M_J = \pm 7/2$ states, which was deducted from theoretical calculations, far-infrared (FIR) spectroscopy and *ac* measurements.

4. The age of lanthanides

The first examples of rare-earth or lanthanide based SMMs were reported by Ishikawa and co-workers in the year 2003 [56]. These were sandwich type coordination compounds previously described by Ohashi *et al.*, in which two phthalocyanine ligands surround the Ln^{III} ions forming double-deckers (**11**, Fig. 14) [57]. Within the lanthanide series, the Tb^{III} (**12**) and Dy^{III} (**13**) counterparts displayed effective energy barriers of 330.9 and 40.3 K (or 230 and 28 cm^{-1}), respectively. This fact confirmed that a single metal center could be enough for the design of high U_{eff} owning compounds with SMM behavior.

In contrast to transition metals, the advantage for lanthanides is that, as indicated above, the 4f orbitals are spatially 'buried' inside the atom and are shielded from the ligand field by the fully occupied $5s^2$ and $5p^6$ orbitals. This implies an almost purely electrostatic interaction between the donor atoms of the ligands and the lanthanide ion and, consequently, the spin–orbit coupling (main cause of the magnetic anisotropy) cannot be quenched so easily as for transition metals. This means that, in principle, the anisotropy value will usually be higher for lanthanides than for transition metal complexes, so that, in theory, one could expect the achievement of SMMs with improved properties. However, as further discussed below, they also exhibit some disadvantages that are not so common for transition metals.

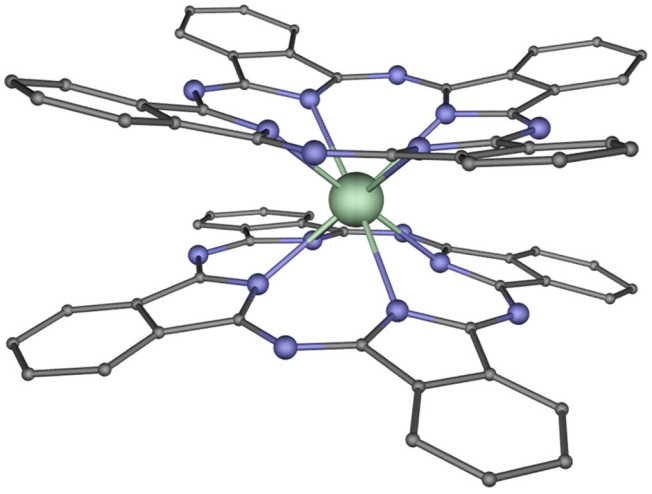

Fig. 14. Perspective view of the cationic sandwich type double-decker described by Ohashi *et al.* [57]. Color code: Nd^{III}, carbon and nitrogen in green, blue and grey, respectively. Hydrogen atoms have been omitted for the sake of clarity. Reproduced from reference [2]. Creative Commons license.

Due to the strong spin–orbit coupling, for most of the lanthanide ions, the spin is not the unique source of the angular momentum. Therefore, when describing their magnetic properties, it is necessary to consider spin–orbit coupling terms (characterized by the quantum number *J*) and their splitting by the ligand field, leading to the sublevels that are described by M_J instead of M_S quantum numbers. Even though the meaning differs from one to another, the interpretation is still similar. Indeed, when designing SMMs, the ground state should possess a well-defined ground state with the highest possible absolute value of M_J, which could be accomplished when the anisotropy of the ground state is axial. Moreover, the energetic separation between M_J and $M_J \pm 1$ states needs to be as high as possible to obtain high U_{eff} values and this implies a rational design of the ligand field.

For the mentioned rational design, Rinehart and Long proposed some very useful guidelines that were conceptually easy to understand [58]. Within the lanthanide series, each of them contains its own characteristics. For instance, although most of them have considerable spin–orbit coupling, the Gd^{III} ion is completely isotropic. Hence, in spite of the fact that it possesses the greatest number of unpaired electron spins possible for a lanthanide ion (which, in principle, would favor a high *S* value in the ground state), its potential for the design of SMMs is null. Among the ions with anisotropic electron density, two main groups may be distinguished (Fig. 15): oblate type ions (Tb^{III} and Dy^{III}, among others) and prolate type ones (Er^{III} and Yb^{III}, among others).

The mere fact of knowing how the shape of the electron density looks like for each rare-earth ion enables a more effective rational design of the specific ligand field with the purpose of achieving large axial magnetic anisotropy (the ground state has the largest M_J value). Thus, for oblate type of ions, the ligand donor atoms with greatest electron density should coordinate at axial positions (Fig. 16, top). This disposition will cause less electronic repulsion between the oblate electronic density of the lanthanide ion and the ligands donor atoms with greatest electron density, stabilizing the ground state with higher M_J values. In this situation, the anisotropy axis, which is perpendicular to the oblate shaped electron density, points to the donor atoms with greater electron density and shorter Ln–X (X being the donor atom) distances. It is worth noting that if no donor ligands are coordinated in the equatorial

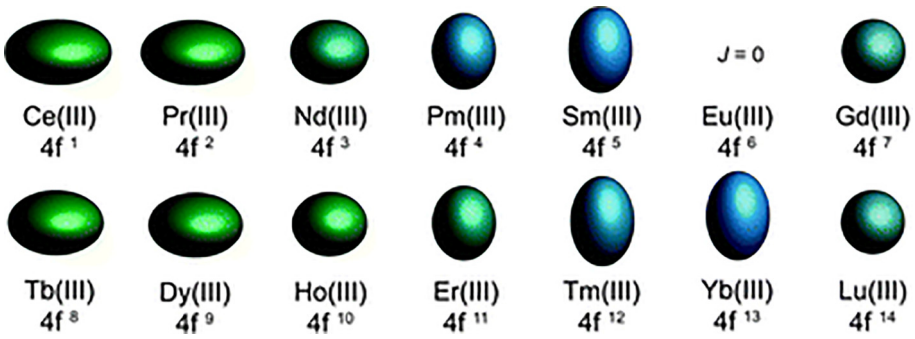

Fig. 15. 4f shell electron distribution shapes for trivalent Ln^{III} ions. Reprinted with permission from [58]. Copyright 2011 The Royal Society of Chemistry.

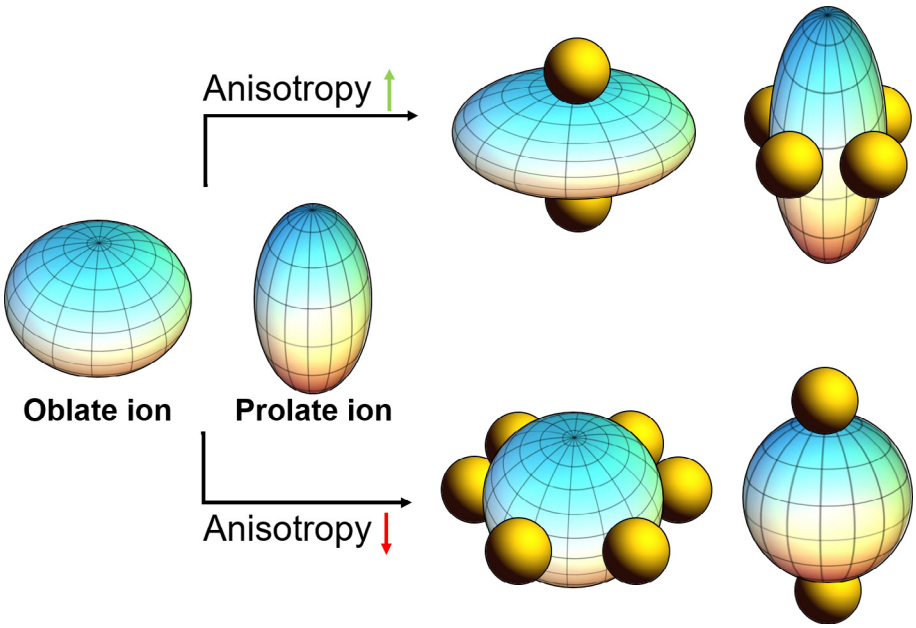

Fig. 16. How to enhance or quench the anisotropy for oblate and prolate type of ions. Modified figure under Creative Commons license.

positions, the electron density will expand along the plane enhancing the axial anisotropy. In contrast, if the donor atoms coordinate within the equatorial plane, the electron distribution will become more isotropic losing the potential to behave as SMM (Fig. 16, bottom).

Regarding the prolate type of ions, the ligand donor atoms with greatest electron density should coordinate at equatorial positions for achieving axial anisotropy. In this disposition, the electronic repulsion between the prolate electronic density of the lanthanide ion and the ligands donor atoms with greatest electron density is smaller and the anisotropic axis, which is parallel to the prolate electron density, lies perpendicular to the plane where are located the ligands donor atoms with greatest electron density. If there are no donor ligands in axial positions, the electron density of the lanthanide metal ion can be expanded along the axial direction leading to a larger axial anisotropy. Conversely, the coordination in axial positions induces a more isotropic electron distribution, so that the anisotropy decreases (Fig. 16, bottom).

Even though the approach looks simple, the great ionic radii of lanthanides becomes a huge obstacle. Indeed, when the ligands are not specifically designed to obtain a certain geometry, it is very common to obtain high coordination numbers (>8). However, here are shown two great impact studies that prove that the guidelines proposed by Rinehart and Long show the way towards the enhancement of the magnetic anisotropy.

In 2013, the group of Murugesu studied the magnetic properties of six very similar Dy^{III} based dinuclear systems, whose main difference resides in the electron donating character of the ancillary bidentate ligands (in the present work only three of them are described) [59]. In order to do that, they were based on their previously studied dinuclear compound **14** (Fig. 17, left) [60,61]. Maintaining the core structure, they were able to substitute the nitrates in the equatorial plane (a phenoxido group provides axiality to the system) by other auxiliary ligands such as acetylacetonate, acac, (**15**, Fig. 17, top) or hexafluoroacetylacetonate, hfac (**16**, Fig. 17, bottom), which are more and less electron-donating groups than nitrate, respectively.

For compound **15**, the switching from nitrates to acetylacetonates provokes a shortening of the Dy-O_{chel} distances due to the greater charge of the donor atoms. Thus, the ligand field in the equatorial plane becomes more prominent. This was proven by measuring the *ac* dynamic magnetic properties and fitting the relaxation times to the Arrhenius law. The fit provided U_{eff} values of 76 and 16 K (or 52.8 and 11.1 cm^{-1}) for **14** and **15**, respectively. When replacing the acac ligands by the hfac counterparts to afford **16**, the oxygen atoms become less donating, even less than the nitrate oxygen atoms (this

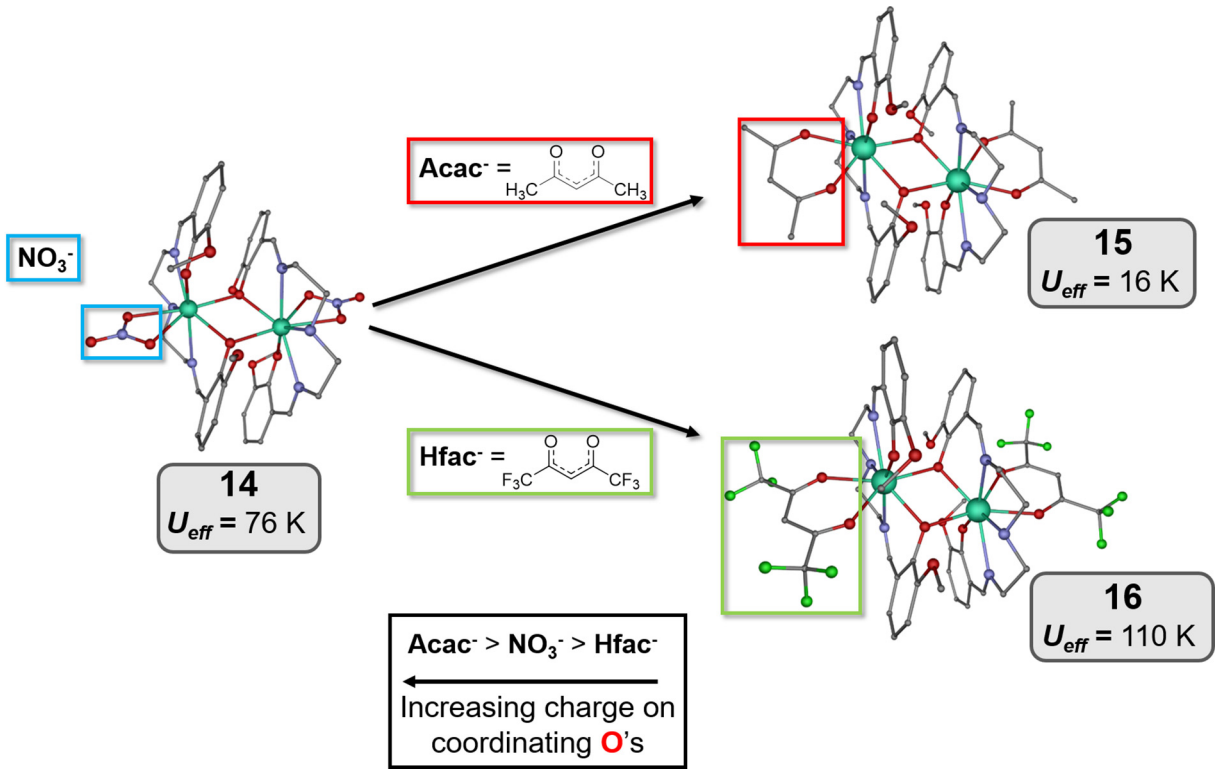

Fig. 17. Compound of reference **14** (left), compound with acac chelates **15** (top right) and compound with hfac chelates **16** (bottom right). Black inset: order of the chelates depending on the charge they provide to the lanthanide ion; based on *ab initio* calculations. Color code: Dy^{III}, carbon, nitrogen, oxygen and fluorine in turquoise, grey, blue, red and green, respectively. Hydrogen atoms have been omitted for the sake of clarity. Generated from the crystal structures in references [59,60].

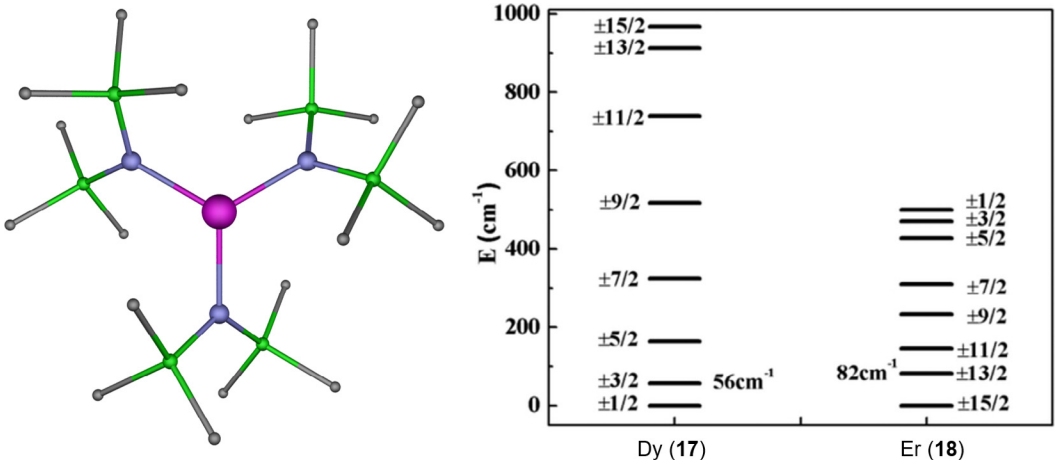

Fig. 18. Structure of **18** (left) and energy diagram of the eight Kramers doublets for **17** and **18** (right). Color code: Er^{III}, carbon, nitrogen and silicon in pink, grey, blue and green, respectively. Hydrogen atoms have been omitted for the sake of clarity. The perspective view of **18** has been generated from the crystal structure downloaded from CCDC (YIBRUW). The energy diagram has been adapted with permission from [62]. Copyright 2014 American Chemical Society.

was proven by *ab initio* calculations). Thereby, Dy-O_{chel} bond distances become larger, the electron density within the equatorial plane diminishes and the U_{eff} value increases up to 110 K (76.4 cm^{-1}).

Among the SMMs containing prolate lanthanide ions, those based on Er^{III} are the most common ones. In a research published by the group of Tang [62], they compared two systems with the general formula $Ln[N(SiMe_3)_2]_3$, where Ln^{III} = Dy^{III} (**17**) and Er^{III} (**18**). Because of the opposite electron cloud distribution for these two lanthanide ions, the crystal field causes reversed effects. As it is shown in Fig. 18, the order of the Kramers doublets (KD) is exactly the opposite for both compounds. The ground state KD is M_J = ±1/2 for **17**, whereas for **18** M_J = ±15/2 KD is the most stable one. These results agree with the model proposed by Rinehart and Long. A strong equatorial ligand field diminishes the electronic repulsions for prolate ions such as Er^{III}, thus stabilizing the KD with the highest M_J value as ground state (axially anisotropic ground state). As aforementioned, one of the most important prerequisites to observe SMM behavior is to stabilize the M_J states with highest absolute values as ground KDs (axially anisotropic ground KD). Hence, it looks reasonable that compound **18** displays an energy

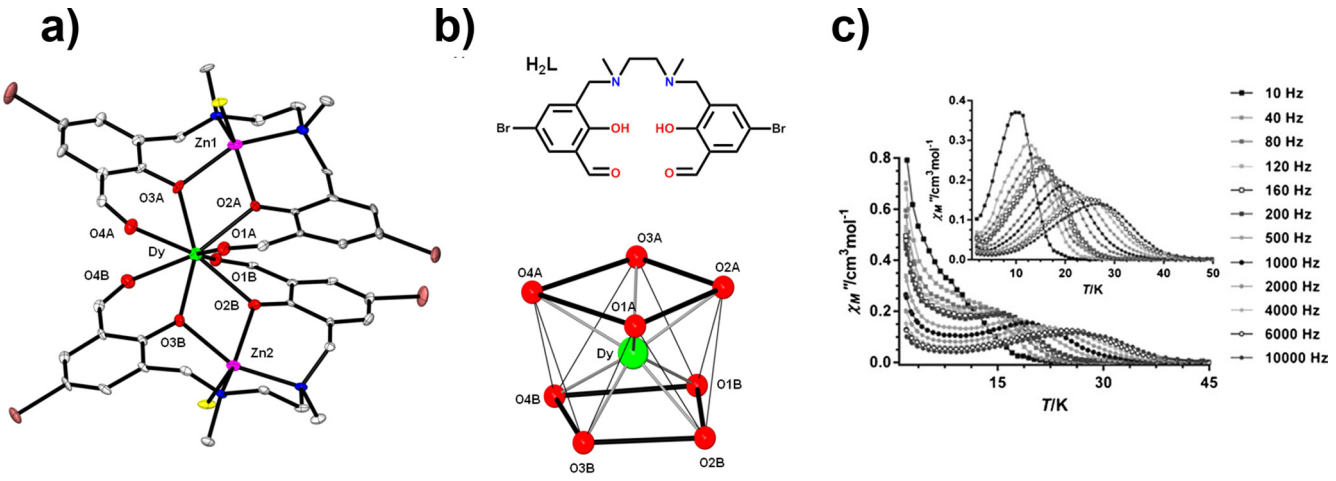

Fig. 19. a) Perspective view of the cationic structure of **19**. b) The Mannich base ligand used in this research (top) and DyO_8 coordination environment of the complex (bottom). c) Temperature dependence of χ_M'' under zero *dc* applied field and at H_{dc} = 1000 Oe (inset) for **19**. Color code: Dy^{III}, Zn^{II}, carbon, oxygen, nitrogen, bromide and chloride in green, pink, grey, red, blue, brown and yellow, respectively. Hydrogen atoms and counterions have been omitted for the sake of clarity. Generated from the crystal structure in reference [63]. Magnetic data reprinted with permission from [63]. Copyright 2014 John Wiley and Sons.

barrier for the reversal of the magnetization of 122 K (84.8 cm^{-1}), while compound **17** does not show slow relaxation of the magnetization.

Based on the described oblate-prolate model, our research group made important contributions to the field of SMMs. For instance, the trinuclear $Zn^{II}Dy^{III}Zn^{II}$ system, **19**, was prepared using a compartmental Mannich base ligand containing bridging phenoxido groups [63]. This kind of assembly was proven to be effective in order to stabilize a ground state with highest M_J state (axial ground state), because the four phenoxido oxygen atoms (those having the highest electron density) are placed by couples in opposite sides of the Dy^{III} ion (Fig. 19). Besides, the incorporation of diamagnetic Zn^{II} ions within the structure may have several benefits. On the one hand, in contrast to diamagnetic Zn^{II}, paramagnetic metal centers are known to create transversal magnetic fields that enable fast relaxation of the magnetization through QTM [64]. On the other hand, Rajaraman *et al.* reported that, for phenoxido containing systems, the inclusion of diamagnetic ions can provoke greater charge polarization for the bridging phenoxido groups, thus creating a bigger energy splitting between the ground and excited states [65].

Compound **19** exhibits a DyO_8 coordination environment that fits best to a square antiprism geometry (calculated by the SHAPE software [66]). Even though the presence of QTM is noticeable in the χ_M'' *(T)* plots (Fig. 19c), it displays zero field SMM behavior. This is in fact due to an almost pure M_J = ±15/2 ground state with a marked axiality and with negligible transverse components calculated from CASSCF + RASSI methods. As expected for an oblate type of ion with well-defined axiality, the magnetic moment points to the stronger electron donating phenoxido oxygen atoms, so that it is oriented roughly collinear with the two shortest Dy-O distances and perpendicular to the oblate electron density.

For further confirming the appropriateness of the ligand field in **19**, electrostatic potential maps caused by the ligands and projected into the Dy^{III} ion were calculated. It was proven that the beta electron density of the oblate ground state was accommodated in the region where the electronic repulsion was less important, whereas in the perpendicular direction the magnetic moment points to the more electron density donating phenoxido oxygen atoms. Finally, as a proof of concept, the isostructural analogue of Er^{III} (**20**) was also studied. As expected, the ligand field was shown to be suitable for stabilizing high magnetic M_J states for oblate ions, but not for prolate ones. The latter ions require strong ligand fields in the equatorial plane. Thus, compound **20** exhibited a field induced SMM with a very modest energy barrier for the reorientation of the magnetization.

As discussed, great efforts were done in synthesizing lanthanide based SMMs and understanding their magnetic properties. Indeed, the rational strategy following the oblate-prolate model allowed the researches to make magneto-structural correlations and be able to modify the ligand fields on demand. Some clear examples of it are the pentagonal-bipyramidal (PB) compounds. Overall, these systems contain strong oxygen donor atoms in the apical positions, for instance: phenoxido groups, phosphine oxides or siloxides. In contrast, the equatorial pentagonal positions are usually occupied by neutral atoms arising from solvents (tetrahydrofuran or pyridine, for example) or weakly coordinating macrocyclic and non-macrocyclic ligands. Within this family, some of the most cutting-edge examples are $[Dy(O^tBu)_2(py)_5][BPh]_4$ (**21**, O^tBu = *tert*-butoxide, py = pyridine) [67] [Dy(bbpen)Br] (**22**, H_2bbpen = N,N′-bis(2-hydroxybenzyl)-N,N′-bis(2-methylpyridyl)ethylenediamine) [68] and $[Dy(Cy_3PO)_2(H_2O)_5]Br_3{\cdot}2(Cy_3PO){\cdot}2H_2O{\cdot}2EtOH$ (**23**, Cy_3PO = tricyclohexyl phosphine oxide) [69]. In all these systems, the axiality is provided by strong oxygen donor atoms in the apical positions while the equatorial planes are occupied by less electron donating atoms with subsequent longer bond distances. The effective energy barriers were experimentally estimated to be of 1815 K, 1025 K and 543 K for **21**, **22** and **23**, respectively. Moreover, even though usually Orbach relaxation pathways occur through the first excited state (which could be better described as TA-QTM), the proper ligand field in those compounds provokes relaxation pathways involving higher excited states achieving high effective energy barriers. Lastly, it is worth mentioning the importance of designing and synthesizing compounds with improved properties, but being air stable. From the last three cited compounds, the one with the highest effective energy barrier (**21**) is air sensitive, a fact that complicates its implementation in future devices. In this sense, some other air stable compounds with high effective energy barriers have been reported, either with PB geometry or by using very electron-donating groups such as F^- to provide an axial ground state very well isolated from excited states [70–73].

One could think about these latter systems as ideal candidates for implementing them in information storage devices. However, the vast majority of lanthanide based SMMs face a common and important handicap: low blocking temperatures. Compound **21**, for example, displays a T_B of "only" 14 K (defined by FC/ZFC experiments), which is mainly due to fast QTM at zero field. This

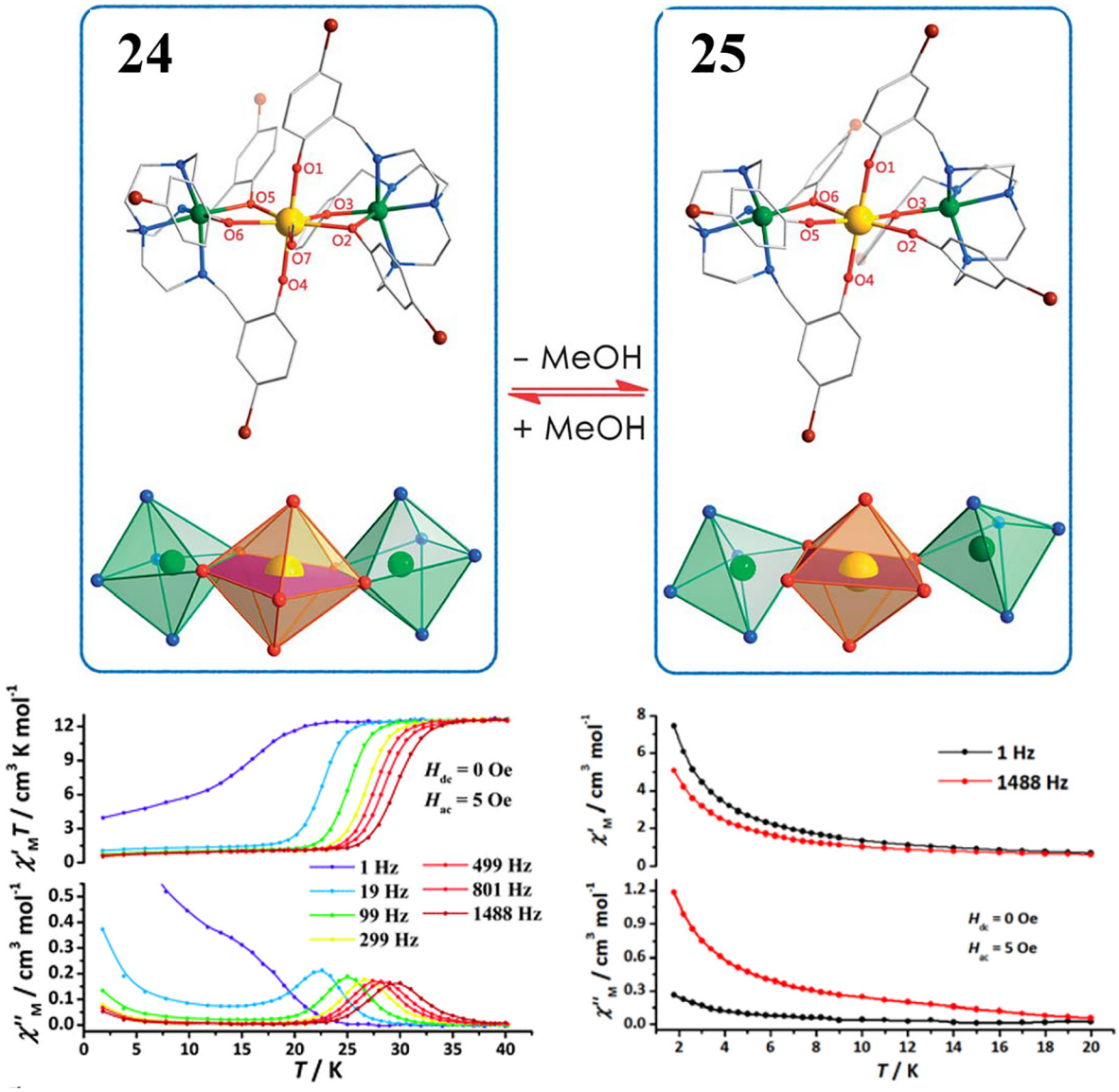

Fig. 20. Structure of the complexes **24** and **25** with their respective coordination polyhedra for Zn^{II} and Dy^{III} (blue insets). Temperature dependence of χ''_M under zero *dc* applied field for **24** and **25** (bottom). Color code: Zn^{II}, Dy^{III}, carbon, nitrogen, oxygen and bromine in green, yellow, grey, blue, red and brown, respectively. Hydrogen atoms have been omitted for the sake of clarity. Adapted with permission from [74]. Copyright 2013 The Royal Society of Chemistry.

is one of the biggest problems that researchers are nowadays facing in the way to achieve high blocking temperature SMMs.

5. QTM: the undesired phenomenon

As previously discussed, it must be said that, in general, it is easier to synthesize a coordination compound with SMM properties when lanthanides are used. Besides, the effective energy barriers that they show are often greater than those found for SMMs based on transition metal ions. However, the QTM is, most of the times, very strong when the external magnetic field is removed and this means that there is not remnant magnetization at zero field. This is a huge problem for using these materials in a future device. Therefore, the QTM effect has been widely studied in the past few years and little by little we are learning how to quench it.

Tong's group, for instance, studied the effect of geometry of the coordination sphere on the QTM [74]. In order to do that, they investigated two very similar trinuclear $Zn^{II}Dy^{III}Zn^{II}$ systems, where the main difference between them consisted in the presence/absence of a methanol molecule within the equatorial plane (Fig. 20). Compound **24**, with methanol, displays a pentagonal bipyramid geometry around the lanthanide ion, whereas **25**, without methanol, shows an octahedral coordination environment. Even though with the exception of the methanol oxygen atom in **24** all the oxygen donor atoms around the Dy^{III} ion belong to phenoxido groups, the ligand field could be considered as optimum in reference to the model suggested by Rinehart and Long. This is because the oxygen atoms in the apical positions of the PB geometry show considerably shorter bond distances than those in the equatorial plane. Being so similar compounds and with a well-defined axial ligand field, it is interesting to remark that compound **24** shows a U_{eff} = 438.8 ± 4.3 K (305 ± 3 cm^{-1}), whereas compound **25** barely displays out-of-phase signals in the $\chi''_M(T)$ plots due to fast QTM (they manage to suppress it with an optimum external magnetic field). With the aim of rationalizing this behavior, they used *ab initio* calculations. They concluded that, as aforementioned, the PB geometry is an ideal candidate to observe SMM behavior, while octahedral ligand fields are prone to present tunneling. It

is worth mentioning that the geometries are never ideal, which leads to adverse effects for the SMM behavior (in fact favors QTM). In connection with this, in compound **24** the SMM behavior is not as good as expected, whereas QTM could be suppressed for **25** by applying an external magnetic field, thus emerging slow magnetic relaxation.

In view of the essential role that plays symmetry for achieving high performance lanthanide-based Single-Molecule Magnets, Tong and col. recently carried out a qualitative study, based on an effective charge model, which showed that certain symmetry groups, such as Cn ($n \geq 7$), S_8/D_{4d}, C_{5h}/D_{5h} and S_{12}/D_{6d} could minimize transverse crystal field parameters (CFs) and then the QTM [75]. It is worth noting that none of these symmetries exists in all the 32 crystallographic point groups and, therefore, it would be impossible to reach such perfect geometries in crystalline complexes. In spite of this, one can attempt to achieve a symmetry as close as possible to the above-indicated symmetries. Experimental results, like those indicated above for compounds **21**–**23**, among others, support these qualitative expectations. It is worth mentioning that, to minimize the transverse CFs and then the QTM, the magnetic anisotropy axis for the $\pm M_J$ ground doublet state should coincide with the principal symmetry axis. When this occurs, the anisotropy axes of the low-lying excited states and the ground state are parallel and the magnetization relaxation does not take place through the first excited state, but through higher excited states, thus leading to higher U_{eff} values. This is the case generally occurring for Dy^{III} complexes with high-performance SMM behavior. For instance, in compound **21**, the anisotropy axes for the three low-lying excited states are almost collinear with that of the ground state, so that the magnetic relaxation occurs via the highly bunched set of states close in energy to the four excited state. It is also worth remarking that the change of charge density distribution around the trivalent lanthanide ion is more essential for determining the symmetry than the molecular geometry.

Another fundamental aspect to quench QTM is to prevent, as much as possible, weak intermolecular interactions. It is of vital importance to have single molecules well isolated within the crystal structure, so that there are no magnetic interactions between adjacent paramagnetic ions. This is because these interactions could provoke transversal magnetic fields favoring QTM. A widely used strategy is that of designing ligands that are not able to form intermolecular hydrogen bonds and thus the molecules should be isolated within the bulk structure [76]. However, this method is not always effective and even though, at first glance, the single molecules might be separated by a considerable distance they could show weak dipolar interactions. Another synthetic strategy could be that of diluting the paramagnetic centers within a diamagnetic matrix. In order to do that, the target compound needs to have isostructural counterparts that crystallize with diamagnetic ions. For instance, when using lanthanides, Y^{III} is usually employed since it contains a similar ionic radius compared to Dy^{III} and Er^{III} (La^{III} is also diamagnetic, but its ionic radius is larger and could not give rise to the same compound). Thus, both paramagnetic and diamagnetic compounds are co-crystallized in different ratios eliminating, at least partly, the undesired intermolecular dipolar interactions. This strategy was already employed by Ishikawa and col. when they discovered the first lanthanide based SMM, and it has been profusely used by other research groups during the last years [77–80].

Probably not at the same level as intermolecular dipolar interactions, the removal of hyperfine interactions between electrons and active nuclei has been proven to be another effective strategy towards diminishing the tunneling effect. In this regard, Cador and co-workers applied this approach firstly in the mononuclear [Dy(tta)$_3$(L)]·C_6H_{14} (**26**, Fig. 21) compound (tta$^-$ = 2-thenoyltrifluoroacetonate and L = 4,5-bis(propylthio)-tetrathiafulvalene-2-(2-pyridyl)-benzimidazole methyl-2-pyridine) [81]. This study aimed to intrinsically improve the magnetic behavior of single molecules, since magnetic dilution strategies are a way to optimize the effect of the environments and not of the molecule itself. For this purpose, they synthesized first **26** with natural Dy^{III} ion, which is mainly a mixing of the four out of seven different isotopes: ^{161}Dy (18.9%) and ^{163}Dy (24.9%) with I = 5/2 and ^{162}Dy (25.5%) and ^{164}Dy (28.2%) without nuclear spin. Then, natural Dy^{III} ions were replaced by ^{161}Dy (I = 5/2) or ^{164}Dy (I = 0) to isotopically enrich them, named **^{161}26** and **^{164}26** from now on. Both isotopically enriched compounds display frequency dependent out-of-phase susceptibility signals below 14 K at zero applied *dc* field, although they show notable differences. The maxima of the $\chi''_M(\upsilon)$ curves are much more shifted to lower frequencies for **^{164}26**. Indeed, even though the thermally activated regime coincides for both compounds regarding τ_0 and U_{eff} values, the relaxation times in the temperature independent regime are increased around an order of magnitude for the compound with a non-active nucleus. To verify that the increment in relaxation times corresponds to the quenching of the hyperfine interactions, they repeated the measurements under an optimum external magnetic field suppressing the residual QTM. The extracted relaxation times

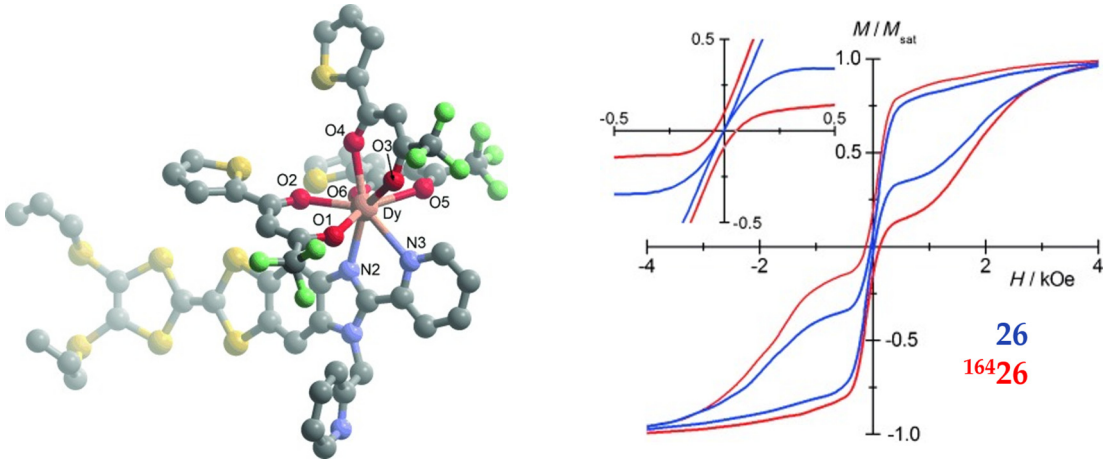

Fig. 21. Structure of the complex **26** (left). Hysteresis loops at 0.46 K for **26** and **^{164}26** (right). Color code: Dy^{III}, carbon, nitrogen, oxygen, sulfur and fluorine in pink, grey, blue, red, yellow and green, respectively. Hydrogen atoms and solvent molecules have been omitted for the sake of clarity. Reproduced with permission from [81]. Copyright 2015 John Wiley and Sons.

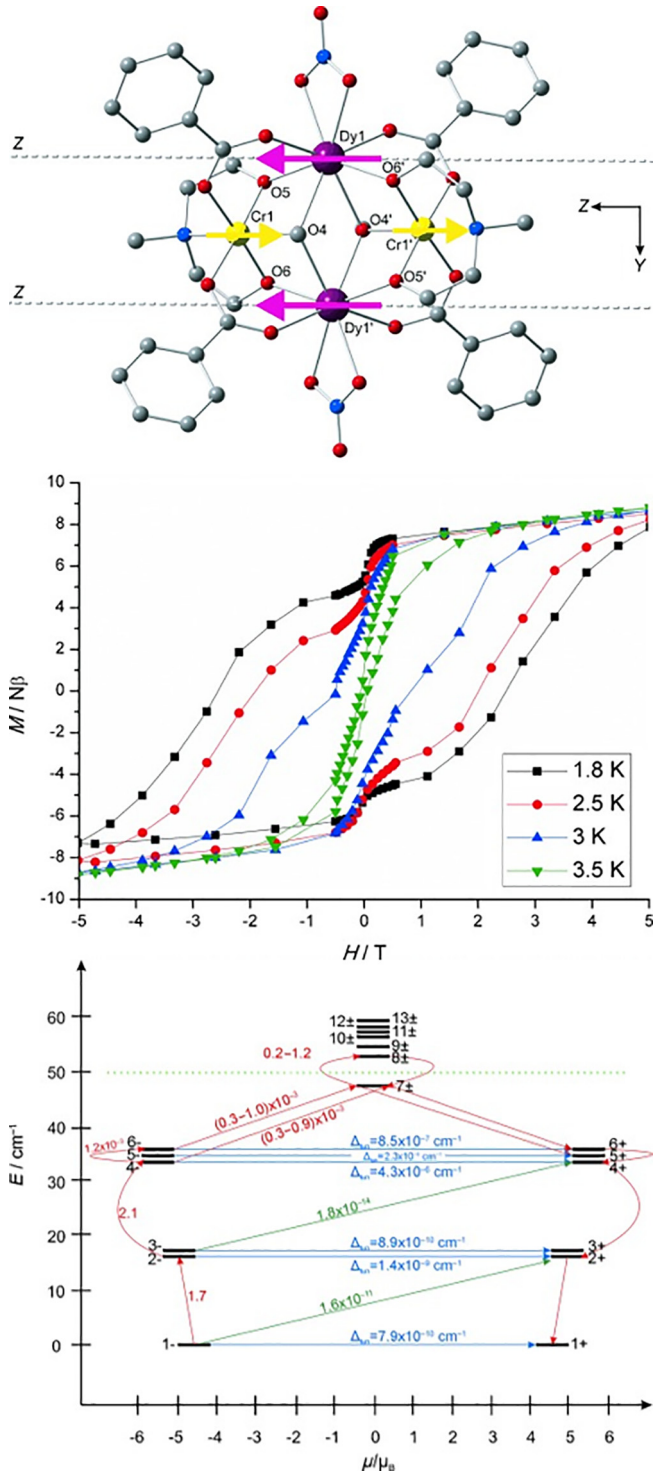

Fig. 22. Structure of the complex **28**. The dashed lines correspond to the main magnetic axes of the Dy^{III} ions. The arrows show the orientation of local magnetic moments in the ground exchange doublet state (top). Hysteresis loops measured with an average sweep rate of 0.003 T/s (middle). Low-lying exchange spectrum with the magnetization blocking barrier indicated by dashed green lines. The numbers for the horizontal blue arrows (Δ_{tun}) indicate an effective quenching of QTM (bottom). Color code: Cr^{III}, Dy^{III}, carbon, nitrogen and oxygen in yellow, purple, grey, blue and red, respectively. Hydrogen atoms have been omitted for the sake of clarity. Reproduced with permission from [83]. Copyright 2013 John Wiley and Sons.

coincide for all the derivatives, which clearly indicates that the isotopic enrichment only influences the temperature-independent regime.

This slowing down of the relaxation times in the temperature-independent regime was further confirmed by hysteresis loop measurements (Fig. 21, right). Compound **26** displays the typical butterfly shape losing the vast majority of the magnetization at low fields. However, for isotopically enriched ^{164}**26**, the opening at zero field is more pronounced, which demonstrates that suppressing hyperfine couplings somehow enhances the SMM properties. Nonetheless, this finding might be cautiously taken, since even combining different strategies including the isotopic enrichment the QTM persists. Related to this work, Chilton and co-workers made an exhaustive field- and temperature-dependent study in a high effective barrier SMM [82]. In that work, although they confirm that magnetic dilution and isotopic enrichment strategies are effective to modify the magnetic behavior at low temperatures, they remark that probably the way forward still resides in the engineering of the molecular structure to avoid tunneling through crystal field effects.

Completely opposite towards the previous strategy of eliminating any possible magnetic interactions of the paramagnetic centers with nuclei or other neighboring ions that could cause transverse magnetic fields, is to look for strong enough metal–metal interactions that might cause the contrary effect. Murray and co-authors reported the comparison between two butterfly type of complexes, namely $Co^{III}_2Dy^{III}_2$ (**27**) and $Cr^{III}_2Dy^{III}_2$ (**28**) systems (Fig. 22, top) [83]. For the former, taking into account that Co^{III} ions are in the diamagnetic low-spin state, the magnetic properties only arise from Dy^{III} ions. For the latter, the exchange interactions between both Cr^{III} and Dy^{III} paramagnetic ions are important. Even though the height of the energy barrier for both compounds is comparable, compound **27** crosses to a pure quantum regime below 2.5 K. In contrast, compound **28** displays open hysteresis loops up to 3.5 K with coercive fields as large as 2.8 T at 1.8 K (Fig. 22, middle). They carried out *ab initio* calculations to explain this huge difference in magnetic behavior. According to them, for the exchange coupled system the ground-state and thermally-assisted QTM are efficiently quenched and, thus, open loops are observable (Fig. 22, bottom). This research reveals the impact of magnetic exchange interactions within relaxation pathways.

Rajaraman *et al.* also made exhaustive studies regarding 3d-4f mixed systems. In a paper published in 2017, they compared four related octanuclear systems, in which they maintained their core structure, but modified either metal–metal bridging ligands and/or 3d metal ions [84]. The compounds **29** and **30** contained $Co^{III}_4Dy^{III}_4$ cores mainly differentiated by bridging OH^- (**29**) or F^- (**30**) groups, whereas **31** and **32** display two types of paramagnetic ions, $Cr^{III}_4Dy^{III}_4$, with bridging F^- (**31**) or N_3^- (**32**) groups (Fig. 23). Noteworthy, compounds **31** and **32** were previously reported [85,86]. Initially, leaving aside the effect of the 3d metal ion, they discovered that F^- bridges provide a bigger splitting between the ground and first excited states. Even though they both (**29** and **30**) have an M_J = ±15/2 as ground state and M_J = ±1/2 as first excited state, the higher electron density in fluoride ensures a better separation between both states. Hence, compound **29** is not an SMM, but **30** it is with a still marked QTM. When switching to structures containing a second type of paramagnetic ion, compound **32** displays two improved features in comparison to **30**. The height of the barrier was increased and QTM was effectively quenched. Moreover, when combining both strategies of implementing Cr^{III} ions and F^- bridges, the resultant compound **31** displayed the best results with the highest U_{eff} and suppression of QTM. This fact was then clearly proved by *ab initio* calculations. Without considering intramolecular exchange interactions, **31** should have even a more marked ground-state tunneling than **30**, which is contrary to what experiments showed. Therefore, Cr···Dy and Dy···Dy exchange pathways should have been included in the calculations. In such case, considering the polynuclear framework for relaxation

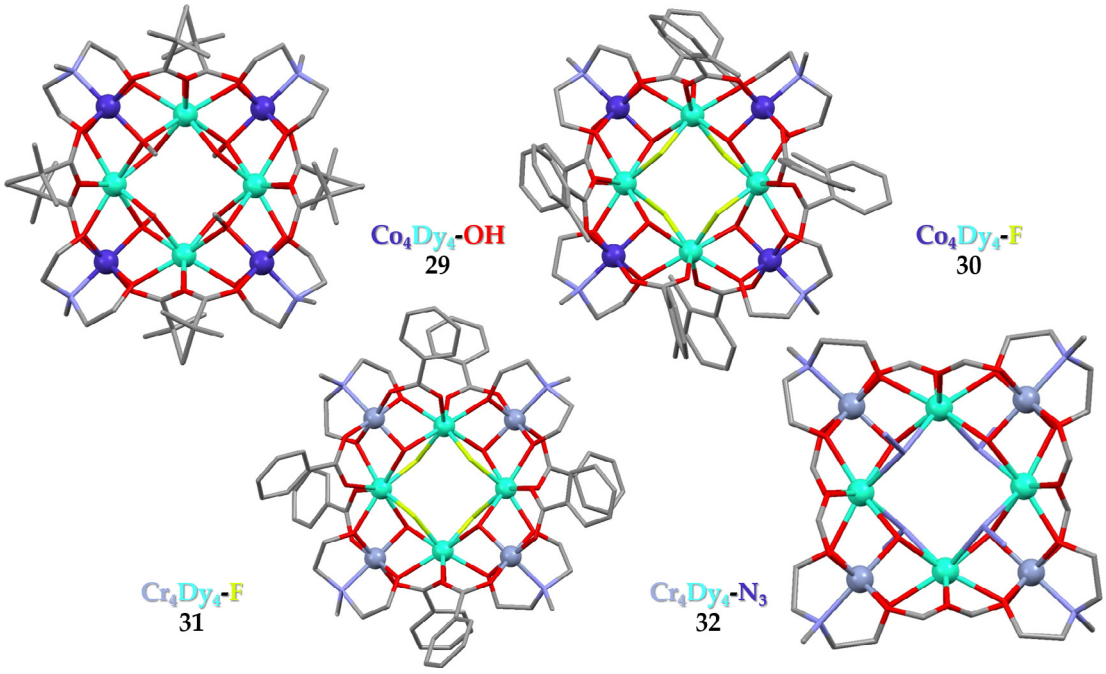

Fig. 23. Structure of the complexes **29**–**32**. Color code: Co^{III}, Cr^{III}, Dy^{III}, carbon, nitrogen, oxygen and fluoride in purple, light grey, turquoise, grey, blue, red and green, respectively. Hydrogen atoms, solvent molecules as well as disordered fragments have been omitted for the sake of clarity. Generated from the crystal structures in references [84–86].

mechanisms, they verified that the presence of paramagnetic Cr^{III} ions were responsible of quenching the low temperature relaxation channels present in compound **30**.

Even though the mentioned examples imply the presence of Cr^{III} ions, more examples including other 3d metals such as Mn^{II}, Fe^{II} and Co^{II} have been also reported [87–90]. Apart from them, the exchange coupled relaxation mechanisms were also investigated by Rajaraman *et al.* [91] for a previously reported Ni_3Dy (**33**) tetranuclear compound (Fig. 24, top) [92]. Although weak, the compound displays zero field SMM behavior. As shown for compound **25**, the octahedral coordination environments are not the most suitable in order to design high performance SMMs. Thus, it is not surprising that the distorted octahedral environment around the Dy^{III} ion in **33** is not able neither to stabilize M_J = ±15/2 states as ground state nor to create huge splitting between the ground and first excited state. In fact, the ground state in this compound is far from being of pure Ising-type with a mixed wavefunction mainly composed of M_J = ±13/2. In addition, even though the *g*-tensor values indicate that the ground-state is axial, the transverse components are not negligible. All in all, the calculations suggest that the compound will show QTM and that is not a potential candidate to be an SMM. However, once again the calculations based on the exchange-coupled system suggest that QTM is partially suppressed due to strong Ni···Dy interactions enabling zero-field SMM behavior (Fig. 24, bottom). Nonetheless, including paramagnetic 3d ions in 3d-4f mixed compounds is not always positive. The relaxation pathways in these complexes are not trivial and slight structural differences might be the line separating systems in which paramagnetic or diamagnetic 3d ions improve or deteriorate the SMM properties [93].

Different bridging groups or heteroatoms could give rise to different exchange, either in nature (ferro- or antiferromagnetic) and strength. However, because the 4f valence electrons are deeply buried below $5s^2$ and $5p^6$ electrons, the metal–ligand interactions are usually purely electrostatic in nature and, thus, when a heteroatom acts as bridging group between two Ln^{III} ions weakly interacting exchange coupled systems are observed. Therefore, for polynuclear Ln^{III} systems the SMM behavior could be directly associated to single ion behavior and, often, the weak interactions may be an unfavorable factor provoking transverse fields. A very promising strategy towards obtaining stronger metal–ligand interactions is to use paramagnetic ligands or, in other words, radicals. Their diffuse feature has been proved to be very effective to penetrate through the lanthanides orbitals and provide strong metal–ligand interactions that cannot be obtained through diamagnetic ligands. Clear examples of it are the N_2^{3-} bridged dinuclear compounds of formula $[K(18\text{-crown-}6)][\{[(Me_3Si)_2N]_2(THF)Ln\}_2(\mu\text{-}\eta^2\text{:}\eta^2\text{-}N_2)]$, where Ln = Gd^{III} (**34**) and Dy^{III} (**35**) compounds (Fig. 25) [94]. The very strong metal-radical interaction was proven by the noticeable rise in $\chi_M T$ observed in the $\chi_M T$ vs T curve below room temperature due to strong antiferromagnetic interactions. In fact, the value at 300 K for **34** was already lower than that expected for two non-interacting S = 7/2 Gd^{III} ions and a single radical S = 1/2 N_2^{3-} unit in agreement with the mentioned antiferromagnetic interactions. The fitting of the data afforded a strong J = -27 cm^{-1} exchange constant, notably higher than those usually found for Gd^{III} systems usually below 3 cm^{-1} [95]. To verify that the strong interaction arises from the diffuse nature of the N_2^{3-} radical, the non-radical N_2^{2-} bridged analogues were also studied (Gd^{III} (**36**) and Dy^{III} (**37**)). Although it was already evident from $\chi_M T$ curves, the fitting of the data for **36** supported a weak antiferromagnetic exchange interaction with J = −0.49 cm^{-1} constant. Noteworthy, the non-radical counterparts displayed some differences regarding structural parameters, but they were the best models to compare it to the data obtained for **34** and **35**.

The lack of spin–orbit coupling in Gd^{III} ion is a good feature in order to evaluate the *dc* data and somehow easily obtain exchange coupling constant values. However, its isotropic character prevents it to be a potential candidate for the design of SMMs. The Dy^{III} based compound **35**, instead, displays zero-field SMM behavior due to its anisotropic nature. The calculated U_{eff} of 177 K (123 cm^{-1}) is comparable to other Dy^{III} based SMMs, whereas the low temperature regime differs from usual. Some other compounds with similar effective energy barriers [96] display devia-

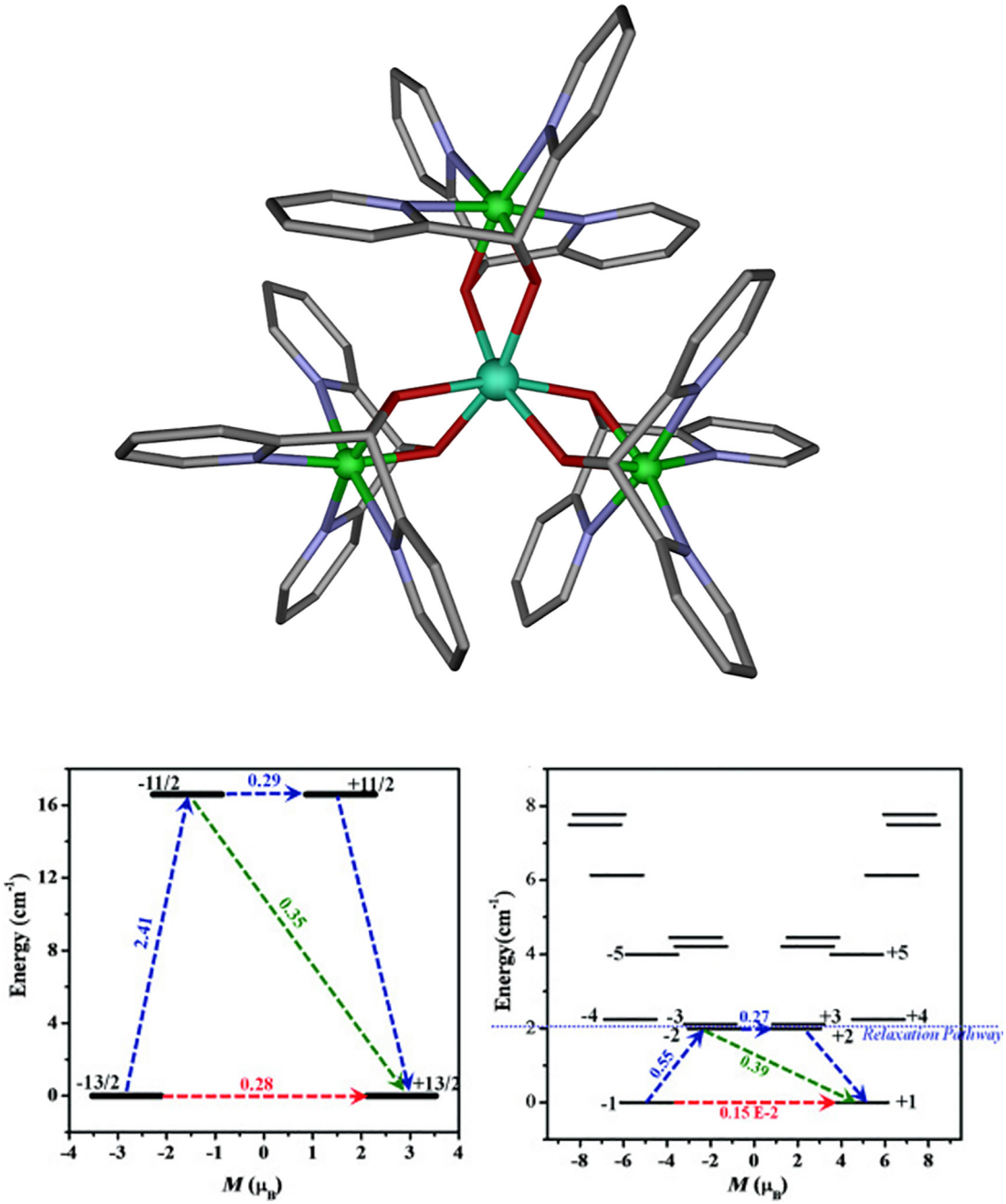

Fig. 24. Structure of the complex **33** (top). *Ab initio* computed magnetization blocking barriers for single ion (bottom left) and exchange-coupled system (bottom right) displaying a major contribution of QTM (dashed red arrow) for the former. Color code: Ni^{II}, Dy^{III}, carbon, nitrogen and oxygen in green, turquoise, grey, blue and red, respectively. Hydrogen atoms and counterions have been omitted for the sake of clarity. Generated from the crystal structure in reference [92]. *Ab initio* plots have been reproduced with permission from [91]. Copyright 2016 John Wiley and Sons.

tions in the Arrhenius plots that are clearly related to under barrier shortcuts. Compound **35** displays a clear linear dependence in the whole studied temperature range related to a pure Orbach mechanism. Moreover, N_2^{2-} bridged **37** displays a modest barrier of 25.9 K (18 cm^{-1}) with nearly constant relaxation times in the low temperature regime indicative of fast tunneling. Differently to **35**, weakly coupled SMMs usually behave as single ion magnets instead of single molecule magnets highlighting the importance of strong exchange coupling constants. Finally, SMM behavior was verified by measuring hysteresis loops up to 8.3 K with large coercive fields.

After the research related to Gd^{III} and Dy^{III} ions, the Long's group continued exploring N_2^{3-} bridged systems. Firstly, maintaining the structure, but switching to Tb^{III} (**38**) they obtained even better results since it showed a blocking temperature as high as 14 K [97]. After that, and in view of the great results obtained for sandwich type of complexes (later discussed) with cyclopentadienide derivatives, they managed to introduce again the N_2^{3-} radical to bridge Dy^{III} and Tb^{III} ions [98]. Among other compounds, they reported on the synthesis, characterization and magnetic properties of four novel compounds with general formula [K(crypt-222)(THF)][$(Cp_2^{Me4H}Ln(THF))_2(\mu - N_2^{\cdot})$] for Tb^{III} (**39**) and Dy^{III} (**40**) and [K(crypt-222)][$(Cp_2^{Me4H}Ln)_2(\mu - N_2^{\cdot})$] for Tb^{III} (**41**) and Dy^{III} (**42**) where crypt-222 = 2.2.2-cryptand and Cp^{Me4H} = tetramethylcyclopentadienyl (Fig. 26). Structurally speaking, the main difference between both structures is the presence/absence of a THF molecule coordi-

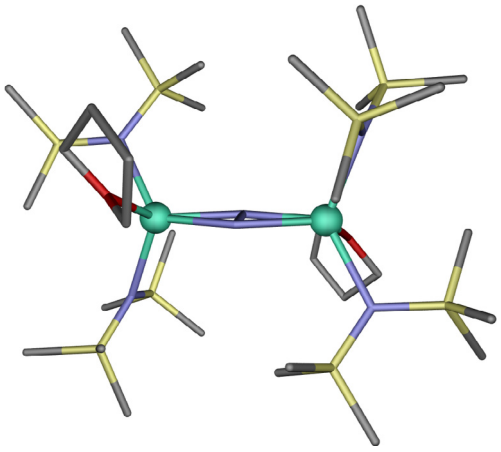

Fig. 25. Structure of the [{[$(Me_3Si)_2N]_2$(THF)Gd}$_2$(μ-η^2: η^2-N_2)] anion in **34** Color code: Gd^{III}, carbon, nitrogen, silicon and oxygen in turquoise, grey, blue, yellow and red, respectively. Hydrogen atoms and counterions have been omitted for the sake of clarity. Generated from the crystal structure in reference [94].

nated to the lanthanide ions. This was then easily removed by dissolution in 2-methyltetrahydrofuran. Even though compounds **39**–**42** are all zero field SMMs, there are some remarkable differences among them. Relaxation times extracted from *ac* measurements follow the Arrhenius law in the whole temperature range except for **40**, which crosses to a pure QTM regime at the lowest temperatures. This was then verified by variable-field magnetization measurements; in which it did not show any remnant magnetization even at 2 K. However, the removal of the THF molecules from the coordination environment substantially improved the magnetic behavior for **40** and open hysteresis loops were observed up to 8 K for **42**. Considering that Tb^{III} based compound **39** was already displaying open loops up to 15 K, great improvements were also predicted for **41** after THF removal. Indeed, open hysteresis loops were measured up to 30 K with a 100 s-magnetic blocking temperature of 20 K. Therefore, these research works regarding radical bridged coordination compounds exhibited great potential in terms of future design of high performance SMMs.

As it will be further discussed in the next section, compounds with a single paramagnetic ion (SIMs) compose the state of the art for SMMs, since so far they have shown the greatest properties. However, it is still necessary and challenging to study polynuclear systems that maintain the high anisotropy. The group of Rinehart employed the $[Er(COT)]^+$ (COT^{2-} = cyclooctatetraenide anion) as building block to construct four novel compounds; a mononuclear one (**43**) and three dinuclear systems (**44**–**46**) [99]. This fragment was selected because it is well known that it is suitable to stabilize the states with highest magnetic moment (M_J = ±15/2) for the Er^{III} ion and the anisotropy axis is known to point along the Er-$COT_{centroid}$ axis. The coordination spheres were completed by I^- ions and weakly coordinating phosphines (Fig. 27). Within the dinuclear systems, the former ones act as magnetic coupling bridges, while the latter non-coupling ligands were introduced to modulate the angles between the magnetic anisotropy axes. Noteworthy, phosphine ligands were selected based on their weakly coordinating character, which was not expected to alter the Er-$COT_{centroid}$ based anisotropy axis. Several interesting conclusions were obtained from the study of these four compounds. On the one hand, the effective energy barriers for **44**–**46** were around 150 K higher than for **43**, and very similar between them. However, the hysteretic behavior at 2 K did not follow the same trend (Fig. 27). Compounds **43** and **44** displayed waist-restricted butterfly-shaped hysteresis loops in agreement with a large influence of QTM. In contrast, compounds **45** and **46**, which show greater angles between Er-COT centroids, displayed open hysteresis loops without clear QTM contribution at zero field. Thus, this study emphasizes the importance of aligning the anisotropy axes in polynuclear systems (as it was previously demonstrated for transition metal clusters). In addition, relaxation times at 2 K were enhanced around six orders of magnitude from **43** to **46**, hence reaffirming the relevance of nuclearity and orientation of the axes in terms of slow relaxation of the magnetization.

6. State of the art: dysprosium metallocenes

As discussed along the paper, during the last decades several SMMs have been reported displaying large effective energy barriers to prevent the reorientation of the magnetization. Blocking temperatures, in contrast, have not been enhanced at the same pace due to the additional relaxation pathways that shortcut the energy barrier. Designated as outliers in this trend, trivalent dysprosium based metallocenes are the current state of the art of SMMs displaying magnetic blocking temperatures already above the liquid nitrogen. In the same way that COT ligands are appropriate for the design of Er^{III} based SMMs, Cp derivatives (Cp = cyclo pentadienyl anion) have provoked a revolution among Dy^{III} based systems. Already from Rinehart and Long's design principles, Cp sandwiched Dy^{III} compounds (without ligands in the equatorial plane) were envisioned as potential candidates, although the large ionic radii of Ln ions hindered or complicated their synthesis. However, Mills *et al.* and Layfield *et al.* almost simultaneously reported on a sandwiched dysprosocenium compound with Cp^{ttt} ligands (Cp^{ttt} = {$C_5H^t_2Bu_3$-1,2,4} and ^{t}Bu = $C(CH_3)_3$) (**47**, Fig. 28, top left) [100,101]. Compound **47**, with general formula $[Dy(Cp^{ttt})_2][B(C_6F_5)_4]$, shows a wide bent Cp-Dy-Cp angle of 152.56(7) ° with relatively short Dy-$Cp_{centroid}$ distances of 2.316(3) Å [100]. Already

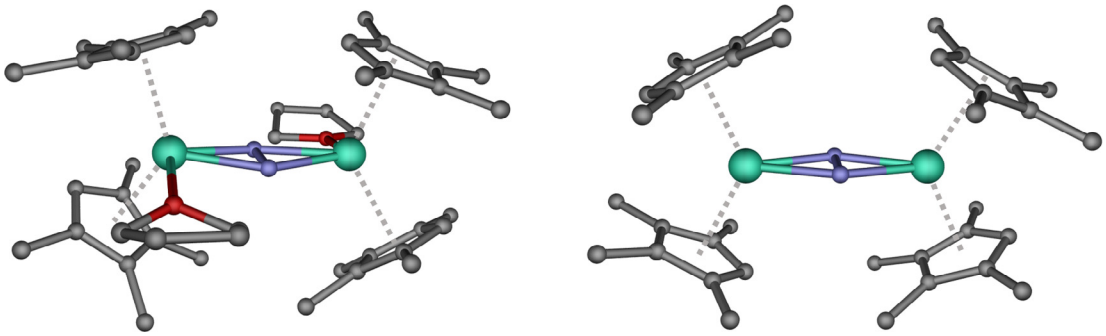

Fig. 26. Structure of the anionic complexes **39** and **41**. Color code: Tb^{III}, carbon, nitrogen and oxygen in turquoise, grey, blue and red, respectively. Hydrogen atoms and counterions have been omitted for the sake of clarity. Generated from the crystal structures in reference [98].

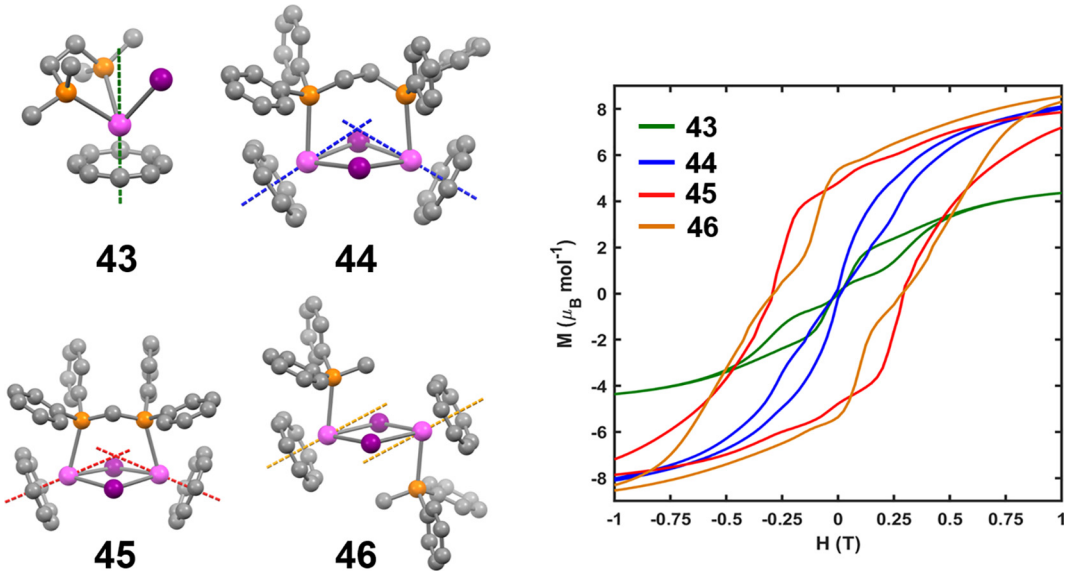

Fig. 27. Structure of the complexes **43**–**46** along with Er-$COT_{centroid}$ vector directions (left). Hysteresis loops at 2 K with a sweep-rate of 10.1 Oe/s (right). Color code: Er^{III}, carbon, phosphor and iodide in pink, grey, orange and purple, respectively. Hydrogen atoms have been omitted for the sake of clarity. Adapted with permission from [99]. Copyright 2019 American Chemical Society.

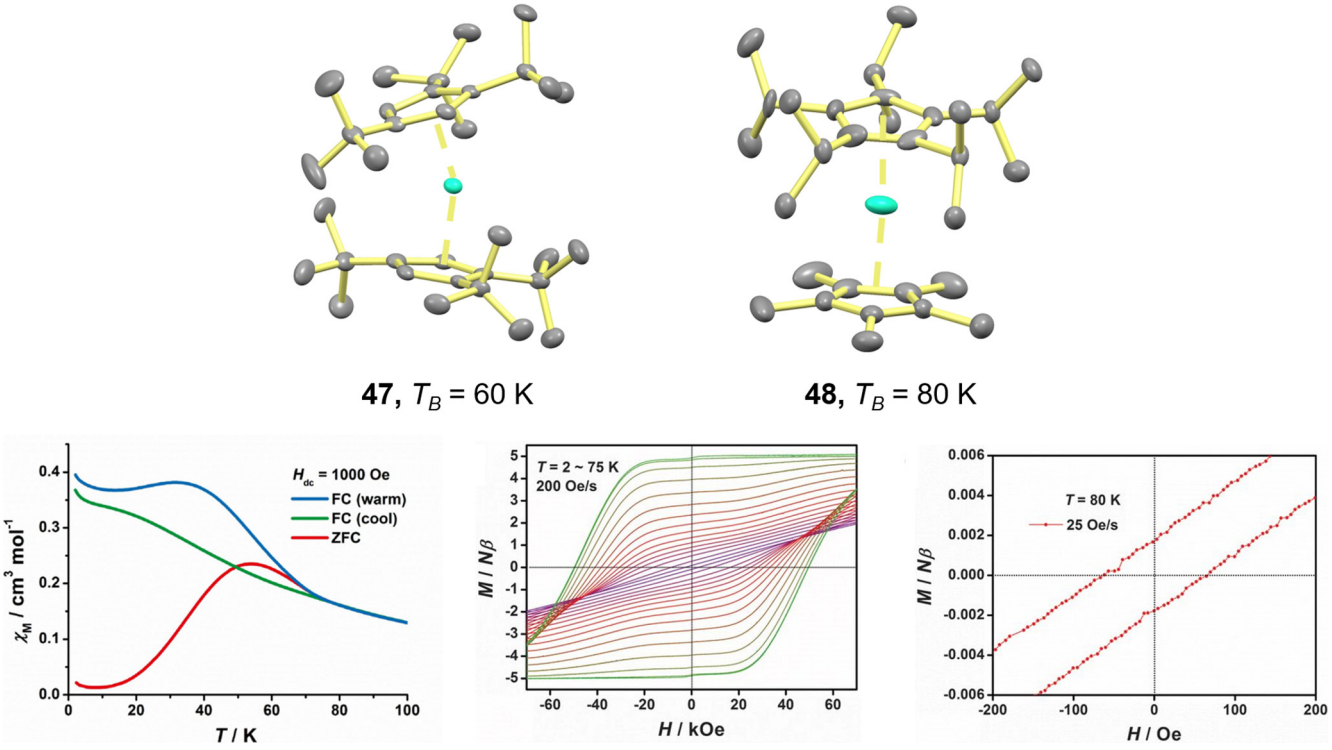

Fig. 28. Cationic structures of complexes **47** and **48** (top). FC/ZFC variable-temperature magnetic susceptibility under 1000 Oe (bottom left), hysteresis loops in the 2–75 K temperature range using a sweep rate of 200 Oe/s (bottom middle) and hysteresis loops at 80 K using a sweep rate of 25 Oe/s for **48** (bottom right). Color code: Dy^{III} and carbon in turquoise and grey, respectively. Hydrogen atoms and counterions have been omitted for the sake of clarity. Generated from the crystal structures in references [100,102]. Magnetic data reproduced with permission from [102]. Copyright 2018 The American Association for the Advancement of Science.

from this structural features, it was evident that the slow relaxation dynamics were going to be really promising. Indeed, open hysteresis loops were observed below 60 K (measured with a sweep rate of 22 Oe/s), although a zero-field step was already observable at 2 K attributed to QTM. FC/ZFC measurements confirmed the value of T_B displaying a bifurcation of both curves at 61 K.

In order to study the mechanism of magnetic relaxation, *ab initio* calculations were performed. Interestingly, the spin-phonon coupling arising from C-H vibrational mode in the Cp^{ttt} ligands was found to be of relevance promoting the first transition from the ground ±15/2 state to the excited ±13/2 one. Thus, pointing out that the substitution of such groups should potentially enhance the hysteretic behavior of dysprosium metallocenes. Furthermore,

the outlier character of this compound was attributed to the particular ligand field around the ion, since the rigid Cp^{ttt} ligands constrain metal–ligand vibrational modes that could enhance the through barrier shortcuts. In fact, the obtained energy barrier of 1760 K (1223 cm^{-1}) was found in the range of other previously reported SMMs such as $[Dy(O^tBu)_2(py)_5][BPh]_4$ (**21**) [67], the blocking temperature, however, is far greater for **47**. When comparing both systems, the former one contains single donor atoms in the first coordination sphere displaying a more pronounced metal–ligand flexibility, which might provide detrimental vibrational modes accelerating relaxation times through barrier shortcuts.

In light of these outstanding results, in 2018 again Layfield and co-workers went further and synthesized another dysprosocenium compound with enhanced performance [102]. By studying compound **47**, the design principles for an improved ligand field were clearer: (i) shorter Dy-Cp bond distances, (ii) wider Cp-Dy-Cp angles and (iii) absence of C—H bonds were targeted. However, in order to fulfil these purposes a compromise needed to be taken, since bulky ligands could provide wide angles (and absence of equatorially coordinated ligands), but too bulky ones favor longer bond distances. All in all, they managed to synthesize the targeted compound **48** (Fig. 28) with general formula $[(\eta^5\text{-}Cp^*)Dy(\eta^5\text{-}Cp^{iPr5})][B(C_6F_5)_4]$ where Cp* = pentamethylcyclopentadienyl and Cp^{iPr5} = pentaisopropylcyclopentadienyl (Fig. 28, top right). As a result of the appropriate ligand design, from the crystal structure analysis they concluded that the Dy-Cp* and Dy-Cp^{iPr5} distances were on average 0.026 Å shorter compared to **47**. Moreover, the Cp*-Dy-Cp^{iPr5} angle showed a notably wider value of 162.507(1)°, almost 10° nearer from the perfectly lineal value of 180°. Thus, already from these considerations, a stronger crystal field effect along with an enhanced magnetic behavior was expected.

Certainly, at a sweep rate of 25 Oe/s the hysteresis loops remained open up to 80 K, a temperature that is already above the liquid nitrogen (Fig. 28, bottom right). This blocking temperature was also certified by FC/ZFC measurements, in which a divergence of both curves was observed at 78 K (Fig. 28, bottom left). The axiality of the system was further confirmed by *ab initio* calculations suggesting a perfectly axial ground state. This was in fair agreement with the hysteresis loops at 2 K. In contrast to what observed for **47**, there was no sign of any zero-field step suggesting a total blocking of QTM (Fig. 28, bottom middle). Finally, taking into account that C—H bonds within the ring were replaced by either isopropyl groups or methyl groups, the vibrational mode initiating the first transition from the ground to the first excited state was found to be the out-of-plane vibration of the Cp* ligand.

Parallel to the discovery of this last metallocene, Harvey and co-authors reported on four other related Dy^{III} sandwich compounds (Fig. 29) with general formula $[Dy(Cp^{iPr4R})_2][B(C_6F_5)_4]$ (R = H (**49**), Me (**50**), Et (**51**), ^{i}Pr (**52**)) [103]. They were also inspired by compound **47**, so they employed four different Cp ligands to mainly modify the Dy-Cp distance, Cp-Dy-Cp angle and vibrational modes around the metal ion. The structural parameters that they found were coherent with the substituents they employed. The more sterically demanding cyclopentadienyl ligands provoked longer bond distances, but wider angles (see Fig. 29). This confirmed the validity of the approach showing that a single modification within the Cp ring modifies the ligand field around the metal ion, possibly modulating magnetization relaxation dynamics. The first evidence of it was observed by FC/ZFC measurements detecting divergences in the wide range of 28–65 K. From *ac* measurements they obtained U_{eff} values of 1849, 2112, 1986 and 1919 K (1285, 1468, 1380 and 1334 cm^{-1}) for **49**, **50**, **51** and **52**, respectively. They were able to rationalize this trend based on magneto-structural correlations. Between the four compounds, **49** displays the most bent angle and, thus, the lowest effective energy barrier. Linearity increases upon introducing bulkier substituents to the fifth position of the Cp ligand. However, they theorize that among them the bond angle is no longer the determinant factor and that the Dy-Cp bond distance comes into play. Therefore, the value of U_{eff}

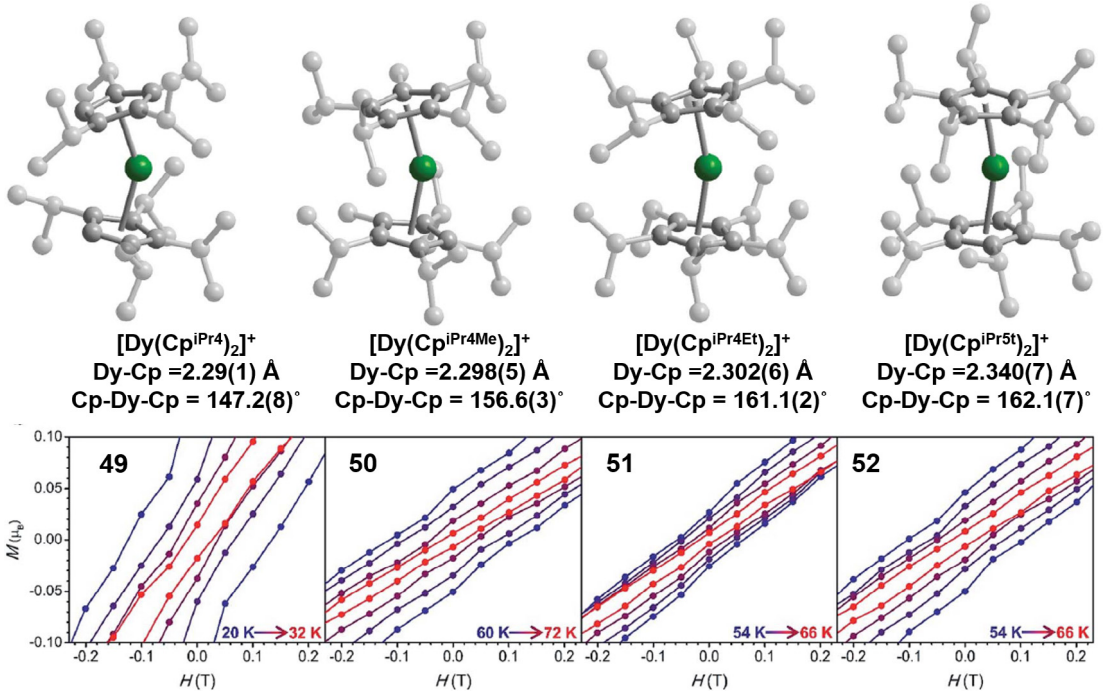

Fig. 29. Cationic structures of complexes **49**–**52** (top). Expanded view of the hysteresis loops near zero field and at high temperatures (sweep rate of 31(4) Oe/s for H < 2 T) (bottom). Color code: Dy^{III} and carbon in green and grey, respectively. Hydrogen atoms, counterions and positional disorder have been omitted for the sake of clarity. [103] – Published by The Royal Society of Chemistry.

increases from **52** to **50** as the Dy-Cp bond distance decreases. Following the observed trend, compound **50** exhibited open hysteresis loops at the highest temperatures. As a general conclusion, they suggest that the ligands that are able to find a compromise between wide Cp-Dy-Cp angles and short Dy-Cp bond distances are the next target, though an exhaustive knowledge in terms of spin-phonon coupling is also fundamental as 100 s blocking temperatures are found in the regime where Raman pathway dominates. Although the effect of molecular vibrations in terms of Orbach relaxation could be evaluated, models are needed for other under-barrier mechanisms.

In view of the exceptional results obtained for all these Dy^{III} metallocenes, in the last few years several new structures have been reported. For instance, Mills *et al.* recently reported a sandwich structure in which the chemical nature of the ligands was modified by changing one carbon atom by a phosphor one in a bis-monophospholyl dysprosium compound [104]. This new system displayed magnetic hysteresis at 48 K. Meng and co-authors studied exchange coupled dinuclear systems varying the bridging ligands (CH_3^-, Cl^-, Br^- and I^-) [105]. Furthermore, isocarbonyl-ligated metallocene coordination polymers have also been studied [106], as well as dinuclear systems in which fulvalene has been used as platform instead of Cp rings [107]. All this research evidences that these systems have revolutionized the field of SMMs and the interested reader is addressed to read further cited literature [108–111].

7. *Ab initio* methods: Valuable tools for a better understanding and improved design principles

Ab initio methods have emerged during the last years enabling a better interpretation, or even prediction, of the experimental magnetic properties, which at the same time facilitates developing improved ligand field design principles. The work of some specific authors in this field is remarkable as they were pioneers setting the basis of the extensively used softwares ORCA [112] and MOLCAS [113]. On the one hand, Frank Neese developed the former one and it has shown its validity for the calculation of *g* values and zero field splitting (ZFS) parameters, as well as the splitting of the d orbitals in transition metal complexes by using the *ab initio* ligand field theory (AILF, [50]). On the other hand, striking efforts of Liviu F. Chibotaru and Liviu Ungur have contributed in a decisive way to the development of the theoretical study of the electronic structure and the magnetic properties of lanthanide based SMMs with the MOLCAS software. In fact, they have built two programs, SINGLE_ANISO and POLY_ANISO for calculating local magnetic properties and the exchange energy spectrum and magnetic properties in polynuclear complexes, respectively, which were implemented in MOLCAS improving its functionality. Interestingly, this program can be used not only for calculating the electronic structure, magnetic properties and the effectiveness of the spin relaxation pathways in lanthanide based SMMs, but also in transition metal based SMMs. Apart from the above cited authors, numerous researchers working in the field of SMMs are notably contributing to the area of theoretical calculations. For instance, the results obtained by Gopalan Rajaraman [114], Eliseo Ruiz [115], Nicholas F. Chilton [116], Roberta Sessoli [117], and Alessandro Soncini [118], among many others, have played an important role in developing and improving this research field. Note that, for example, Soncini and co-authors recently developed a novel *ab initio* code called CERES (Computational Emulator of Rare Earth Systems), which is able to efficiently calculate the electronic structure and magnetic properties in lanthanide complexes [118]. In this section, we have tried to briefly remark some of the cutting-edge studies that have been carried out in the last years in the field of theory.

Chilton and co-workers have very recently reported a theoretical study for the prediction of relaxation rates based on *ab initio* methods [116]. Within this work, they have implemented a refined *ab initio* method to theoretically calculate the relaxation dynamics of several dysprosium based metallocenes including compounds **47**, **48** and **49**, which are intermediate, best and worst performing SMMs, respectively, among compounds that have been considered in the cited work. Between the latter two, they have concluded that the most influencing factor regarding relaxation dynamics is the crystal field splitting related to the static crystal structure. Namely, the larger energy gaps between ground and excited states for **48** in comparison to **49** are the reason for a better performance. When considering **47** and **48**, the initial prediction was related to an improved spin-phonon engineering; in other words, the substitution of C—H bonds was expected to be the discriminant factor for the enhanced magnetic properties. In this work, however, they found out that both a larger CF splitting and a reduced spin-phonon coupling were responsible of slowing down relaxation rates, but being the former one the prevailing reason. More interestingly, they also studied some other model compounds with general formula $[Dy(C_5R_5)_2]^+$ and $[Dy(C_4R_4)_2]^-$. From it, they concluded that organometallic sandwich compounds have probably reached their limit in terms of U_{eff} with a value of around 2100 K. Nevertheless, based on their study, the mentioned spin-phonon engineering may be now crucial to develop SMMs with improved properties. In fact, some of the studied model compounds displayed theoretical U_{eff} values that were similar to that of **48**, but relaxation rates were expected to be orders of magnitude slower. As they state, this can be explained by the presence of far fewer available vibrational modes that are not, at the same time, so frequently on-resonance with electronic transitions. Hence, they finally remark the relevance of removing detrimental vibrational modes that provoke faster relaxation times.

Theoretical studies have shown to be important to figure out some other issues that are not obvious based on experimental data. The qualitative crystal field design principles proposed by Rinehart and Long have given rise to a large amount of SMMs with huge U_{eff} values and blocking temperatures. However, the results that have been obtained based on these principles are not always easy to understand. For instance, why Er^{III} based SMMs have not shown such a good performance as Dy^{III} based ones? Switching the chemical design from an axial ligand field to an equatorial one is not enough? Theoretical studies based on *ab initio* calculations are very useful to understand the reasons behind.

For this purpose, Zhang *et al.* [119] selected the equatorially three coordinated compounds **18** ($Er[N(SiMe_3)_2]_3$), **53** ($Er(dbpc)_3$; dbpc = tris(2,6-di-*tert*-butyl-*p*-cresol)) and **54** ($Er(btmsm)_3$; btmsm = tris(bis(trimethylsilyl)methyl)), being the latter two previously reported by Yamashita and co-authors [120]. For the three compounds shown in Fig. 30, they observed by theoretical calculations that the axiality of the systems was quite modest in contrast to what was expected by crystal field considerations. Indeed, the $g_{x,y}$ values that they obtained for the first excited Kramers doublets were no longer close to zero. Thus, these transverse components would be the reason for a fast QTM in the first excited state limiting the value of U_{eff} to the energy difference between the ground and first excited state. Additionally, they also studied theoretically the influence that would have the modulation of θ angles (angle between the vector connecting Er^{III} and L ligands and the anisotropy axis, see Fig. 30) and Er-L distances in the height of the energy barrier. The calculations were partially in agreement with the design principles proposed by Long *et al.* On the one hand, the highest U_{eff}'s were calculated for θ = 90° angles and, in the other hand, a lengthening of Er-L bond distances would give rise to a smaller energy splitting between the ground and first excited states. In contrast, a shortening of Er-L bond distances would lead

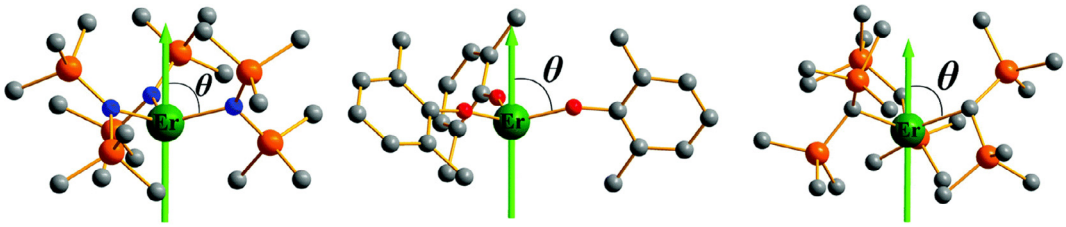

18 53 54

Fig. 30. Structural view of complexes **18**, **53** and **54**. The green axes show the orientations of the local main magnetic axes on Er^{III} in the ground KDs. Color code: Er^{III}, carbon, nitrogen, silicon and oxygen in green, grey, orange and red, respectively. Hydrogen atoms and *tert*-butyl groups in **53** have been omitted for the sake of clarity. Adapted with permission from [119]. Copyright 2020 The Royal Society of Chemistry.

to an undesired competing effect, since the equatorially coordinated ligands would produce larger transverse components (higher $g_{x,y}$) in the ground and first excited states allowing fast QTM. Therefore, they conclude that for equatorially coordinated Er^{III} mononuclear compounds will be difficult to obtain energy barriers as high as for Dy^{III} compounds.

Another very interesting theoretical work was recently reported by Chibotaru and co-workers [121]. They made an *ab initio* study on robust divalent [LnO] units for enhanced SMM properties. Note that previously was done for the $[DyO]^+$ unit [122]. Furthermore, being aware of the importance of depositing SMMs on surfaces (see next section) for future devices, they also studied a model [DyO] unit deposited on the hexagonal boron nitride (h-BN) surface. As they state, the findings they made are important for two main reasons. Firstly, as it has been shown for several recently reported Dy^{III} metallocenes, the limit of the blocking barrier seems to have been enhanced to the maximum and, thus, it seems to be hardly surpassable. This is directly related to the extreme difficulty of synthesizing low coordinated lanthanide based compounds. For this reason, switching to [LnO] units is presented as an attractive alternative towards SMMs with an improved efficiency. The energy splitting of the eight Ising doublets and a singlet for $J = 8$ in [DyO] spreads over 2500 cm^{-1} due to the strong covalent contribution and short Dy-O distance. Therefore, this system could be a potential candidate for future experimental studies. Finally, even though the model [DyO] system deposited on h-BN would theoretically be in a horizontal fashion (parallel to the surface), it is expected to preserve intrinsic axiality over the possible low-symmetric contributions from the surface. Consequently, this system is supposed to have a blocking barrier still exceeding 2000 cm^{-1} and to preserve excellent magnetic blocking properties even after depositing it into a surface.

During last years, there has been a more exhaustive study in order to try to understand how molecular or lattice vibrations affect the demagnetization process. As another recent example, Irländer and Schnack showed how phonons could open tunneling gaps between otherwise degenerate ground states in SMMs [123]. They believe that these kind of studies are very useful for future rational designs, since it enables identifying vibrations that are detrimental and facilitate demagnetization processes.

As a last example in this section, we would also like to remark an interesting recent paper by Aravena [124]. As it states, *ab initio* calculations have been and are very useful to rationalize the observed experimental magnetic properties. However, these are often case specific and approaches that could be generalized to bigger families of compounds are lacking. Fascinatingly, in this work a new method was proposed for the prediction of tunneling demagnetization times (named as τ_{QTM} in the present work) and effective energy barriers (U_{eff}). This method could be used by introducing the orientation of the molecule in the crystal structure, the ground and excited states energies and *g* factors to give rise to an *ab initio* prediction. To prove the validity of it, it was evaluated by considering 18 previously reported Ln^{III} based compounds (15 Dy^{III} based and 3 Er^{III} based) and comparing the obtained results with the experimental ones. As mentioned, we also consider this approach a valuable tool for evaluating a bigger family of SMMs by the same method.

8. Hybrid materials based on SMMs for future applications

During the last decades an enormous amount of SMMs have been reported in the literature. For the vast majority of them, the magnetic properties were studied in the bulk. However, with the aim of developing a future device and for reading/writting purposes, incorporating these systems in surfaces is imperative while preserving their magnetic properties, which could be a handicap due to potential surface-molecule interactions [125–128]. Moreover, a long range ordering, as well as high density of molecules is desirable for these hybrid systems. Although numerous examples of hybrid materials have been reported so far, here we will only describe a few selected examples of them.

Among different options [129,130], the use of three dimensional metal–organic frameworks (MOFs) could be an attractive one. Indeed, some of these systems possess pores that could be suitable to load guest molecules. Even though few of these hybrid systems have been previously reported [131,132], the problem usually arises when designing specific pore sizes and functional groups that point towards the pore stabilizing the guests and providing great loading capacities. In a recently reported research by Yuan and co-workers, they synthesized a La^{III} based mesoporous MOF based on short and rigid ligands showing 2 nm long pore diameter [133], suitable for incorporating Mn12-ac molecules inside (Fig. 31). By dipping samples of the MOF into saturated solutions of Mn12-ac, the colorless crystals turned from colorless to brown already indicating that the guest molecules were loaded. PXRD experiments showed that the 3D network remained intact after the process and N_2 adsorption isotherms as well as BET surface measurements were used to prove that the target molecules were encapsulated within the pores. They concluded that the designed system had special features that allowed a large loading. On the one hand, the hydrogen bonds between the —OH groups pointing to the center of the pores and acetate oxygen atoms (see red dashed lines in Fig. 31) stabilize the guests and, on the other hand, the flexibility of the material was essential since the interactions between the MOF and SMMs provoked a shrinking of the pores improving the loading capacity. Based on EDX, ICP-MS and ^1H NMR techniques, they calculated a record-breaking

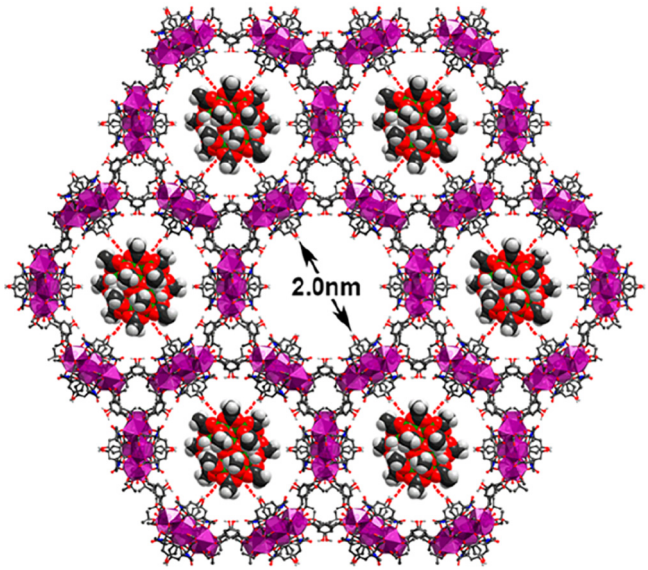

Fig. 31. Crystal structure of the MOF reported by Yuan and co-workers with a loading suggestion of Mn12-ac. Reproduced with permission from [133]. Copyright 2019 American Chemical Society.

loading capacity of 40.15 mol%. Finally, by measuring the magnetic properties of the hybrid system, they proved that the SMM properties were well preserved since maxima were visible in the $\chi''_M(T)$ and open hysteresis loops were observed at 2 K.

As seen in the previous example and also in previous reported studies, indirect methods to prove the loading of the SMMs into the channels of the MOFs are well stablished. However, it was not until a couple of years that a direct method was employed in order to visualize guest molecules inside the pores. More specifically, Wriedt *et al.* synthesized a SMM@MOF composite using Mn12-ac as the guest molecule and the Zr^{IV} based MOF NU-1000 [134], named **Mn12-ac@NU-1000** [135]. By using a low-dose High-Resolution Transmission Electron Microscopy (HRTEM) technique they were able to unequivocally probe the incorporation of the SMMs into the channels of the MOF. As depicted in Fig. 32, the image that was acquired along the [001] direction displayed discrete particles of a ~2 nm size in the hexagonal channels. This particle size was in fair agreement with the expected size of 1.6 nm for Mn12-ac. In order to discard the possibility of these particles arising from the decomposition of the MOF due to prolonged exposure times, several other images were taken and compared to unmodified NU-1000, demonstrating that the observed particles were corresponding to Mn12-ac.

They finally studied the magnetic properties of the hybrid composite showing that the nanoconfinement of the SMM within the pores of NU-1000 only slightly modified the SMM properties that are observed for bulk samples of Mn12-ac, thus maintaining the slow relaxation of the magnetization. Interestingly, the authors extended their work to the synthesis and characterization of a thin film of the composite, which would be the next step to implementing them in future devices.

In those previous two examples, the SMMs were successfully introduced in diamagnetic MOFs. Therefore, the metal–organic architectures acted only as scaffolds to organize the systems without influencing the magnetic properties. Another intriguing approach could be to combine magnetically active MOFs with SMMs. Pardo and co-authors [136] reported on hybrid systems combining the field-induced SMM $[Mn^{III}(TPP)(H_2O)_2]ClO_4$ (TPP = 5,10,15,20-tetraphenylporphyrin) [137,138] with the Mn^{II} and Cu^{II} based 3D MOF $Na_4\{Mn_4[Cu_2(Me_3mpba)_2]_3\}\cdot 60H_2O$ (Me_3mpba^{4-} = N,N′-2,4,6-trimethyl-1,3-phenylenebis(oxamate)) [139], which shows long-range magnetic ordering below 15 K. The SMM was introduced within the MOF by a single-crystal to single-crystal post-synthetic procedure obtaining the hybrid **MnTPP@1**. Interestingly, the magnetic properties of both the MOF and SMM were modulated. On the one hand, measurements that were carried out with an alternating current displayed frequency independent χ''_M signals below 20 K, indicating a long range magnetic ordering 5 K above respect to the 3D system without any incorporated SMM. Regarding slow magnetic relaxation, the hybrid system displayed frequency dependent χ''_M signal in the absence of any external field. This unequivocally showed that the internal magnetic

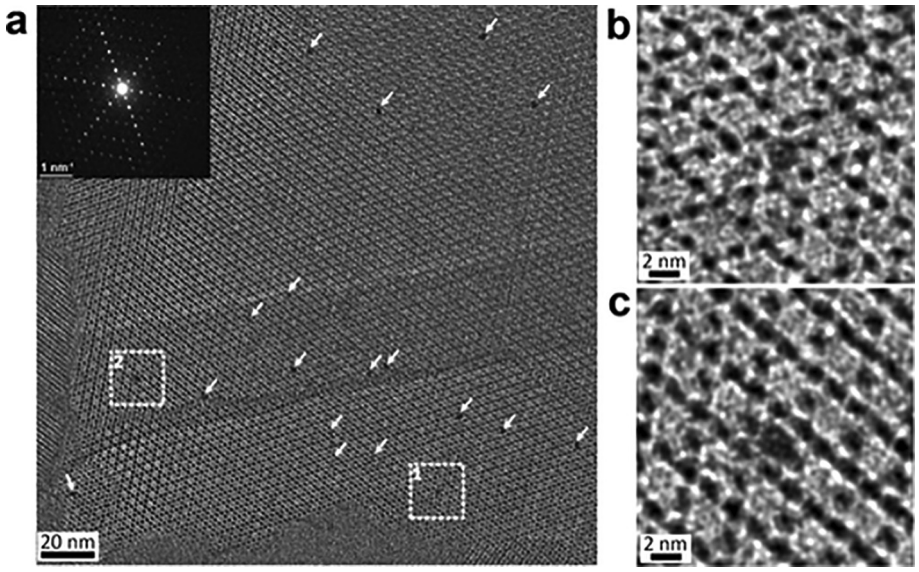

Fig. 32. Structural characterization by HRTEM of **Mn12-ac@NU-1000**. a) HRTEM image and electron diffraction pattern (inset) of **Mn12-ac@ NU-1000** acquired along the [001] zone axis of NU-1000. Arrows indicate the observed particles that correspond to Mn12Ac. b) and c) Enlarged images of the highlighted areas in areas 1 and 2, respectively, showing that the clusters of Mn12-ac are precisely encapsulated and perfectly fitted in the hexagonal channels of NU-1000. Images were processed by using a Gaussian filter to enhance the signal-to-noise ratio. Reproduced with permission from [135]. Copyright 2019 American Chemical Society.

field provided by the ferrimagnetic MOF was able to somehow quench the fast QTM present in the unsupported compound. Moreover, an isostructural 3D compound was also synthesized by changing Mn^{II} with Mg^{II} ($Mg_2\{Mg_4[Cu_2(Me_3mpba)_2]_3\}\cdot 45H_2O$ [140]), a compound that does not show any long range magnetic ordering. By post-synthetically modifying it, they obtained another hybrid system **MnTPP@2**. Confirming the previously suggested hypothesis, no χ''_M signal was observed in the absence of an external magnetic field, pointing out the importance of the intrinsic magnetic field in quenching the fast QTM.

Another essential feature for reading/writing processes is to orient the magnetic easy axis of the molecules perpendicular to the surface, so that many other systems have been reported which were anchored to two-dimensional layers. For example, Dreiser *et al.* reported on Er(trensal) molecules (H_3trensal = 2,2′,2″-tris-(salicylideneimino)-triethylamine) anchored to graphene (G) decoupling layers that were grown on Ru(0001) and Ir(111) single crystal surfaces [141]. For comparative purposes, they also studied Er(trensal) molecules grown in bare Ru(0001). Thus, three hybrid systems were targeted and named as **Er(trensal)/G/Ru(0001)**, **Er(trensal)/G/Ir(111)** and **Er(trensal)/Ru(0001)**. For the two former ones, scanning tunneling microscopy (STM) images showed that the lateral size of the unit cell of Er(trensal) molecules anchored to the surface was comparable to the unit cell of the model system, suggesting a similar molecular packing on the hybrid materials. In contrast, the molecules that were grown in bare Ru(0001) did not display any long-range ordering revealing the importance of implementing a decoupling graphene layer between the molecules and the metallic surfaces.

This different packing behavior was then noticeable in the *M(H)* curves obtained from low-temperature X-ray magnetic circular dichroism (XMCD) data. This technique is capable of measuring the projection of the magnetic moment onto the beam direction. Thus, if in a certain surface all the molecules have the same orientation, the magnetic anisotropy axes of all these systems will also have the same direction. Therefore, normal and grazing incidences of the beam will show different magnetization data. When the molecules are not properly ordered within the mentioned surface, the response to the magnetic field will be the same for normal or grazing incidence. In the present case, the difference between the hybrid systems containing a decoupling G layer respect to the bare Ru(0001) was remarkable (Fig. 33). For both hybrid systems with G, the Er^{III} magnetic moment projected onto the surface normal (black data) is notably stronger than the one measured in grazing geometry (red data). Which means that the magnetic easy axes of the molecules are oriented perpendicular to the G surface, consistent with the STM data. In contrast, for Er(trensal) on bare Ru (0001), there was not any angular dependence, confirming the different adsorption conformations to the surface with random directions for the magnetic anisotropy axes. In addition to this work, other research papers such as the one reported by Marocchi and co-workers points out the importance of implementing a decoupling graphene monolayer between the SMMs and the metallic surface [142]. Besides the influence that it can have regarding the orientation and long-range ordering of the molecules, in this latter research work the graphene layer was of vital importance to maintain the nature of the target molecule. They anchored the so well-known $TbPc_2$ sandwich compounds to G/Ni (111) substrate, but when G was not used, the radical character of the phthalocyanine was lost.

Another interesting material for anchoring SMMs is a carbon nanotube (CNT). For data storage, spintronics or quantum information processing purposes, an electrical control of the material is fundamental [143,144], and since CNTs are excellent electrical conductors [145], CNT-SMM hybrids are of great interest. Moreover, due to their chemical and thermal stability, they are great candidates for fabrication [146]. CNT hybrid materials have been previously studied with gold or magnetic nanoparticles, proteins, enzymes or luminescent molecules [147–152]. These materials, however, usually display large amounts of anchored molecules per carbon nanotube, while CNT-SMM hybrids should display a very controlled amount of magnets within the nanotube.

With this purpose, Bogani *et al.* designed and synthesized the compound **55** with general formula $[Fe_4(L)_2(dpm)_6]$ where Hdpm = dipivaloylmethane and H_3L = 2-hydroxymethyl-2-(4-(pyren-1-yl)butoxy)methylpropane-1,3-diol [153]. Noteworthy, other derivatives of this tetranuclear Fe^{III} based structures have also been extensively studied for their implementation in gold or graphene based surfaces [154–156]. For the present case, H_3L was rationally designed containing pyrene groups in the side chains, which are suitable for π ··· π interactions. Compound **55** was proven to be an SMM displaying open hysteresis loops below 1 K. By immersion of the CNTs into solutions containing complex **55**, they managed to synthesize the hybrid systems. AFM (Atomic Force Microscopy) techniques were then used to prove the link between **55** and CNTs. However, this strategy allowed developing systems in which the SMM is anchored in the outer surface of the CNT, thus being exposed to the outside world. Perhaps, a more interesting

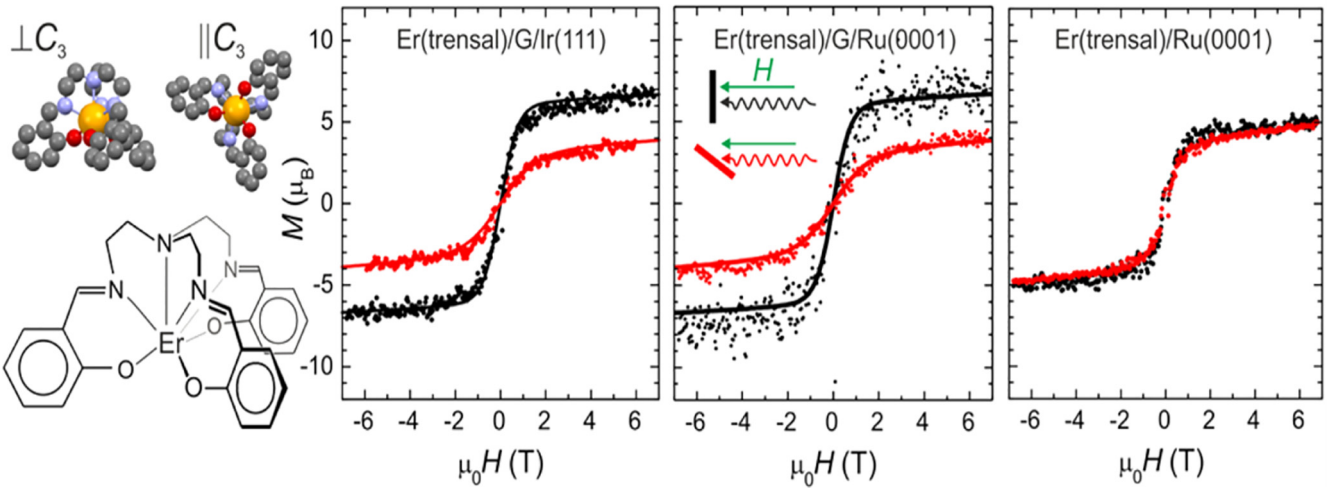

Fig. 33. Structural views and scheme for Er(trensal) (left). Er *M(H)* from XMCD at 3 K in normal (θ = 0°) and grazing (θ = 65°) geometry for **Er(trensal)/G/Ru(0001)**, **Er(trensal)/G/Ir(111)** and **Er(trensal)/Ru(0001)**, respectively. Reproduced from [141] with *ACS Author Choice*.

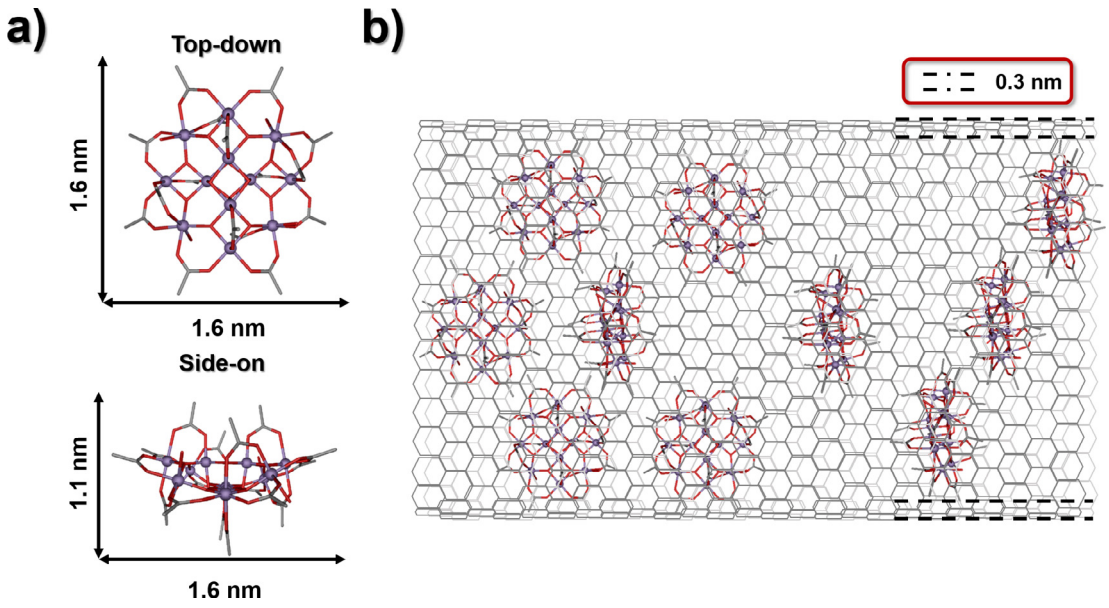

Fig. 34. a) Structure of Mn12-ac with its dimensions. b) Schematic representation of the innermost layer of a GMWNT hosting Mn12-ac molecules. The representation is based on the original work [158].

approach would be encapsulating the guest SMM within the carbon nanotube protecting it from the surrounding and preventing an undesired decoherence, which is fundamental for information processing purposes [157].

A clear example of this approach is the research carried out by Khlobystov and co-workers, who encapsulated Mn12-ac molecules within CNTs [158]. Firstly, considering the size of Mn12-ac, and taking into account a minimum van der Waals gap of 0.3 nm necessary between the molecules and CNTs [146], multiwalled carbon nanotubes (MWNT) were employed, whose internal diameters are found in the range of 5–50 nm (for this specific case, graphitized MWNTs, GMWNT, with internal diameter of 6.5 ± 1.8 nm were used). Hybrid **Mn12-ac@GMWNT** (Fig. 34) were characterized by TEM (Transmission Electron Microscopy) showing that the SMMs were inside the nanotubes and not in the outer surface of the tubes as reported in other works where single-walled carbon nanotubes were used [153,159,160]. In addition, PXRD and TG experiments were carried out to prove that the molecules were interacting more strongly with the interior than with the exterior. The χ''_M *(T)* plots for the hybrid material confirmed the retention of original SMM properties for **Mn12-ac@GMWNT**. However, the fact that two different sets of maxima appeared in this plot was justified by a tilt in a Jahn-Teller axis for a Mn^{III} species allowing an additional faster relaxation process. Hysteresis loops were found to be more influenced by QTM in the hybrid material due to larger transverse anisotropy, in fair agreement with the lower calculated energy barrier. All in all, though, these hybrid materials where the molecules were encapsulated within the nanotubes showed their great potential retaining the original SMM behavior.

To end this section, we would like to emphasize the relevance of implementing theory upon hybrid systems. The main handicap in these cases is that (normally) there is not a crystal structure that defines the explicit position of every single atom when the SMM is adsorbed or anchored to a surface. Therefore, this makes much harder to unequivocally define magneto-structural correlations. In this context, in 2015 Sessoli, Totti and co-workers [117] used *ab initio* molecular dynamics (AIMD) for the first time to examine the structural evolution of a previously reported SMM once adsorbed in a gold surface and, thus, they were able to predict changes in magnetic properties when going from the bulk to the anchored systems. Interestingly, they found out that structural rearrangements induced by the surface were more relevant than electronic coupling (with gold) in the final magnetic properties of the system, which highlights the role of an appropriate ligand design.

9. Multifunctional SMMs

It is very common to find in the literature SMMs that display different functionalities and this is very interesting when the sum of them is synergistic in nature. In words of the philosopher Aristotle, multiple functionalities for a single system are justified as long as the *"whole is greater than the sum of its parts*". The most common synergy for Ln-SMMs occurs when magnetic and luminescent properties are combined. As mentioned above, the unquenched spin–orbit coupling in Ln^{III} ions arises from the deeply buried 4f valence electrons. At the same time, the low sensitivity of these 4f electrons towards the coordination environment causes minor variations in the energy level spectrum of each Ln^{III} and, thus absorption and emission bands are very narrow giving rise to extremely pure colors. Each emission band, therefore, is a fingerprint of the ion. Along the lanthanide series, emission bands are found either in the visible (Tm^{III}, Tb^{III}, Dy^{III}, Eu^{III} and Sm^{III}; Fig. 35a) or near infrared range (Yb^{III}, Nd^{III} and Er^{III}; Fig. 35a).

The main problem to overcome arises from the fact that 4f-4f electronic transitions are parity-forbidden by the Laporte rule, which causes low brightness emissions. In addition, direct Ln^{III} excitation is not an effective strategy due to low absorption coefficients (ε). Hence, an effective way to overcome this problem is introducing the emissive ion within an organic matrix in order to sensitize the photoluminescent properties. With this purpose, organic ligands that contain wide absorption bands (ligands containing aromatic or conjugated unsaturated groups, for instance) are selected to achieve a good sensitization by the so-called *antenna-effect*. Such effect, among other factors, depends on the position of the lowest ligand triplet state (T_1, Fig. 35b) respect to the excited emissive state of the Ln^{III}. By use of the excitation light, the ligand is excited to a singlet state (S_n) from where can relax giving rise to fluorescence or it could relax to the triplet T_1 state. At the same time, from this level two things could happen: (i) the ligand can relax to the initial state emitting phosphorescence

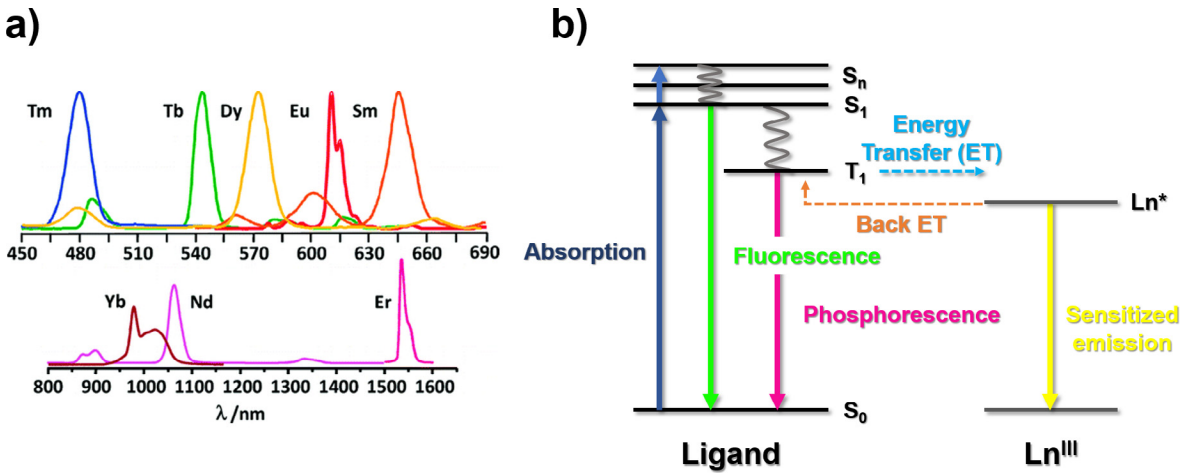

Fig. 35. a) Emission spectra of tris-β-diketonate compounds. b) Simplified Jablonsky diagram. Reproduced with permission from [168]. Copyright 2010 American Chemical Society. Original data can be found in [169].

or (ii) if the energy difference between the ligand T_1 and emitting level of the Ln^{III} is in the optimal range, an energy transfer may occur sensitizing the emission of the Ln^{III} (Fig. 35b). For each trivalent lanthanide, the optimum energy difference range between these two states has been previously reported [161]. After the sensitization process, though, the deactivation can occur through non-radiative pathways diminishing the quantum yield (Φ) of the emission. Even though we are not going to explain deep inside, these non-radiative processes, on the one hand, occur more or less depending on the Ln^{III} ion (intrinsic to the nature of the metal ion), but, on the other hand, could be enhanced by external factors. The smaller the energy gap between the emitting state and the first lower-lying energy level, the bigger the probability to observe non-radiative deactivating processes (this is one of the reasons why usually Tb^{III} based compounds display brighter emission than Dy^{III} ones, for example). Moreover, among the external luminescence quenchers, oscillators such as O—H, N—H and C—H groups are known to enhance the undesired non-radiative deactivation pathways. Thus, it is of vital importance to avoid these functional groups in close approximation of the luminophores [162,163]. Since only some of the most important features are going to be discussed along this section, the reader interested in luminescent Ln-SMMs is encouraged to read the cited literature [164–167].

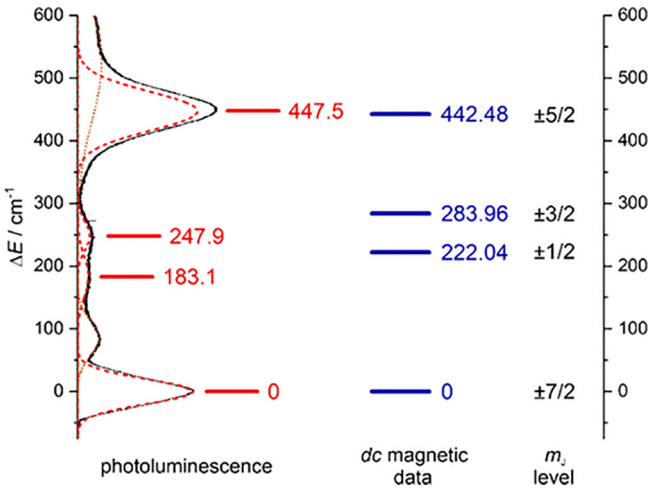

Fig. 36. The energy level diagram of a Yb^{III} compound is shown as an example. The crystal field splitting of the ground $^2F_{7/2}$ multiplet was constructed based on the emission spectrum at 6 K (left) and based on the fitting of the *dc* magnetic data starting from *ab initio* studies (right). The presented M_J levels in the right side represent the components with the highest contribution. Reproduced with permission from [174]. Copyright 2020 American Chemical Society.

One of the exciting benefits of combining both magnetic and photoluminescent properties is the fact that once the molecules are anchored or attached to a surface, their emission could be used to verify the position and quantify the concentration of them in the material. Noteworthy, in order to develop bright emissions, asymmetric environments are beneficial in comparison to highly symmetric ones. This is somehow incompatible for enhanced magnetic properties, since as it has been discussed, asymmetric features could provide the systems with transverse magnetic fields that provoke faster relaxation times and through barrier shortcuts. Therefore, when designing these bifunctional materials a compromise should be targeted.

Another interesting aspect of studying the luminescent properties is to obtain information about the crystal-field energy splitting of the ground multiplet. Usually, SMMs relax through the first excited state (or higher excited states when a strong axiality is provided to the system) and the energy splitting between the ground and this excited state is often calculated by *ab initio* computational methods. However, the narrow emission "lines" are in reality multiplets that could give us the energy splitting of the M_J sublevels [170–173]. When the excited emitting state of the Ln^{III} ion relaxes, the relaxation occurs to every M_J sublevels giving rise to the mentioned multiplet. Therefore, according to the position of each peak, the energy distribution of the states could be calculated (Fig. 36). Nevertheless, this process is not trivial. The emission multiplets are not composed only by transitions between the lowest emitting M_J and the different M_J in the ground state (these transitions are called zero-phonon bands), hot-bands and vibronic sidebands are usually present within the multiplet complicating its interpretation. Hot-bands correspond to transitions between higher M_J states of the emitting level and the ground M_J sublevels, while vibronic sidebands are a consequence of the electron–phonon coupling. Despite these drawbacks, the "quality" of the spectra could be improved by carrying out the measurements at low temperatures diminishing the contribution of the non-desired bands.

Another emerging and interesting synergy between magnetic and luminescent properties is related to SMM luminescence thermometry. As it has been shown along the entire review, temperature is a pivotal factor in determining the magnetic behavior of the systems. Below certain temperature SMMs are able to store infor-

mation, while above it, the magnetization is lost at zero field and, thus there is not memory effect. Therefore, the control of the temperature within the system is essential, and taking into account that we are talking about the temperature of single molecules, conventional contact thermometers are no longer a valid alternative. An attractive opportunity to substitute these thermometers is to take advantage of the thermal variations that could be seen in the emission spectra of Ln^{III} ions. According to the temperature, the profile of the spectra may notably change and, hence, this thermal dependence of the emission signal can be used as a contactless and precise thermometer [174–178]. Anyway, the key point in combining these two features for a single system lies on the fact that the working temperature related to magnetic memory and thermal dependence of the emission signal should overlap, which would allow to determine the temperature while the system works.

Related to photoluminescence, another emerging field is the one of circularly polarized luminescence (CPL), which could be detected when left/right circularly polarized emitted light is more intense than right/left one. Combining SMM and CPL features is captivating due to the fact that, just like SMMs (see next section), systems showing this chiroptical property are potential candidates for spintronic devices [179] and information storage [180] among other applications [181,182]. CPL is induced by chiral compounds, though the influence of achiral components such as solvent [183] or counterions [184] may play an essential role in the final result [185]. In order to quantify the effect, the luminescence dissymmetry factor g_{lum} is calculated by the following equation (the value ranges between −2 and +2):

$$g_{lum} = \frac{I_L - I_R}{1/2(I_L + I_R)} = \frac{\Delta I}{I} \quad (6)$$

I_L and I_R stand for left and right circularly polarized emission intensity, respectively. Whereas for organic molecules or transition metal based coordination compounds small g_{lum} values ($\leq$0.2) are usually found [186–191], the nature of the f-f transitions in Ln^{III} ions makes them potential candidates for this effect showing g_{lum} values as high as 1.45 [192]. As an example, the results of two chiral $Zn^{II}Dy^{III}$ (**56-Λ** and **56-Δ**) based coordination compounds are shown in Fig. 37, which have been recently reported by Sutter *et al.* [193]. These compounds exhibited slow magnetic relaxation below 12 K while g_{lum} values ranging between 0.04 and 0.18 for **56-Λ** and between −0.04 and −0.16 for **56-Δ** were observed vanishing at 25 K. Since CPL can be induced by magnetic fields (whether applied or intrinsic to the material) and not only by chiral environments [194], the CPL of $Zn^{II}Eu^{III}$ analogues was also studied in order to determine the nature of the optical property. Interestingly, the emission of the two circular polarizations remained exactly the same down to 5 K obtaining g_{lum} values near to zero and confirming that the structure originated CPL in those compounds was very low.

When chirality is introduced within the molecular structure, this may give rise to a non-centrosymmetric crystal structure adopting a space group associated with one of the ten polar point groups: C_1, C_S, C_2, C_{2V}, C_3, C_{3V}, C_4, C_{4V}, C_6 and C_{6V}. These materials are potential candidates to display ferroelectricity [195]. Ferroelectrics are materials that display a spontaneous electric polarization that can be reversed by the application of an electric field. In synergy with magnetic and luminescent properties, materials with all these functionalities are considered very attractive target compounds due to their potential applicability as four-level density data storage or multifunctional sensors [196,197]. However, the many requirements (appropriate ligand fields to enhance anisotropy, good sensitization of the ion for a good emission and concrete crystallization in a space group, among others) that are needed to incorporate all these functionalities leads to a rather scarce group of materials found in the literature [198–201]. Moreover, in terms of potential applications, all the ferroelectric materials are at the same time piezoelectric, pyroelectric and they also exhibit second-harmonic generation (SHG). In contrast to perovskites, molecular materials display a much higher grade of tunability due to the flexibility of the ligands and besides they display lower density. Hence, they are an attractive alternative to them.

As last remarks for this section, SMMs with additional electrical properties have also been studied. For instance, when protic polar solvents such as alcohols or water are used, as well as counterions like sulfate, perchlorate or nitrate, it is possible to obtain hydrogen bonding networks that lie along an axis. In such cases, the materials are potential candidates to show proton conductivity [174,202]. Additionally, the idea of combining single-molecule magnetism with electrical conductivity is also promising. In this sense, a bi-component approach has been usually employed in which the cationic or anionic extended π -structures act as electrical conductors, while the counterions contain paramagnetic ions that provide slow relaxation of the magnetization [203,204].

10. Other potential applications for SMMs

In general, the introduction of this review paper has been focused on implementing SMMs in information storage devices. However, nowadays society needs more effective technologies either for information storage or information processing. For the first approach SMMs are potential candidates due to the fact that a molecule with a diameter in the 1–2 nm range would represent

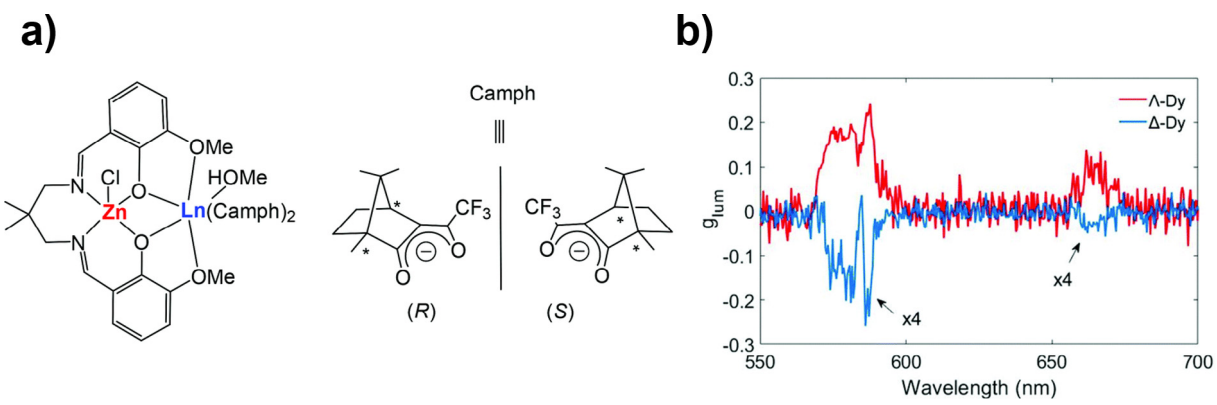

Fig. 37. a) Scheme of the $Zn^{II}Ln^{III}$ based compounds. b) CPL dissymmetry factor g_{lum} as a function of the wavelength for **56-Λ** and **56-Δ** at 5 K. Reproduced with permission from [193]. Copyright 2020 the Partner Organisations.

an information storage density of about ~30 Tbit/cm^2. For comparative purposes, in 2015 Seagate launched a hard drive with a density of 0.21 Tbit/cm^2, which is more than two orders of magnitude below the capacity of SMMs. The second approach related to a faster information processing drives us to quantum computing [205]. The traditional bit can "only" store binary information, while the qubits (quantum bits) can have both values at the same time due to their quantum nature. Since SMMs are within the interphase of classical and quantum nature, they are potential candidates for quantum computing. Shor and Grover showed that quantum computers can surpass the performance of any classical computers in terms of factoring numbers and in searching a database [206,207]. Interestingly, Grover's algorithm was successfully implemented for molecular magnets proving their candidature for this purpose [208].

Moreover, the general necessity of miniaturizing magnetic devices leads to the possibility of studying SMMs for other emerging applications such as molecular spintronics [130,143], electronics [209] or magneto-optics [210]. The physics behind these other applications have been widely studied during the last years and even it is not within the scope of this research work, the interested reader is addressed to the cited literature for more details.

11. Outlook and future perspectives

The global trend of miniaturizing devices, including information storage devices, led to scientists to the discovery of the first SMM, Mn12-ac, a milestone in the area of molecular materials. Along this entire review paper, we have shown that the trends towards synthesizing these materials have completely changed: starting from high spin and high nuclearity metal clusters to highly anisotropic low nuclearity systems. The last cutting-edge discoveries of Dy^{III} metallocenes have somehow showed the way to follow, since one of the biggest handicaps towards incorporating them in future devices has been overcome; surpassing the temperature limit of liquid nitrogen. The unique coordination environment around the Dy^{III} ion constrains unfavorable vibrational modes that provoke QTM, an under-barrier shortcut that eclipsed the outstanding performance of several SMMs in terms of U_{eff}. Definitely, the discovery of these new systems has allowed the scientific community to create new magneto-structural correlations that facilitate novel ligand designs. In this direction, Zheng and co-workers [211] recently reported a research paper in which they improved the performance, in terms of magnetic blocking temperature, of the previously cited compound **21** ([Dy(O^{t}Bu)$_2$(py)$_5$][BPh]$_4$). They rationally selected another alkoxide containing a phenyl group and prepared compound **57** with general formula [Dy(L)$_2$(py)$_5$][BPh$_4$] (HL = (S)-(-)-1-phenylethanol). The aim of including a phenyl substituent was to provoke intra- or intermolecular interactions to stiffen the molecule and suppress QTM. As targeted, the metric parameters (bond distances and angles) for **21** and **57** were found to be comparable. But, additionally, **57** displayed the expected C—H··· π intramolecular interactions between hydrogen atoms belonging to equatorial pyridines and the aromatic rings in the apical chiral ligands (Fig. 38a). Moreover, intermolecular C—H··· π and π ··· π interactions were also observed (Fig. 38b). According to density functional theory (DFT) calculations, the observed interactions must be strong enough to enhance the stiffness of the structure. When measuring the hysteresis loops, they found out that complex **57** showed open hysteresis loops at con-

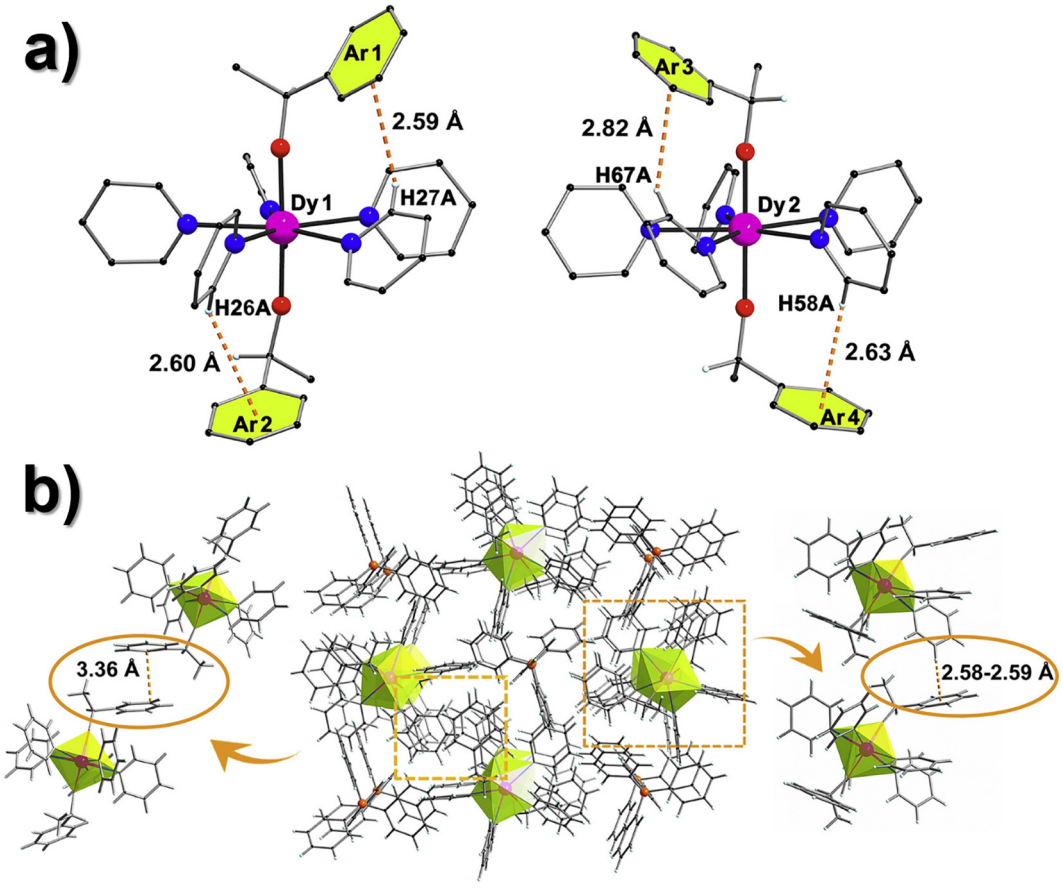

Fig. 38. a) Structural view of compound **57** along with intramolecular C—H··· π interactions. b) Intermolecular π ··· π and C—H··· π interactions. Color code: Dy^{III}, nitrogen, oxygen, carbon and hydrogen in fuchsia, blue, red, black and white, respectively. Reproduced from [211].

siderably higher temperatures compared to **21** and the step at zero field was less pronounced indicative of a quenching of QTM. Considering that the electronic structure calculated by *ab initio* calculations was found to be very similar for both of the compounds, the authors suggested that the alterations in the ligand periphery and modulation of vibrational modes must be the reasons of the observed magnetic properties. This work is also in agreement with a previously reported study in which Liddle and co-authors empirically proved that the molecular flexibility is related to QTM efficiency [212].

However, as discussed, new theoretical basis is of vital importance in order to deeply understand spin-phonon interactions and under-barrier shortcuts that determine the T_B. In fact, even though we are able to evaluate the effect of these interactions in terms of Orbach process, it has been seen that the blocking temperatures are highly influenced by Raman mechanism [213]. Chilton *et al.* made a study selecting some of the reported high performing SMMs (U_{eff} > 600 K) and concluded that there could be a correlation between T_B and the point at which Raman relaxation starts to operate [214]. Note that the T_B values that we mention in this work are referred to the ones obtained by FC/ZFC measurements. This specific relaxation time at which Raman starts to operate was named as τ_{switch}. By plotting $log_{10}(T_B)$ vs $log_{10}(\tau_{switch})$ they found a clear linear correlation. Thus, as mentioned, there might be a strong link between T_B and the relaxation time at the point at which Raman mechanism operates over the Orbach. Hence, the authors emphasize that further studies are of vital importance in order to better understand this mechanism and to be able to improve chemical design principles for improved SMMs.

A last worth mentioning branch related to lanthanides is the field of clusterfullerenes. Very promising research works have been reported encapsulating Ln^{III} ions inside fullerenes [215–217]. These kind of materials show favorable properties such as thermal and chemical stability in contrast to the air sensitivity of the record breaking metallocenes. Moreover, the particularly short Ln-X (X = N^{3-}, S^{2-} or O^{2-}) bonds that can be obtained inside the fullerenes provide strong magnetic anisotropy as well as strong exchange interactions. The interested reader is encouraged to read the cited papers as well as the research progress that has been done implementing these materials into surfaces [218–220] and theoretical calculations [114] that have been carried out for a deeper understanding of these systems.

In general, it seems that the employment of lanthanides is a very promising way to follow. Indeed, they have opened a wide variety of possibilities to combine multiple functionalities in a single system breaking new ground with synergistic applications. However, this does not mean that transition metals are discarded for future devices. In fact, very recently some researchers have successfully combined large magnetic anisotropy along with strong ferromagnetic interactions for high spin ground states in transition metal clusters. Nevertheless, this was done in a novel way, since direct metal–metal orbital overlap was involved opening a new variant in the design of SMMs.

Long and co-workers synthesized the isostructural tetranuclear $M_4(NP^tBu_3)_4{\cdot}n\text{-}C_6H_{14}$ (M^I = Ni^I (**58**) or Cu^I (**59**); ^{t}Bu = *tert*-butyl) compounds [221] following a modified previously reported procedure [222] and by protonolysis of mesitylcopper(I), respectively (Fig. 39, left). Furthermore, the oxidized $[M_4(NP^tBu_3)_4][B(C_6F_5)_4]$ ($M^{I/II}$ = $Ni^{I/II}$ (**60**) or $Cu^{I/II}$ (**61**) were also studied. In **58**, the two coordinate Ni^I ions lie in the same plane displaying almost linear N-Ni-N angles (174.4(6)° in average), which has been shown to be effective in order to enhance magnetic anisotropy. Moreover, the average Ni-Ni distances are of 2.3631(1) Å falling in the range of metal–metal interactions [223]. After one electron oxidation in **60**, the fact that all bond distances decrease precludes identifying a localized oxidized site within the structure confirming the delocalized character of the electrons in the metal–metal bonded cluster (further electrochemical experiments, as well as *dc* magnetic measurements were carried out to confirm this fact).

Easy axis and easy plane types of magnetic anisotropy were calculated for **58** and **60**, respectively with relatively high values of D (D = −1.93 and −1.74 cm^{-1} for **58** calculated from magnetic and EPR measurements, respectively and D = +7.95 and +9.2 cm^{-1} for **60**). However, the easy axis type compound **58** did not displayed any slow magnetic relaxation probably due to a small energy separation between the ground and first excited state. As shown in the literature [224,225], Kramers ions with D > 0 can show SMM behavior under an external magnetic field and thus, **60** was also a potential candidate. At zero field, no out-of-phase signal was detected, but under a small external field of 400 Oe χ''_M peaks were observed in the 1.85–2.05 K temperature range with a calculated U_{eff} of 23.78 K (16.53 cm^{-1}). Furthermore, the fit of the relaxation times suggested that only Orbach mechanism was operative within the examined temperature range in contrast to other reported easy plane SMMs [226]. More interestingly, *ac* measurements carried out in frozen solution of **60** showed slow magnetic relaxation under zero applied *dc* field confirming that dipolar interactions were at least partially responsible of originating zero field QTM. As far as we know, this is the first reported example of a zero field SMM with D > 0. Finally, compound **61** displayed field induced SMM behavior relaxing through Raman and direct processes, since there is no magnetic excited state for a S = 1/2 system. Unequivo-

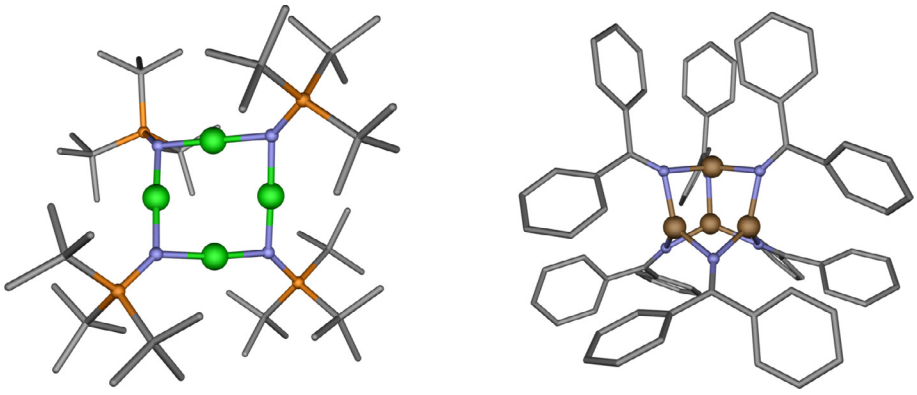

Fig. 39. Perspective view of compounds **58** (left) and a Fe based compound (right). Color code: Ni^I, Fe^I/Fe^{II}, carbon, nitrogen and phosphor in green, brown, grey, blue and orange, respectively. Hydrogen atoms, counterions and solvent molecules have been omitted for the sake of clarity. Generated from the crystal structures in references [221,228].

cally, these new type of clusters with direct metal–metal orbital overlap open a new route for the design of SMMs. In fact, very recently some other systems have been reported for Co^{II} [227] or $Fe^{I/II}$ systems [228], for example (see Fig. 39).

The interest regarding high nuclearity metal clusters remains also intact. For instance, Stamatatos and co-authors recently published a novel mixed valence Mn_{31} structure with the general formula $[Mn_{31}O_{24}(OH)_2(OMe)_{24}(O_2CPh)_{16}(rac\text{-mpm})_2]$ (**62**), where mpmH = α-methyl-2-pyridine-methanol [229]. Within the structure, $\{Mn^{II}_2Mn^{III}_{28}Mn^{IV}\}$ ions were found, where most of the Mn^{III} ions displayed Jahn-Teller axes parallel to each other indicative of a possible $D \neq 0$. Consequently, slow magnetic relaxation was observed for **62** with a calculated U_{eff} of 58 K and hysteresis loops below 5 K. This value of the effective energy barrier is large when talking about 3d based SMMs [230,231]. But more interestingly, although **62** is comparable in size to other magnetic nanoparticles, below 0.5 K displays quantum phenomena. Therefore, these kind of compounds could be very interesting to investigate the limit between SMMs and magnetic nanoparticles.

Even though their impact or future perspectives are not potentially so promising, field induced SMMs based on isotropic metal ions also have their own place in this field. More specifically, complexes containing almost isotropic Mn^{II} [232], Fe^{III} [233] or Gd^{III} [234–238] ions have been reported showing slow magnetic relaxation under the presence of an external magnetic field. Moreover, the use of actinides is also being studied [239,240]. They show stronger spin–orbit coupling and, in consequence, they may show enhanced magnetic anisotropy. Within the series, particularly U^{III} based compounds have been reported [241–243], though uranium compounds in other oxidation states or SMMs with other actinides such as Np have also been studied [244].

All in all, the field of SMMs can be considered as a young field barely reaching three decades of life since the discovery of Mn12-ac. In all these years synthetic and computational chemists, as well as physicists, have coexisted combining new synthetic strategies and theoretical knowledge, fundamental to understand quantum physics determining the slow relaxation of the magnetization. Thus, we would like to remark the importance of combining these two fields. Synthetic chemists have shown the ability to design and synthesize compounds almost *à la carte*, but theoretical chemists and physicists have a pivotal role in explaining the quantum phenomena behind SMMs.

CRediT authorship contribution statement

Andoni Zabala-Lekuona: Conceptualization, Investigation, Writing - original draft, Visualization. **José Manuel Seco:** Writing - review & editing, Funding acquisition. **Enrique Colacio:** Investigation, Writing - review & editing, Supervision, Funding acquisition.

Declaration of Competing Interest

The authors declare that they have no known competing financial interests or personal relationships that could have appeared to influence the work reported in this paper.

Acknowledgments

This work was supported by the Spanish Ministerio de Innovación, Ciencia y Universidades (PGC2018 102052-B-C21) and by the University of the Basque Country (GIU 17/13). E.C. is gratefully acknowledged to the Junta de Andalucía (FQM-195 and the Project financed by FEDER funds A-FQM-172-UGR18). A.Z.-L. is grateful for his predoctoral fellowship from GV/EJ.

References

[1] R. Sessoli, D. Gatteschi, A. Caneschi, M.A. Novak, Magnetic bistability in a metal-ion cluster, Nature 365 (1993) 141–143, https://doi.org/10.1038/365141a0.
[2] A. Zabala-Lekuona, Iman Molekularrak: informazio unitate txikienaren bila, Ekaia 35 (2019) 85–99, https://doi.org/10.1387/ekaia.19692.
[3] A. Abragam, B. Bleaney, in: Electron Paramagnetic Resonance of Transition Ions, Clarendon Press, Oxford, UK, 1970, p. 925.
[4] J.H. Van Vleck, Paramagnetic relaxation times for titanium and chrome alum, Phys. Rev. 57 (1940) 426–447, https://doi.org/10.1103/PhysRev.57.426.
[5] H.B.G. Casimir, D. Bijl, F.K. Du Pré, Measurememts on paramagnetic relaxation in chromium potassium alum, Physica. 8 (1941) 449–460, https://doi.org/10.1016/S0031-8914(41)90066-6.
[6] K.S. Cole, R.H. Cole, Dispersion and absorption in dielectrics I. Alternating current characteristics, J. Chem. Phys. 9 (1941) 341–351, https://doi.org/10.1063/1.1750906.
[7] I.F. Díaz-Ortega, J.M. Herrera, D. Aravena, E. Ruiz, T. Gupta, G. Rajaraman, H. Nojiri, E. Colacio, Designing a Dy_2 single-molecule magnet with two well-differentiated relaxation processes by using a nonsymmetric bis-bidentate bipyrimidine-N-oxide Ligand: a comparison with mononuclear counterparts, Inorg. Chem. 57 (2018) 6362–6375, https://doi.org/10.1021/acs.inorgchem.8b00427.
[8] L. Zhang, J. Jung, P. Zhang, M. Guo, L. Zhao, J. Tang, B. Le Guennic, Site-resolved two-step relaxation process in an asymmetric Dy_2 single-molecule magnet, Chem. - A Eur. J. 22 (2016) 1392–1398, https://doi.org/10.1002/chem.201503422.
[9] E. Echenique-Errandonea, A. Zabala-Lekuona, J. Cepeda, A. Rodríguez-Diéguez, J.M. Seco, I. Oyarzabal, E. Colacio, Effect of the change of the ancillary carboxylate bridging ligand on the SMM and luminescence properties of a series of carboxylate-diphenoxido triply bridged dinuclear ZnLn and tetranuclear Zn_2Ln_2 complexes (Ln = Dy, Er), Dalton Trans. 48 (2019) 190–201, https://doi.org/10.1039/c8dt03800g.
[10] C. Shi, R. Nie, X. Yao, S. Fan, G. An, Y. Dong, G. Li, Asymmetry-unit-dominated double slow-relaxation modes of 2,6-dimethyl-3,5-heptanedione dysprosium SMMs, RSC Adv. 7 (2017) 49701–49709, https://doi.org/10.1039/c7ra09711e.
[11] J. Ruiz, A.J. Mota, A. Rodríguez-Diéguez, S. Titos, J.M. Herrera, E. Ruiz, E. Cremades, J.P. Costes, E. Colacio, Field and dilution effects on the slow relaxation of a luminescent DyO9 low-symmetry single-ion magnet, Chem. Commun. 48 (2012) 7916–7918, https://doi.org/10.1039/c2cc32518g.
[12] B. Liu, B. Wang, Z. Wang, S. Gao, Static field induced magnetic relaxations in dinuclear lanthanide compounds of $[phen_2Ln_2(HCOO)_4(HCOO)_{2-2x}(NO_3)_{2x}]$ (1, Ln = Gd and x = 0.52; 2, Ln = Er and x = 0.90; Phen = 1,10-phenanthroline), Sci. China Chem. 55 (2012) 926–933, https://doi.org/10.1007/s11426-012-4599-5.
[13] A. Arauzo, A. Lazarescu, S. Shova, E. Bartolomé, R. Cases, J. Luzón, J. Bartolomé, C. Turta, Structural and magnetic properties of some lanthanide (Ln = Eu(III), Gd(iii) and Nd(iii)) cyanoacetate polymers: Field-induced slow magnetic relaxation in the Gd and Nd substitutions, Dalton Trans. 43 (2014) 12342–12356, https://doi.org/10.1039/c4dt01104j.
[14] D. Reta, N.F. Chilton, Uncertainty estimates for magnetic relaxation times and magnetic relaxation parameters, Phys. Chem. Chem. Phys. 21 (2019) 23567–23575, https://doi.org/10.1039/c9cp04301b.
[15] O. Kahn, Molecular Magnetism, VCH, Weinheim, Germany, 1993.
[16] T. Glaser, H. Theil, I. Liratzis, T. Weyhermüller, E. Bill, Ferromagnetic coupling by orthogonal magnetic orbitals in a heterodinuclear $Cu^{II}V^{IV}$=O complex and in a homodinuclear CuSalts of the two-coordinate homoleptic manganese$^{II}Cu^{II}$ complex, Inorg. Chem. 45 (2006) 4889–4891, https://doi.org/10.1021/ic0606328.
[17] T. Glaser, M. Gerenkamp, R. Fröhlich, Targeted Synthesis of Ferromagnetically Coupled Complexes with Modified 1,3,5-Trihydroxybenzene Ligands, Angew. Chem. Int. Ed. 41 (2002) 3823–3825, https://doi.org/10.1002/1521-3773(20021018)41:20<3823::AID-ANIE3823>3.0.CO;2-I.
[18] T. Glaser, T. Beissel, E. Bill, T. Weyhermüller, V. Schünemann, W. Meyer-Klaucke, A.X. Trautwein, K. Wieghardt, Electronic structure of linear thiophenolate-bridged heterotrinuclear complexes $[LFeMFeL]^{n+}$ (M = Cr Co, Fe; n = 1–3): Localized vs delocalized models, J. Am. Chem. Soc. 121 (1999) 2193–2208, https://doi.org/10.1021/ja982898m.
[19] C. Beghidja, G. Rogez, J. Kortus, M. Wesolek, R. Welter, Very strong ferromagnetic interaction in a new binuclear μ-methoxo-bridged Mn(III) complex: Synthesis, crystal structure, magnetic properties, and DFT calculations, J. Am. Chem. Soc. 128 (2006) 3140–3141, https://doi.org/10.1021/ja0575023.
[20] A. Ferguson, J. Lawrence, A. Parkin, J. Sanchez-Benitez, K.V. Kamenev, E.K. Brechin, W. Wernsdorfer, S. Hill, M. Murrie, Synthesis and characterisation of a Ni_4 single-molecule magnet with S_4 symmetry, J. Chem. Soc. Dalt. Trans. (2008) 6409–6414, https://doi.org/10.1039/b807447j.
[21] G.S. Papaefstathiou, A. Escuer, C.P. Raptopoulou, A. Terzis, S.P. Perlepes, R. Vicente, Defective double-cubane, tetranuclear manganese(II) and cobalt(II) complexes with simultaneous μ1,1-azido and μ-O bridges, Eur. J. Inorg.

Chem. 2001 (2001) 1567–1574, https://doi.org/10.1002/1099-0682(200106)2001:6<1567::aid-ejic1567>3.0.co;2-7.
[22] G.S. Papaefstathiou, A. Escuer, R. Vicente, M. Font-Bardia, X. Solans, S.P. Perlepes, Reactivity in polynuclear transition metal chemistry as a means to obtain high-spin molecules: substitution of μ_4-OH^- by η^1, μ_4-N_3^- increases nine times the ground-state S value of a nonanuclear nickel(II) cage, Chem. Commun. 1 (2001) 2414–2415, https://doi.org/10.1039/b106472j.
[23] D.M. Low, L.F. Jones, A. Bell, E.K. Brechin, T. Mallah, E. Rivière, S.J. Teat, E.J.L. McInnes, Solvothermal synthesis of a tetradecametallic Fe^{III} cluster, Angew. Chem. Int. Ed. 42 (2003) 3781–3784, https://doi.org/10.1002/anie.200351865.
[24] J. Larionova, M. Gross, M. Pilkington, H. Andres, H. Stoeckli-Evans, H.U. Güdel, S. Decurtins, High-spin molecules: a novel cyano-bridged $Mn_9^{II}Mo_6^V$ molecular cluster with a S = 51/2 ground state and ferromagnetic intercluster ordering at low temperatures, Angew. Chem. Int. Ed. 39 (2000) 1605–1609, https://doi.org/10.1002/(SICI)1521-3773(20000502)39:9<1605::AID-ANIE1605>3.0.CO;2-5.
[25] M. Affronte, J.C. Lasjaunias, W. Wernsdorfer, R. Sessoli, D. Gatteschi, S.L. Heath, A. Fort, A. Rettori, Magnetic ordering in a high-spin Fe_{19} molecular nanomagnet, Phys. Rev. B. 66 (2002) 644081–644087, https://doi.org/10.1103/PhysRevB.66.064408.
[26] A.M. Ako, I.J. Hewitt, V. Mereacre, R. Clérac, W. Wernsdorfer, C.E. Anson, A.K. Powell, A ferromagnetically coupled Mn_{19} aggregate with a record S = 83/2 ground spin state, Angew. Chem. Int. Ed. 45 (2006) 4926–4929, https://doi.org/10.1002/anie.200601467.
[27] M. Murugesu, M. Habrych, W. Wernsdorfer, K.A. Abboud, G. Christou, Single-Molecule Magnets: A Mn_{25} Complex with a Record S = 51/2 Spin for a Molecular Species, J. Am. Chem. Soc. 126 (2004) 4766–4767, https://doi.org/10.1021/ja0316824.
[28] J. Cirera, E. Ruiz, S. Alvarez, F. Neese, J. Kortus, How to build molecules with large magnetic anisotropy, Chem. - A Eur. J. 15 (2009) 4078–4087, https://doi.org/10.1002/chem.200801608.
[29] A. Sieber, R. Bircher, O. Waldmann, G. Carver, G. Chaboussant, H. Mutka, H.-U. Güdel, Effect of pressure on the magnetic anisotropy in the single-molecule magnet Mn12-acetate: an inelastic neutron scattering study, Angew. Chem. Int. Ed. 44 (2005) 4239–4242, https://doi.org/10.1002/anie.200500171.
[30] F. Neese, D.A. Pantazis, What is not required to make a single molecule magnet, Faraday Discuss 148 (2011) 229–238, https://doi.org/10.1039/c005256f.
[31] P.P. Power, Stable two-coordinate, open-shell (d^1-d^9) transition metal complexes, Chem. Rev. 112 (2012) 3482–3507, https://doi.org/10.1021/cr2004647.
[32] R. Ruamps, L.J. Batchelor, R. Maurice, N. Gogoi, P. Jiménez-Lozano, N. Guihéry, C. Degraaf, A.L. Barra, J.P. Sutter, T. Mallah, Origin of the magnetic anisotropy in heptacoordinate Ni^{II} and Co^{II} complexes, Chem. - A Eur. J. 19 (2013) 950–956, https://doi.org/10.1002/chem.201202492.
[33] Y. Rechkemmer, F.D. Breitgoff, M. Van Der Meer, M. Atanasov, M. Hakl, M. Orlita, P. Neugebauer, F. Neese, B. Sarkar, J. Van Slageren, A four-coordinate cobalt(II) single-ion magnet with coercivity and a very high energy barrier, Nat. Commun. 7 (2016) 10467, https://doi.org/10.1038/ncomms10467.
[34] J.M. Frost, K.L.M. Harriman, M. Murugesu, The rise of 3-d single-ion magnets in molecular magnetism: towards materials from molecules?, Chem Sci. 7 (2016) 2470–2491, https://doi.org/10.1039/c5sc03224e.
[35] S. Gómez-Coca, D. Aravena, R. Morales, E. Ruiz, Large magnetic anisotropy in mononuclear metal complexes, Coord. Chem. Rev. 289–290 (2015) 379–392, https://doi.org/10.1016/j.ccr.2015.01.021.
[36] M. Feng, M.L. Tong, Single ion magnets from 3d to 5f: developments and strategies, Chem. - A Eur. J. 24 (2018) 7574–7594, https://doi.org/10.1002/chem.201705761.
[37] S. Tripathi, A. Dey, M. Shanmugam, R.S. Narayanan, V. Chandrasekhar, Cobalt (II) complexes as single-ion magnets, in: Top. Organomet. Chem., Springer, 2019, pp. 35–75, https://doi.org/10.1007/3418_2018_8.
[38] G.A. Craig, M. Murrie, 3d single-ion magnets, Chem. Soc. Rev. 44 (2015) 2135–2147, https://doi.org/10.1039/c4cs00439f.
[39] W.M. Reiff, A.M. LaPointe, E.H. Witten, Virtual free ion magnetism and the absence of Jahn-Teller distortion in a linear two-coordinate complex of high-spin iron(II), J. Am. Chem. Soc. 126 (2004) 10206–10207, https://doi.org/10.1021/jă32w.
[40] W.M. Reiff, C.E. Schulz, M.H. Whangbo, J.I. Seo, Y.S. Lee, G.R. Potratz, C.W. Spicer, G.S. Girolami, Consequences of a linear two-coordinate geometry for the orbital magnetism and Jahn-Teller distortion behavior of the high spin iron(II) complex $Fe[N(t\text{-}Bu)_2]_2$, J. Am. Chem. Soc. 131 (2009) 404–405, https://doi.org/10.1021/ja806660f.
[41] W.A. Merrill, T.A. Stich, M. Brynda, G.J. Yeagle, J.C. Fettinger, R. De Hont, W.M. Reiff, C.E. Schulz, R.D. Britt, P.P. Power, Direct spectroscopic observation of large quenching of first-order orbital angular momentum with bending in monomeric, two-coordinate Fe(II) primary amido complexes and the profound magnetic effects of the absence of Jahnand- and Renner-Teller distortions in rigorously linear coordination, J. Am. Chem. Soc. 131 (2009) 12693–12702, https://doi.org/10.1021/ja903439t.
[42] J.M. Zadrozny, M. Atanasov, A.M. Bryan, C.Y. Lin, B.D. Rekken, P.P. Power, F. Neese, J.R. Long, Slow magnetization dynamics in a series of two-coordinate iron(II) complexes, Chem. Sci. 4 (2013) 125–138, https://doi.org/10.1039/c2sc20801f.
[43] M. Atanasov, J.M. Zadrozny, J.R. Long, F. Neese, A theoretical analysis of chemical bonding, vibronic coupling, and magnetic anisotropy in linear iron(II) complexes with single-molecule magnet behavior, Chem. Sci. 4 (2013) 139–156, https://doi.org/10.1039/c2sc21394j.
[44] J.M. Zadrozny, D.J. Xiao, M. Atanasov, G.J. Long, F. Grandjean, F. Neese, J.R. Long, Magnetic blocking in a linear iron(I) complex, Nat. Chem. 5 (2013) 577–581, https://doi.org/10.1038/nchem.1630.
[45] M. Dey, N. Gogoi, Geometry-mediated enhancement of single-ion anisotropy: a route to single-molecule magnets with a high blocking temperature, Angew. Chem. Int. Ed. 52 (2013) 12780–12782, https://doi.org/10.1002/anie.201304982.
[46] Y.S. Meng, Z. Mo, B.W. Wang, Y.Q. Zhang, L. Deng, S. Gao, Observation of the single-ion magnet behavior of d8 ions on two-coordinate Co(I)-NHC complexes, Chem. Sci. 6 (2015) 7156–7162, https://doi.org/10.1039/c5sc02611c.
[47] X.N. Yao, J.Z. Du, Y.Q. Zhang, X.B. Leng, M.W. Yang, S. Da Jiang, Z.X. Wang, Z.W. Ouyang, L. Deng, B.W. Wang, S. Gao, Two-coordinate Co(II) imido complexes as outstanding single-molecule magnets, J. Am. Chem. Soc. 139 (2017) 373–380, https://doi.org/10.1021/jacs.6b11043.
[48] J. Du, L. Wang, M. Xie, L. Deng, A Two-coordinate Cobalt(II) Imido complex with NHC ligation: synthesis, structure, and reactivity, Angew. Chem. Int. Ed. 54 (2015) 12640–12644, https://doi.org/10.1002/anie.201505937.
[49] P.C. Bunting, M. Atanasov, E. Damgaard-Møller, M. Perfetti, I. Crassee, M. Orlita, J. Overgaard, J. Van Slageren, F. Neese, J.R. Long, A linear cobalt(II) complex with maximal orbital angular momentum from a non-Aufbau ground state, Science 362 (2018) 3719, https://doi.org/10.1126/science.aat7319.
[50] M. Atanasov, D. Aravena, E. Suturina, E. Bill, D. Maganas, F. Neese, First principles approach to the electronic structure, magnetic anisotropy and spin relaxation in mononuclear 3d-transition metal single molecule magnets, Coord. Chem. Rev. 289–290 (2015) 177–214, https://doi.org/10.1016/j.ccr.2014.10.015.
[51] T. Viefhaus, W. Schwarz, K. Hübler, K. Locke, J. Weidlein, Das unterschiedliche Reaktionsverhalten von basefreiem Tris(trimethylsilyl)methyl-Lithium gegenüber den Trihalogeniden der Erdmetalle und des Eisens, Zeitschrift Fur Anorg. Und Allg. Chemie. 627 (2001) 715–725, https://doi.org/10.1002/1521-3749(200104)627:4<715::aid-zaac715>3.0.co;2-0.
[52] N.H. Buttrus, C. Eaborn, P.B. Hitchcock, J.D. Smith, A.C. Sullivan, Preparation and crystal structure of a two-co-ordinate manganese compound, bis[tris(trimethyl)silylmethyl]manganese, J. Chem. Soc., Chem. Commun. (1985) 1380–1381, https://doi.org/10.1039/c39850001380.
[53] C.Y. Lin, J.C. Fettinger, N.F. Chilton, A. Formanuik, F. Grandjean, G.J. Long, P.P. Power, Salts of the two-coordinate homoleptic manganese(I) dialkyl anion $[Mn\{C(SiMe_3)_3\}_2]^-$ with quenched orbital magnetism, Chem. Commun. 51 (2015) 13275–13278, https://doi.org/10.1039/c5cc05166e.
[54] P.E. Kazin, M.A. Zykin, L.A. Trusov, A.A. Eliseev, O.V. Magdysyuk, R.E. Dinnebier, R.K. Kremer, C. Felser, M. Jansen, A Co-based single-molecule magnet confined in a barium phosphate apatite matrix with a high energy barrier for magnetization relaxation, Chem. Commun. 53 (2017) 5416–5419, https://doi.org/10.1039/c7cc02453c.
[55] I.G. Rau, S. Baumann, S. Rusponi, F. Donati, S. Stepanow, L. Gragnaniello, J. Dreiser, C. Piamonteze, F. Nolting, S. Gangopadhyay, O.R. Albertini, R.M. Macfarlane, C.P. Lutz, B.A. Jones, P. Gambardella, A.J. Heinrich, H. Brune, Reaching the magnetic anisotropy limit of a 3d metal atom, Science 344 (2014) 988–992, https://doi.org/10.1126/science.1252841.
[56] N. Ishikawa, M. Sugita, T. Ishikawa, S.Y. Koshihara, Y. Kaizu, Lanthanide double-decker complexes functioning as magnets at the single-molecular level, J. Am. Chem. Soc. 125 (2003) 8694–8695, https://doi.org/10.1021/ja029629n.
[57] N. Koike, H. Uekusa, Y. Ohashi, C. Harnoode, F. Kitamura, T. Ohsaka, K. Tokuda, Relationship between the Skew Angle and Interplanar Distance in Four Bis(phthalocyaninato)lanthanide(III) Tetrabutylammonium Salts $([NBu_4^n][Ln^{III}Pc_2]$; Ln = Nd, Gd, Ho, Lu), Inorg. Chem. 35 (1996) 5798–5804, https://doi.org/10.1021/ic960158d.
[58] J. Rinehart, J. Long, Exploiting single-ion anisotropy in the design of f-element single-molecule magnets, Chem. Sci. 2 (2011) 2078–2085, https://doi.org/10.1039/c1sc00513h.
[59] F. Habib, G. Brunet, V. Vieru, I. Korobkov, L.F. Chibotaru, M. Murugesu, Significant enhancement of energy barriers in dinuclear dysprosium single-molecule magnets through electron-withdrawing effects, J. Am. Chem. Soc. 135 (2013) 13242–13245, https://doi.org/10.1021/ja404846s.
[60] J. Long, F. Habib, P.H. Lin, I. Korobkov, G. Enright, L. Ungur, W. Wernsdorfer, L. F. Chibotaru, M. Murugesu, Single-molecule magnet behavior for an antiferromagnetically superexchange-coupled dinuclear dysprosium(III) complex, J. Am. Chem. Soc. 133 (2011) 5319–5328, https://doi.org/10.1021/ja109706y.
[61] F. Habib, P.H. Lin, J. Long, I. Korobkov, W. Wernsdorfer, M. Murugesu, The use of magnetic dilution to elucidate the slow magnetic relaxation effects of a Dy2 single-molecule magnet, J. Am. Chem. Soc. 133 (2011) 8830–8833, https://doi.org/10.1021/ja2017009.
[62] P. Zhang, L. Zhang, C. Wang, S. Xue, S.Y. Lin, J. Tang, Equatorially coordinated lanthanide single ion magnets, J. Am. Chem. Soc. 136 (2014) 4484–4487, https://doi.org/10.1021/ja500793x.
[63] I. Oyarzabal, J. Ruiz, J.M. Seco, M. Evangelisti, A. Camón, E. Ruiz, D. Aravena, E. Colacio, Rational electrostatic design of easy-axis magnetic anisotropy in a Zn^{II}-Dy^{III}-Zn^{II} single-molecule magnet with a high energy barrier, Chem. - A Eur. J. 20 (2014) 14262–14269, https://doi.org/10.1002/chem.201403670.

[64] L. Ungur, M. Thewissen, J.P. Costes, W. Wernsdorfer, L.F. Chibotaru, Interplay of strongly anisotropic metal ions in magnetic blocking of complexes, Inorg. Chem. 52 (2013) 6328–6337, https://doi.org/10.1021/ic302568x.
[65] A. Upadhyay, S.K. Singh, C. Das, R. Mondol, S.K. Langley, K.S. Murray, G. Rajaraman, M. Shanmugam, Enhancing the effective energy barrier of a Dy(III) SMM using a bridged diamagnetic Zn(II) ion, Chem. Commun. 50 (2014) 8838–8841, https://doi.org/10.1039/c4cc02094d.
[66] M. Llunell, D. Casanova, J. Cirera, J.M. Bofill, P. Alemany, S. Alvarez, M. Pinsky, D. Avnir, SHAPE, (2005).
[67] Y.S. Ding, N.F. Chilton, R.E.P. Winpenny, Y.Z. Zheng, On approaching the limit of molecular magnetic anisotropy: a near-perfect pentagonal bipyramidal dysprosium(III) single-molecule magnet, Angew. Chem. Int. Ed. 55 (2016) 16071–16074, https://doi.org/10.1002/anie.201609685.
[68] J. Liu, Y.C. Chen, J.L. Liu, V. Vieru, L. Ungur, J.H. Jia, L.F. Chibotaru, Y. Lan, W. Wernsdorfer, S. Gao, X.M. Chen, M.L. Tong, A Stable pentagonal bipyramidal Dy(III) single-ion magnet with a record magnetization reversal barrier over 1000 K, J. Am. Chem. Soc. 138 (2016) 5441–5450, https://doi.org/10.1021/jacs.6b02638.
[69] Y.C. Chen, J.L. Liu, L. Ungur, J. Liu, Q.W. Li, L.F. Wang, Z.P. Ni, L.F. Chibotaru, X. M. Chen, M.L. Tong, Symmetry-supported magnetic blocking at 20 K in pentagonal bipyramidal Dy(III) single-ion magnets, J. Am. Chem. Soc. 138 (2016) 2829–2837, https://doi.org/10.1021/jacs.5b13584.
[70] S.K. Gupta, T. Rajeshkumar, G. Rajaraman, R. Murugavel, An air-stable Dy(III) single-ion magnet with high anisotropy barrier and blocking temperature, Chem. Sci. 7 (2016) 5181–5191, https://doi.org/10.1039/c6sc00279j.
[71] Z. Jiang, L. Sun, Q. Yang, B. Yin, H. Ke, J. Han, Q. Wei, G. Xie, S. Chen, Excess axial electrostatic repulsion as a criterion for pentagonal bipyramidal Dy^{III} single-ion magnets with high: U eff and T B, J. Mater. Chem. C 6 (2018) 4273–4280, https://doi.org/10.1039/c8tc00353j.
[72] A.B. Canaj, S. Dey, C. Wilson, O. Céspedes, G. Rajaraman, M. Murrie, Engineering macrocyclic high performance pentagonal bipyramidal Dy(III) single-ion magnets, Chem. Commun. 56 (2020) 12037–12040, https://doi.org/10.1039/d0cc04559d.
[73] L. Norel, L.E. Darago, B. Le Guennic, K. Chakarawet, M.I. Gonzalez, J.H. Olshansky, S. Rigaut, J.R. Long, A terminal fluoride ligand generates axial magnetic anisotropy in dysprosium complexes, Angew. Chem. Int. Ed. 57 (2018) 1933–1938, https://doi.org/10.1002/anie.201712139.
[74] J. Liu, Y. Chen, Y. Zheng, W. Lin, L. Ungur, W. Wernsdorfer, L. Chibotaru, M. Tong, Switching the anisotropy barrier of a single-ion magnet by symmetry change from quasi-D5h to quasi-Oh, Chem. Sci. 4 (2013) 3310, https://doi.org/10.1039/c3sc50843a.
[75] J.L. Liu, Y.C. Chen, M.L. Tong, Symmetry strategies for high performance lanthanide-based single-molecule magnets, Chem. Soc. Rev. 47 (2018) 2431–2453, https://doi.org/10.1039/c7cs00266a.
[76] E. Colacio, J. Ruiz-Sanchez, F.J. White, E.K. Brechin, Strategy for the rational design of asymmetric triply bridged dinuclear 3d–4f single-molecule magnets, Inorg. Chem. 50 (2011) 7268–7273, https://doi.org/10.1021/ic2008599.
[77] S. Titos-Padilla, J. Ruiz, J.M. Herrera, E.K. Brechin, W. Wersndorfer, F. Lloret, E. Colacio, Dilution-triggered SMM behavior under zero field in a luminescent Zn_2Dy_2 tetranuclear complex incorporating carbonato-bridging ligands derived from atmospheric CO_2 fixation, Inorg. Chem. 52 (2013) 9620–9626, https://doi.org/10.1021/ic401378k.
[78] T. Han, M.J. Giansiracusa, Z. Li, Y. Ding, N.F. Chilton, R.E.P. Winpenny, Y. Zheng, Exchange-biasing in a Dinuclear Dysprosium(III) single-molecule magnet with a large energy barrier for magnetisation reversal, Chem. – A Eur. J. 26 (2020) 6773–6777, https://doi.org/10.1002/chem.202000719.
[79] R.J. Blagg, L. Ungur, F. Tuna, J. Speak, P. Comar, D. Collison, W. Wernsdorfer, E. J.L. McInnes, L.F. Chibotaru, R.E.P. Winpenny, Magnetic relaxation pathways in lanthanide single-molecule magnets, Nat. Chem. 5 (2013) 673–678, https://doi.org/10.1038/nchem.1707.
[80] K.R. Meihaus, J.D. Rinehart, J.R. Long, Dilution-induced slow magnetic relaxation and anomalous hysteresis in trigonal prismatic dysprosium(III) and Uranium(III) complexes, Inorg. Chem. 50 (2011) 8484–8489, https://doi.org/10.1021/ic201078r.
[81] F. Pointillart, K. Bernot, S. Golhen, B. Le Guennic, T. Guizouarn, L. Ouahab, O. Cador, Magnetic memory in an isotopically enriched and magnetically isolated mononuclear dysprosium complex, Angew. Chem. Int. Ed. 54 (2015) 1504–1507, https://doi.org/10.1002/anie.201409887.
[82] Y.S. Ding, K.X. Yu, D. Reta, F. Ortu, R.E.P. Winpenny, Y.Z. Zheng, N.F. Chilton, Field- and temperature-dependent quantum tunnelling of the magnetisation in a large barrier single-molecule magnet, Nat. Commun. 9 (2018) 3134, https://doi.org/10.1038/s41467-018-05587-6.
[83] S.K. Langley, D.P. Wielechowski, V. Vieru, N.F. Chilton, B. Moubaraki, B.F. Abrahams, L.F. Chibotaru, K.S. Murray, A $Cr^{III}_2Dy^{III}_2$ single-molecule magnet: enhancing the blocking temperature through 3d magnetic exchange, Angew. Chem. Int. Ed. 52 (2013) 12014–12019, https://doi.org/10.1002/anie.201306329.
[84] K.R. Vignesh, S.K. Langley, K.S. Murray, G. Rajaraman, Quenching the quantum tunneling of magnetization in heterometallic octanuclear TM^{III}_4 DyI^{II}_4 (TM=Co and Cr) single-molecule magnets by modification of the bridging ligands and enhancing the magnetic exchange coupling, Chem. - A Eur. J. 23 (2017) 1654–1666, https://doi.org/10.1002/chem.201604835.
[85] S.K. Langley, C.M. Forsyth, B. Moubaraki, K.S. Murray, A fluoride bridged $Cr^{III}_4Dy^{III}_4$ single molecule magnet, Dalton Trans. 44 (2014) 912–915, https://doi.org/10.1039/c4dt03100h.
[86] J. Rinck, G. Novitchi, W. Van Den Heuvel, L. Ungur, Y. Lan, W. Wernsdorfer, C. E. Anson, L.F. Chibotaru, A.K. Powell, An octanuclear $[Cr^{III}_4Dy^{III}_4]$ 3d–4f single-molecule magnet, Angew. Chem. Int. Ed. 49 (2010) 7583–7587, https://doi.org/10.1002/anie.201002690.
[87] X.L. Li, F.Y. Min, C. Wang, S.Y. Lin, Z. Liu, J. Tang, Utilizing 3d–4f magnetic interaction to slow the magnetic relaxation of heterometallic complexes, Inorg. Chem. 54 (2015) 4337–4344, https://doi.org/10.1021/acs.inorgchem.5b00019.
[88] J.L. Liu, J.Y. Wu, Y.C. Chen, V. Mereacre, A.K. Powell, L. Ungur, L.F. Chibotaru, X. M. Chen, M.L. Tong, A heterometallic Fe^{II}-Dy^{III} single-molecule magnet with a record anisotropy barrier, Angew. Chem. Int. Ed. 53 (2014) 12966–12970, https://doi.org/10.1002/anie.201407799.
[89] M. Hołyńska, D. Premužić, I.R. Jeon, W. Wernsdorfer, R. Clérac, S. Dehnen, $[Mn^{III}_6O_3Ln_2]$ single-molecule magnets: increasing the energy barrier above 100 K, Chem. - A Eur. J. 17 (2011) 9605–9610, https://doi.org/10.1002/chem.201101807.
[90] K.C. Mondal, A. Sundt, Y. Lan, G.E. Kostakis, O. Waldmann, L. Ungur, L.F. Chibotaru, C.E. Anson, A.K. Powell, Coexistence of distinct single-ion and exchange-based mechanisms for blocking of magnetization in a $Co^{II}_2Dy^{III}_2$ single-molecule magnet, Angew. Chem. Int. Ed. 51 (2012) 7550–7554, https://doi.org/10.1002/anie.201201478.
[91] S.K. Singh, M.F. Beg, G. Rajaraman, Role of magnetic exchange interactions in the magnetization relaxation of 3d–4f single-molecule magnets: a theoretical perspective, Chem. - A Eur. J. 22 (2016) 672–680, https://doi.org/10.1002/chem.201503102.
[92] C.G. Efthymiou, T.C. Stamatatos, C. Papatriantafyllopoulou, A.J. Tasiopoulos, W. Wernsdorfer, S.P. Perlepes, G. Christou, Nickel/lanthanide single-molecule magnets: Ni_3Ln "stars" with a ligand derived from the metal-promoted reduction of di-2-pyridyl ketone under solvothermal conditions, Inorg. Chem. 49 (2010) 9737–9739, https://doi.org/10.1021/ic101504c.
[93] T. Gupta, M.F. Beg, G. Rajaraman, Role of single-ion anisotropy and magnetic exchange interactions in suppressing zero-field tunnelling in 3d–4f single molecule magnets, Inorg. Chem. 55 (2016) 11201–11215, https://doi.org/10.1021/acs.inorgchem.6b01831.
[94] J.D. Rinehart, M. Fang, W.J. Evans, J.R. Long, Strong exchange and magnetic blocking in N_2^{3-}-radical-bridged lanthanide complexes, Nat. Chem. 3 (2011) 538–542, https://doi.org/10.1038/nchem.1063.
[95] C. Benelli, D. Gatteschi, Magnetism of lanthanides in molecular materials with transition-metal ions and organic radicals, Chem. Rev. 102 (2002) 2369–2387, https://doi.org/10.1021/cr010303r.
[96] Y.N. Guo, G.F. Xu, P. Gamez, L. Zhao, S.Y. Lin, R. Deng, J. Tang, H.J. Zhang, Two-step relaxation in a linear tetranuclear dysprosium(III) aggregate showing single-molecule magnet behavior, J. Am. Chem. Soc. 132 (2010) 8538–8539, https://doi.org/10.1021/ja103018m.
[97] J.D. Rinehart, M. Fang, W.J. Evans, J.R. Long, A N_2^{3-} radical-bridged terbium complex exhibiting magnetic hysteresis at 14 K, J. Am. Chem. Soc. 133 (2011) 14236–14239, https://doi.org/10.1021/ja206286h.
[98] S. Demir, M.I. Gonzalez, L.E. Darago, W.J. Evans, J.R. Long, Giant coercivity and high magnetic blocking temperatures for N_2^{3-} radical-bridged dilanthanide complexes upon ligand dissociation, Nat. Commun. 8 (2017) 2144, https://doi.org/10.1038/s41467-017-01553-w.
[99] J.D. Hilgar, M.G. Bernbeck, J.D. Rinehart, Million-fold Relaxation Time Enhancement across a Series of Phosphino-Supported Erbium Single-Molecule Magnets, J. Am. Chem. Soc. 141 (2019) 1913–1917, https://doi.org/10.1021/jacs.8b13514.
[100] C.A.P. Goodwin, F. Ortu, D. Reta, N.F. Chilton, D.P. Mills, Molecular magnetic hysteresis at 60 kelvin in dysprosocenium, Nature 548 (2017) 439–442, https://doi.org/10.1038/nature23447.
[101] F.S. Guo, B.M. Day, Y.C. Chen, M.L. Tong, A. Mansikkamäki, R.A. Layfield, A dysprosium metallocene single-molecule magnet functioning at the axial limit, Angew. Chem. Int. Ed. 56 (2017) 11445–11449, https://doi.org/10.1002/anie.201705426.
[102] F.S. Guo, B.M. Day, Y.C. Chen, M.L. Tong, A. Mansikkamäki, R.A. Layfield, Magnetic hysteresis up to 80 kelvin in a dysprosium metallocene single-molecule magnet, Science 362 (2018) 1400–1403, https://doi.org/10.1126/science.aav0652.
[103] K.R. McClain, C.A. Gould, K. Chakarawet, S.J. Teat, T.J. Groshens, J.R. Long, B.G. Harvey, High-temperature magnetic blocking and magneto-structural correlations in a series of dysprosium(III) metallocenium single-molecule magnets, Chem. Sci. 9 (2018) 8492–8503, https://doi.org/10.1039/C8SC03907K.
[104] P. Evans, D. Reta, G.F.S. Whitehead, N.F. Chilton, D.P. Mills, Bis-monophospholyl dysprosium cation showing magnetic hysteresis at 48 K, J. Am. Chem. Soc. 141 (2020) 19935–19940, https://doi.org/10.1021/jacs.9b11515.
[105] Y. Meng, J. Xiong, M. Yang, Y. Qiao, Z. Zhong, H. Sun, J. Han, T. Liu, B. Wang, S. Gao, Experimental determination of magnetic anisotropy in exchange-bias dysprosium metallocene single-molecule magnets, Angew. Chem. Int. Ed. 59 (2020) 13037–13043, https://doi.org/10.1002/anie.202004537.
[106] R. Collins, M.J. Heras Ojea, A. Mansikkamäki, J. Tang, R.A. Layfield, Carbonyl back-bonding influencing the rate of quantum tunnelling in a dysprosium metallocene single-molecule magnet, Inorg. Chem. 59 (2020) 642–647, https://doi.org/10.1021/acs.inorgchem.9b02895.
[107] M. He, F.S. Guo, J. Tang, A. Mansikkamäki, R.A. Layfield, Fulvalene as a platform for the synthesis of a dimetallic dysprosocenium single-molecule

magnet, Chem. Sci. 11 (2020) 5745–5752, https://doi.org/10.1039/d0sc02033h.
[108] B.M. Day, F.S. Guo, R.A. Layfield, Cyclopentadienyl ligands in lanthanide single-molecule magnets: one ring to rule them all?, Acc Chem. Res. 51 (2018) 1880–1889, https://doi.org/10.1021/acs.accounts.8b00270.
[109] T. Pugh, N.F. Chilton, R.A. Layfield, A low-symmetry dysprosium metallocene single-molecule magnet with a high anisotropy barrier, Angew. Chem. Int. Ed. 55 (2016) 11082–11085, https://doi.org/10.1002/anie.201604346.
[110] P. Evans, D. Reta, C.A.P. Goodwin, F. Ortu, N.F. Chilton, D.P. Mills, A double-dysprosocenium single-molecule magnet bound together with neutral ligands, Chem. Commun. 56 (2020) 5677–5680, https://doi.org/10.1039/c9cc08945d.
[111] D. Errulat, B. Gabidullin, A. Mansikkamäki, M. Murugesu, Two heads are better than one: Improving magnetic relaxation in the dysprosium metallocene $DyCp_2^*BPh_4$ upon dimerization by use of an exceptionally weakly-coordinating anion, Chem. Commun. 56 (2020) 5937–5940, https://doi.org/10.1039/d0cc01980a.
[112] F. Neese, The ORCA program system, WIREs Comput. Mol. Sci. 2 (2012) 73–78, https://doi.org/10.1002/wcms.81.
[113] F. Aquilante, J. Autschbach, R.K. Carlson, L.F. Chibotaru, M.G. Delcey, L. De Vico, I. Fdez Galván, N. Ferré, L.M. Frutos, L. Gagliardi, M. Garavelli, A. Giussani, C.E. Hoyer, G. Li Manni, H. Lischka, D. Ma, P.Å. Malmqvist, T. Müller, A. Nenov, M. Olivucci, T.B. Pedersen, D. Peng, F. Plasser, B. Pritchard, M. Reiher, I. Rivalta, I. Schapiro, J. Segarra-Martí, M. Stenrup, D.G. Truhlar, L. Ungur, A. Valentini, S. Vancoillie, V. Veryazov, V.P. Vysotskiy, O. Weingart, F. Zapata, R. Lin, Molcas 8: new capabilities for multiconfigurational quantum chemical calculations across the periodic table, J. Comput. Chem. 37 (2016) 506–541, https://doi.org/10.1002/jcc.24221.
[114] A. Swain, A. Sarkar, G. Rajaraman, Role of Ab initio calculations in the design and development of organometallic lanthanide-based single-molecule magnets, Chem. – An Asian J. 14 (2019) 4056–4073, https://doi.org/10.1002/asia.201900828.
[115] D. Aravena, E. Ruiz, Shedding light on the single-molecule magnet behavior of mononuclear Dy^{III} complexes, Inorg. Chem. 52 (2013) 13770–13778, https://doi.org/10.1021/ic402367c.
[116] D. Reta, J.G.C. Kragskow, N.F. Chilton, Ab initio prediction of high-temperature magnetic relaxation rates in single-molecule magnets, J. Am. Chem. Soc. (2021), https://doi.org/10.1021/jacs.1c01410.
[117] A. Lunghi, M. Iannuzzi, R. Sessoli, F. Totti, Single molecule magnets grafted on gold: magnetic properties from ab initio molecular dynamics †, J. Mater. Chem. C. 7294 (2015) 7294, https://doi.org/10.1039/c5tc00394f.
[118] S. Calvello, M. Piccardo, S.V. Rao, A. Soncini, CERES: An ab initio code dedicated to the calculation of the electronic structure and magnetic properties of lanthanide complexes, J. Comput. Chem. 39 (2018) 328–337, https://doi.org/10.1002/jcc.25113.
[119] F. Lu, M.M. Ding, J.X. Li, B.L. Wang, Y.Q. Zhang, Why lanthanide Er^{III}SIMs cannot possess huge energy barriers: a theoretical investigation, Dalton Trans. 49 (2020) 14576–14583, https://doi.org/10.1039/d0dt02868a.
[120] H. Zhang, R. Nakanishi, K. Katoh, B.K. Breedlove, Y. Kitagawa, M. Yamashita, Low coordinated mononuclear erbium(III) single-molecule magnets with C3v symmetry: a method for altering single-molecule magnet properties by incorporating hard and soft donors, Dalton Trans. 47 (2018) 302–305, https://doi.org/10.1039/c7dt04053a.
[121] W. Zhang, A. Muhtadi, N. Iwahara, L. Ungur, L.F. Chibotaru, Magnetic anisotropy in divalent lanthanide compounds, Angew. Chem. Int. Ed. 59 (2020) 12720–12724, https://doi.org/10.1002/anie.202003399.
[122] L. Ungur, L.F. Chibotaru, Magnetic anisotropy in the excited states of low symmetry lanthanide complexes, PCCP 13 (2011) 20086–20090, https://doi.org/10.1039/c1cp22689d.
[123] K. Irländer, J. Schnack, Spin-phonon interaction induces tunnel splitting in single-molecule magnets, Phys. Rev. B. 102 (2020), https://doi.org/10.1103/PhysRevB.102.054407 054407.
[124] D. Aravena, Ab initio prediction of tunneling relaxation times and effective demagnetization barriers in kramers lanthanide single-molecule magnets, J. Phys. Chem. Lett. 9 (2018) 5327–5333, https://doi.org/10.1021/acs.jpclett.8b02359.
[125] L. Bogani, L. Cavigli, M. Gurioli, R.L. Novak, M. Mannini, A. Caneschi, F. Pineider, R. Sessoli, M. Clemente-León, E. Coronado, A. Cornia, D. Gatteschi, Magneto-optical investigations of nanostructured materials based on single-molecule magnets monitor strong environmental effects, Adv. Mater. 19 (2007) 3906–3911, https://doi.org/10.1002/adma.200700594.
[126] Z. Salman, K.H. Chow, R.I. Miller, A. Morello, T.J. Parolin, M.D. Hossain, T.A. Keeler, C.D.P. Levy, W.A. MacFarlane, G.D. Morris, H. Saadaoui, D. Wang, R. Sessoli, G.G. Condorelli, R.F. Kiefl, Local magnetic properties of a monolayer of Mn12 single molecule magnets, Nano Lett. 7 (2007) 1551–1555, https://doi.org/10.1021/nl070366a.
[127] F. Moro, R. Biagi, V. Corradini, M. Evangelisti, A. Gambardella, V. De Renzi, U. Del Pennino, E. Coronado, A. Forment-Aliaga, F.M. Romero, Electronic and magnetic properties of Mn 12 molecular magnets on sulfonate and carboxylic acid prefunctionalized gold surfaces, J. Phys. Chem. C 116 (2012) 14936–14942, https://doi.org/10.1021/jp3031896.
[128] C. Wäckerlin, F. Donati, A. Singha, R. Baltic, S. Rusponi, K. Diller, F. Patthey, M. Pivetta, Y. Lan, S. Klyatskaya, M. Ruben, H. Brune, J. Dreiser, Giant hysteresis of single-molecule magnets adsorbed on a nonmagnetic insulator, Adv. Mater. 28 (2016) 5195–5199, https://doi.org/10.1002/adma.201506305.
[129] D. Aulakh, H.K. Bilan, M. Wriedt, Porous substrates as platforms for the nanostructuring of molecular magnets, CrystEngComm 20 (2018) 1011–1030, https://doi.org/10.1039/c7ce01978e.
[130] E. Coronado, Molecular magnetism: from chemical design to spin control in molecules, materials and devices, Nat. Rev. Mater. 5 (2020) 87–104, https://doi.org/10.1038/s41578-019-0146-8.
[131] D. Aulakh, J.B. Pyser, X. Zhang, A.A. Yakovenko, K.R. Dunbar, M. Wriedt, Metal-organic frameworks as platforms for the controlled nanostructuring of single-molecule magnets, J. Am. Chem. Soc. 137 (2015) 9254–9257, https://doi.org/10.1021/jacs.5b06002.
[132] D. Aulakh, H. Xie, Z. Shen, A. Harley, X. Zhang, A.A. Yakovenko, K.R. Dunbar, M. Wriedt, Systematic investigation of controlled nanostructuring of Mn12 single-molecule magnets templated by metal-organic frameworks, Inorg. Chem. 56 (2017) 6965–6972, https://doi.org/10.1021/acs.inorgchem.7b00514.
[133] H.-J. Chen, X.-Y. Zheng, Y.-R. Zhao, D.-Q. Yuan, X.-J. Kong, L.-S. Long, L.-S. Zheng, A record-breaking loading capacity for single-molecule magnet Mn 12 clusters achieved in a mesoporous Ln-MOF, ACS Appl. Electron. Mater. 1 (2019) 804–809, https://doi.org/10.1021/acsaelm.9b00088.
[134] T.C. Wang, N.A. Vermeulen, I.S. Kim, A.B.F. Martinson, J. Fraser Stoddart, J.T. Hupp, O.K. Farha, Scalable synthesis and post-modification of a mesoporous metal-organic framework called NU-1000, Nat. Protoc. 11 (2016) 149–162, https://doi.org/10.1038/nprot.2016.001.
[135] D. Aulakh, L. Liu, J.R. Varghese, H. Xie, T. Islamoglu, K. Duell, C.W. Kung, C.E. Hsiung, Y. Zhang, R.J. Drout, O.K. Farha, K.R. Dunbar, Y. Han, M. Wriedt, Direct imaging of isolated single-molecule magnets in metal-organic frameworks, J. Am. Chem. Soc. 141 (2019) 2997–3005, https://doi.org/10.1021/jacs.8b11374.
[136] M. Mon, A. Pascual-Álvarez, T. Grancha, J. Cano, J. Ferrando-Soria, F. Lloret, J. Gascon, J. Pasán, D. Armentano, E. Pardo, Solid-state molecular nanomagnet inclusion into a magnetic metal-organic framework: interplay of the magnetic properties, Chem. - A Eur. J. 22 (2016) 441, https://doi.org/10.1002/chem.201504827.
[137] B.J. Kennedy, K.S. Murray, Magnetic properties and zero-field splitting in high-spin manganese(III) complexes. 2. Axially ligated manganese(III) porphyrin complexes, Inorg. Chem. 24 (1985) 1557–1560, https://doi.org/10.1021/ic00204a030.
[138] M.M. Williamson, C.L. Hill, Molecular Stereochemistry Of Aquamanganese (III) porphyrins. demonstrable Effect of π-arene-porphyrin interaction on the metal coordination environment in a metalloporphyrin, Inorg. Chem. 26 (1987) 4155–4160, https://doi.org/10.1021/ic00272a005.
[139] J. Ferrando-Soria, P. Serra-Crespo, M. De Lange, J. Gascon, F. Kapteijn, M. Julve, J. Cano, F. Lloret, J. Pasán, C. Ruiz-Pérez, Y. Journaux, E. Pardo, Selective gas and vapor sorption and magnetic sensing by an isoreticular mixed-metal-organic framework, J. Am. Chem. Soc. 134 (2012) 15301–15304, https://doi.org/10.1021/ja3045822.
[140] T. Grancha, J. Ferrando-Soria, H.-C. Zhou, J. Gascon, B. Seoane, J. Pasán, O. Fabelo, M. Julve, E. Pardo, Postsynthetic improvement of the physical properties in a metal-organic framework through a single crystal to single crystal transmetallation, Angew. Chem. Int. Ed. 54 (2015) 6521–6525, https://doi.org/10.1002/anie.201501691.
[141] J. Dreiser, G.E. Pacchioni, F. Donati, L. Gragnaniello, A. Cavallin, K.S. Pedersen, J. Bendix, B. Delley, M. Pivetta, S. Rusponi, H. Brune, Out-of-plane alignment of Er(trensal) easy magnetization axes using graphene, ACS Nano 10 (2016) 2887–2892, https://doi.org/10.1021/acsnano.5b08178.
[142] S. Marocchi, A. Candini, D. Klar, W. Van Den Heuvel, H. Huang, F. Troiani, V. Corradini, R. Biagi, V. De Renzi, S. Klyatskaya, K. Kummer, N.B. Brookes, M. Ruben, H. Wende, U. Del Pennino, A. Soncini, M. Affronte, V. Bellini, Relay-like exchange mechanism through a spin radical between $TbPc_2$ molecules and graphene/Ni(111) substrates, ACS Nano 10 (2016) 9353–9360, https://doi.org/10.1021/acsnano.6b04107.
[143] L. Bogani, W. Wernsdorfer, Molecular spintronics using single-molecule magnets, Nat. Mater. 7 (2008) 179–186, https://doi.org/10.1038/nmat2133.
[144] M. Trif, F. Troiani, D. Stepanenko, D. Loss, Spin-electric coupling in molecular magnets, Phys. Rev. Lett. 101 (2008), https://doi.org/10.1103/PhysRevLett.101.217201 217201.
[145] A. Saywell, G. Magnano, C.J. Satterley, L.M.A. Perdigão, A.J. Britton, N. Taleb, M. Del Carmen Giménez-López, N.R. Champness, J.N. O'Shea, P.H. Beton, Self-assembled aggregates formed by single-molecule magnets on a gold surface, Nat. Commun. 1 (2010) 75, https://doi.org/10.1038/ncomms1075.
[146] T.W. Chamberlain, M.C. Giménez-López, A.N. Khlobystov, Carbon Nanotubes and Related Structures: Synthesis, Characterization, Functionalization, and Applications, Wiley-VCH, 2010 (accessed January 28, 2021).
[147] K. Jiang, A. Eitan, L.S. Schadler, P.M. Ajayan, R.W. Siegel, N. Grobert, M. Mayne, M. Reyes-Reyes, H. Terrones, M. Terrones, Selective attachment of gold nanoparticles to nitrogen-doped carbon nanotubes, Nano Lett. 3 (2003) 275–277, https://doi.org/10.1021/nl025914t.
[148] V. Georgakilas, D. Gournis, V. Tzitzios, L. Pasquato, D.M. Guldi, M. Prato, Decorating carbon nanotubes with metal or semiconductor nanoparticles, J. Mater. Chem. 17 (2007) 2679–2694, https://doi.org/10.1039/b700857k.
[149] Y.B. Zhang, M. Kanungo, A.J. Ho, P. Freimuth, D. Van Der Lelie, M. Chen, S.M. Khamis, S.S. Datta, A.T.C. Johnson, J.A. Misewich, S.S. Wong, Functionalized carbon nanotubes for detecting viral proteins, Nano Lett. 7 (2007) 3086–3091, https://doi.org/10.1021/nl071572l.
[150] K. Besteman, J.O. Lee, F.G.M. Wiertz, H.A. Heering, C. Dekker, Enzyme-coated carbon nanotubes as single-molecule biosensors, Nano Lett. 3 (2003) 727–730, https://doi.org/10.1021/nl034139u.

[151] S. Banerjee, T. Hemraj-Benny, S.S. Wong, Covalent surface chemistry of single-walled carbon nanotubes, Adv. Mater. 17 (2005) 17–29, https://doi.org/10.1002/adma.200401340.
[152] J. Kong, N.R. Franklin, C. Zhou, M.G. Chapline, S. Peng, K. Cho, H. Dai, Nanotube molecular wires as chemical sensors, Science 287 (2000) 622–625, https://doi.org/10.1126/science.287.5453.622.
[153] L. Bogani, C. Danieli, E. Biavardi, N. Bendiab, A.-L. Barra, E. Dalcanale, W. Wernsdorfer, A. Cornia, Single-molecule-magnet carbon-nanotube hybrids, Angew. Chem. Int. Ed. 48 (2009) 746–750, https://doi.org/10.1002/anie.200804967.
[154] L. Malavolti, V. Lanzilotto, S. Ninova, L. Poggini, I. Cimatti, B. Cortigiani, L. Margheriti, D. Chiappe, E. Otero, P. Sainctavit, F. Totti, A. Cornia, M. Mannini, R. Sessoli, Magnetic bistability in a submonolayer of sublimated Fe_4 single-molecule magnets, Nano Lett. 15 (2015) 535–541, https://doi.org/10.1021/nl503925h.
[155] L. Gragnaniello, F. Paschke, P. Erler, P. Schmitt, N. Barth, S. Simon, H. Brune, S. Rusponi, M. Fonin, Uniaxial 2D superlattice of Fe4 molecular magnets on graphene, Nano Lett. 17 (2017) 7177–7182, https://doi.org/10.1021/acs.nanolett.6b05105.
[156] C. Cervetti, A. Rettori, M.G. Pini, A. Cornia, A. Repollés, F. Luis, M. Dressel, S. Rauschenbach, K. Kern, M. Burghard, L. Bogani, The classical and quantum dynamics of molecular spins on graphene, Nat. Mater. 15 (2016) 164–168, https://doi.org/10.1038/nmat4490.
[157] S.C. Benjamin, A. Ardavan, G.A.D. Briggs, D.A. Britz, D. Gunlycke, J. Jefferson, M.A.G. Jones, D.F. Leigh, B.W. Lovett, A.N. Khlobystov, S.A. Lyon, J.J.L. Morton, K. Porfyrakis, M.R. Sambrook, A.M. Tyryshkin, Towards a fullerene-based quantum computer, J. Phys. Condens. Matter. 18 (2006) S867, https://doi.org/10.1088/0953-8984/18/21/S12.
[158] M. Del Carmen Giménez-López, F. Moro, A. La Torre, C.J. Gómez-García, P.D. Brown, J. Van Slageren, A.N. Khlobystov, Encapsulation of single-molecule magnets in carbon nanotubes, Nat. Commun. 2 (2011) 407, https://doi.org/10.1038/ncomms1415.
[159] S. Kyatskaya, J.R.G. Mascarós, L. Bogani, F. Hennrich, M. Kappes, W. Wernsdorfer, M. Ruben, Anchoring of rare-earth-based single-molecule magnets on single-walled carbon nanotubes, J. Am. Chem. Soc. 131 (2009) 15143–15151, https://doi.org/10.1021/ja906165e.
[160] A. Giusti, G. Charron, S. Mazerat, J.-D. Compain, P. Mialane, A. Dolbecq, E. Rivière, W. Wernsdorfer, R. Ngo Biboum, B. Keita, L. Nadjo, A. Filoramo, J.-P. Bourgoin, T. Mallah, Magnetic bistability of individual single-molecule magnets grafted on single-wall carbon nanotubes, Angew. Chem. Int. Ed. 48 (2009) 4949–4952, https://doi.org/10.1002/anie.200901806.
[161] J.C.G. Bünzli, On the design of highly luminescent lanthanide complexes, Coord. Chem. Rev. 293–294 (2015) 19–47, https://doi.org/10.1016/j.ccr.2014.10.013.
[162] M.J. Weber, Radiative and multiphonon relaxation of rare-earth ions in Y_2O_3, Phys. Rev. 171 (1968) 283–291, https://doi.org/10.1103/PhysRev.171.283.
[163] C.P. Montgomery, D. Parker, L. Lamarque, Effective and efficient sensitisation of terbium luminescence at 355 nm with cell permeable pyrazoyl-1-azaxanthone macrocyclic complexes, Chem. Commun. (2007) 3841–3843, https://doi.org/10.1039/b709805g.
[164] J. Long, Y. Guari, R.A.S. Ferreira, L.D. Carlos, J. Larionova, Recent advances in luminescent lanthanide based Single-Molecule Magnets, Coord. Chem. Rev. 363 (2018) 57–70, https://doi.org/10.1016/j.ccr.2018.02.019.
[165] J.H. Jia, Q.W. Li, Y.C. Chen, J.L. Liu, M.L. Tong, Luminescent single-molecule magnets based on lanthanides: design strategies, recent advances and magneto-luminescent studies, Coord. Chem. Rev. 378 (2019) 365–381, https://doi.org/10.1016/j.ccr.2017.11.012.
[166] J. Long, Luminescent Schiff-base lanthanide single-molecule magnets: the association between optical and magnetic properties, Front. Chem. 7 (2019) 63, https://doi.org/10.3389/fchem.2019.00063.
[167] F. Pointillart, O. Cador, B. Le Guennic, L. Ouahab, Uncommon lanthanide ions in purely 4f Single Molecule Magnets, Coord. Chem. Rev. 346 (2017) 150–175, https://doi.org/10.1016/j.ccr.2016.12.017.
[168] J.C.G. Bünzli, Lanthanide luminescence for biomedical analyses and imaging, Chem. Rev. 110 (2010) 2729–2755, https://doi.org/10.1021/cr900362e.
[169] S.V. Eliseeva, M. Ryazanov, F. Gumy, S.I. Troyanov, L.S. Lepnev, J.-C.G. Bünzli, N.P. Kuzmina, Dimeric Complexes of Lanthanide(III) hexafluoroacetylacetonates with4-cyanopyridinen-oxide: synthesis, crystal structure, magnetic and photoluminescent properties, Eur. J. Inorg. Chem. (2006) 4809–4820, https://doi.org/10.1002/ejic.200600673.
[170] D. Errulat, R. Marin, D.A. Gálico, K.L.M. Harriman, A. Pialat, B. Gabidullin, F. Iikawa, O.D.D. Couto, J.O. Moilanen, E. Hemmer, F.A. Sigoli, M. Murugesu, A luminescent thermometer exhibiting slow relaxation of the magnetization: toward self-monitored building blocks for next-generation optomagnetic devices, ACS Cent. Sci. 5 (2019) 1187–1198, https://doi.org/10.1021/acscentsci.9b00288.
[171] F. Pointillart, J. Jung, R. Berraud-Pache, B. Le Guennic, V. Dorcet, S. Golhen, O. Cador, O. Maury, Y. Guyot, S. Decurtins, S.X. Liu, L. Ouahab, Luminescence and single-molecule magnet behavior in lanthanide complexes involving a tetrathiafulvalene-fused dipyridophenazine ligand, Inorg. Chem. 54 (2015) 5384–5397, https://doi.org/10.1021/acs.inorgchem.5b00441.
[172] F. Pointillart, B. Le Guennic, S. Golhen, O. Cador, O. Maury, L. Ouahab, A redox-active luminescent ytterbium based single molecule magnet, Chem. Commun. 49 (2013) 615–617, https://doi.org/10.1039/c2cc37635k.
[173] G. Brunet, R. Marin, M.J. Monk, U. Resch-Genger, D.A. Gálico, F.A. Sigoli, E.A. Suturina, E. Hemmer, M. Murugesu, Exploring the dual functionality of an ytterbium complex for luminescence thermometry and slow magnetic relaxation, Chem. Sci. 10 (2019) 6799–6808, https://doi.org/10.1039/c9sc00343f.
[174] J. Wang, J.J. Zakrzewski, M. Heczko, M. Zychowicz, K. Nakagawa, K. Nakabayashi, B. Sieklucka, S. Chorazy, S.I. Ohkoshi, Proton conductive luminescent thermometer based on near-infrared emissive $YbCo_2$ molecular nanomagnets, J. Am. Chem. Soc. 142 (2020) 3970–3979, https://doi.org/10.1021/jacs.9b13147.
[175] J. Wang, J.J. Zakrzewski, M. Zychowicz, V. Vieru, L.F. Chibotaru, K. Nakabayashi, S. Chorazy, S. Ohkoshi, Holmium(iii) molecular nanomagnets for optical thermometry exploring the luminescence re-absorption effect, Chem. Sci. 12 (2021) 730–741, https://doi.org/10.1039/d0sc04871b.
[176] A.A. Kitos, D.A. Gálico, R. Castañeda, J.S. Ovens, M. Murugesu, J.L. Brusso, Stark sublevel-based thermometry with Tb(III) and Dy(III) complexes cosensitized via the 2-amidinopyridine ligand, Inorg. Chem. 59 (2020) 11061–11070, https://doi.org/10.1021/acs.inorgchem.0c01534.
[177] M. Fondo, J. Corredoira-Vázquez, A.M. García-Deibe, J. Sanmartín-Matalobos, M. Amoza, A.M.P. Botas, R.A.S. Ferreira, L.D. Carlos, E. Colacio, Field-induced slow magnetic relaxation and luminescence thermometry in a mononuclear ytterbium complex, Inorg. Chem. Front. 7 (2020) 3019–3029, https://doi.org/10.1039/d0qi00637h.
[178] R. Marin, G. Brunet, M. Murugesu, Shining new light on multifunctional lanthanide single-molecule magnets, Angew. Chem. Int. Ed. 60 (2021) 1728–1746, https://doi.org/10.1002/anie.201910299.
[179] R. Farshchi, M. Ramsteiner, J. Herfort, A. Tahraoui, H.T. Grahn, Optical communication of spin information between light emitting diodes, Appl. Phys. Lett. 98 (2011), https://doi.org/10.1063/1.3582917 162508.
[180] J.F. Sherson, H. Krauter, R.K. Olsson, B. Julsgaard, K. Hammerer, I. Cirac, E.S. Polzik, Quantum teleportation between light and matter, Nature 443 (2006) 557–560, https://doi.org/10.1038/nature05136.
[181] M.C. Heffern, L.M. Matosziuk, T.J. Meade, Lanthanide probes for bioresponsive imaging, Chem. Rev. 114 (2014) 4496–4539, https://doi.org/10.1021/cr400477t.
[182] M. Schadt, Liquid crystal materials and liquid crystal displays, Annu. Rev. Mater. Sci. 27 (1997) 305–379, https://doi.org/10.1146/annurev.matsci.27.1.305.
[183] M. Leonzio, M. Bettinelli, L. Arrico, M. Monari, L. Di Bari, F. Piccinelli, Circularly polarized luminescence from an Eu(III) complex based on 2-thenoyltrifluoroacetyl-acetonate and a tetradentate chiral ligand, Inorg. Chem. 57 (2018) 10257–10264, https://doi.org/10.1021/acs.inorgchem.8b01480.
[184] L. Arrico, C. De Rosa, L. Di Bari, A. Melchior, F. Piccinelli, Effect of the counterion on circularly polarized luminescence of europium(III) and samarium(III) complexes, Inorg. Chem. 59 (2020) 5050–5062, https://doi.org/10.1021/acs.inorgchem.0c00280.
[185] S. Wada, Y. Kitagawa, T. Nakanishi, M. Gon, K. Tanaka, K. Fushimi, Y. Chujo, Y. Hasegawa, Electronic chirality inversion of lanthanide complex induced by achiral molecules, Sci. Rep. 8 (2018) 16395, https://doi.org/10.1038/s41598-018-34790-0.
[186] K. Dhbaibi, L. Favereau, J. Crassous, Enantioenriched helicenes and helicenoids containing main-group elements (B, Si, N, P), Chem. Rev. 119 (2019) 8846–8953, https://doi.org/10.1021/acs.chemrev.9b00033.
[187] Z.P. Yan, K. Liao, H.B. Han, J. Su, Y.X. Zheng, J.L. Zuo, Chiral iridium(III) complexes with four-membered Ir-S-P-S chelating rings for high-performance circularly polarized OLEDs, Chem. Commun. 55 (2019) 8215–8218, https://doi.org/10.1039/c9cc03915e.
[188] G. Park, H. Kim, H. Yang, K.R. Park, I. Song, J.H. Oh, C. Kim, Y. You, Amplified circularly polarized phosphorescence from co-assemblies of platinum(II) complexes, Chem. Sci. 10 (2019) 1294–1301, https://doi.org/10.1039/c8sc04509g.
[189] R. Aoki, R. Toyoda, J.F. Kögel, R. Sakamoto, J. Kumar, Y. Kitagawa, K. Harano, T. Kawai, H. Nishihara, Bis(dipyrrinato)zinc(II) complex chiroptical wires: exfoliation into single strands and intensification of circularly polarized luminescence, J. Am. Chem. Soc. 139 (2017) 16024–16027, https://doi.org/10.1021/jacs.7b07077.
[190] J.R. Jiménez, B. Doistau, C.M. Cruz, C. Besnard, J.M. Cuerva, A.G. Campaña, C. Piguet, Chiral molecular ruby $[Cr(dqp)_2]^{3+}$ with long-lived circularly polarized luminescence, J. Am. Chem. Soc. 141 (2019) 13244–13252, https://doi.org/10.1021/jacs.9b06524.
[191] M. Deng, N.F.M. Mukthar, N.D. Schley, G. Ung, Yellow circularly polarized luminescence from C_1 -symmetrical copper(I) complexes, Angew. Chem. Int. Ed. 59 (2020) 1228–1231, https://doi.org/10.1002/anie.201913672.
[192] J. Kumar, B. Marydasan, T. Nakashima, T. Kawai, J. Yuasa, Chiral supramolecular polymerization leading to eye differentiable circular polarization in luminescence, Chem. Commun. 52 (2016) 9885–9888, https://doi.org/10.1039/c6cc05022k.
[193] B. El Rez, J. Liu, V. Béreau, C. Duhayon, Y. Horino, T. Suzuki, L. Coolen, J.P. Sutter, Concomitant emergence of circularly polarized luminescence and single-molecule magnet behavior in chiral-at-metal Dy complex, Inorg. Chem. Front. 7 (2020) 4527–4534, https://doi.org/10.1039/d0qi00919a.
[194] J.P. Riehl, F.S. Richardson, Circularly polarized luminescence spectroscopy, Chem. Rev. 86 (1986) 1–16, https://doi.org/10.1021/cr00071a001.

[195] W. Zhang, H.Y. Ye, R.G. Xiong, Metal-organic coordination compounds for potential ferroelectrics, Coord. Chem. Rev. 253 (2009) 2980–2997, https://doi.org/10.1016/j.ccr.2009.02.028.
[196] M. Gajek, M. Bibes, S. Fusil, K. Bouzehouane, J. Fontcuberta, A. Barthélémy, A. Fert, Tunnel junctions with multiferroic barriers, Nat. Mater. 6 (2007) 296–302, https://doi.org/10.1038/nmat1860.
[197] J.F. Scott, Multiferroic memories, Nat. Mater. 6 (2007) 256–257, https://doi.org/10.1038/nmat1868.
[198] P.H. Guo, Y. Meng, Y.C. Chen, Q.W. Li, B.Y. Wang, J.D. Leng, D.H. Bao, J.H. Jia, M. L. Tong, A zigzag Dy^{III}_4 cluster exhibiting single-molecule magnet, ferroelectric and white-light emitting properties, J. Mater. Chem. C 2 (2014) 8858–8864, https://doi.org/10.1039/c4tc01275e.
[199] X.L. Li, C.L. Chen, H.P. Xiao, A.L. Wang, C.M. Liu, X. Zheng, L.J. Gao, X.G. Yang, S. M. Fang, Luminescent, magnetic and ferroelectric properties of noncentrosymmetric chain-like complexes composed of nine-coordinate lanthanide ions, Dalton Trans. 42 (2013) 15317–15325, https://doi.org/10.1039/c3dt51743h.
[200] P.-H. Guo, J.-L. Liu, J.-H. Jia, J. Wang, F.-S. Guo, Y.-C. Chen, W.-Q. Lin, J.-D. Leng, D.-H. Bao, X.-D. Zhang, J.-H. Luo, M.-L. Tong, Multifunctional Dy^{III}_4 cluster exhibiting white-emitting, ferroelectric and single-molecule magnet behavior, Chem. - A Eur. J. 19 (2013) 8769–8773, https://doi.org/10.1002/chem.201300299.
[201] J. Long, J. Rouquette, J.-M. Thibaud, R.A.S. Ferreira, L.D. Carlos, B. Donnadieu, V. Vieru, L.F. Chibotaru, L. Konczewicz, J. Haines, Y. Guari, J. Larionova, A high-temperature molecular ferroelectric Zn/Dy complex exhibiting single-ion-magnet behavior and lanthanide luminescence, Angew. Chemie. 127 (2015) 2264–2268, https://doi.org/10.1002/ange.201410523.
[202] S.D. Zhu, J.J. Hu, L. Dong, H.R. Wen, S.J. Liu, Y.B. Lu, C.M. Liu, Multifunctional Zn(II)-Yb(III) complex enantiomers showing second-harmonic generation, near-infrared luminescence, single-molecule magnet behaviour and proton conduction, J. Mater. Chem. C 8 (2020) 16032–16041, https://doi.org/10.1039/d0tc03687k.
[203] G. Cosquer, Y. Shen, M. Almeida, M. Yamashita, Conducting single-molecule magnet materials, Dalton Trans. 47 (2018) 7616–7627, https://doi.org/10.1039/c8dt01015c.
[204] N.D. Kushch, L.I. Buravov, P.P. Kushch, G.V. Shilov, H. Yamochi, M. Ishikawa, A. Otsuka, A.A. Shakin, O.V. Maximova, O.S. Volkova, A.N. Vasiliev, E.B. Yagubskii, Multifunctional compound combining conductivity and single-molecule magnetism in the same temperature range, Inorg. Chem. 57 (2018) 2386–2389, https://doi.org/10.1021/acs.inorgchem.7b03152.
[205] A. Jones, Fast Searches with Nuclear Magnetic Resonance Computers, Science. 280 (1998) 229, https://doi.org/10.1126/science.280.5361.229.
[206] P.W. Shor, Algorithms for quantum computation: discrete logarithms and factoring, in: Institute of Electrical and Electronics Engineers (IEEE), Santa Fe, NM, USA, 1994, pp. 124–134, https://doi.org/10.1109/sfcs.1994.365700.
[207] L.K. Grover, Quantum computers can search arbitrarily large databases by a single query, Phys. Rev. Lett. 79 (1997) 4709–4712, https://doi.org/10.1103/PhysRevLett.79.4709.
[208] M.N. Leuenberger, D. Loss, Quantum computing in molecular magnets, Nature 410 (2001) 789–793, https://doi.org/10.1038/35071024.
[209] C. Joachim, J.K. Gimzewski, A. Aviram, Electronics using hybrid-molecular and mono-molecular devices, Nature 408 (2000) 541–548, https://doi.org/10.1038/35046000.
[210] M. Affronte, Molecular nanomagnets for information technologies, J. Mater. Chem. 19 (2009) 1731–1737, https://doi.org/10.1039/b809251f.
[211] K.X. Yu, J.G.C. Kragskow, Y.S. Ding, Y.Q. Zhai, D. Reta, N.F. Chilton, Y.Z. Zheng, Enhancing magnetic hysteresis in single-molecule magnets by ligand functionalization, Chem. 6 (2020) 1777–1793, https://doi.org/10.1016/j.chempr.2020.04.024.
[212] F. Ortu, D. Reta, Y.S. Ding, C.A.P. Goodwin, M.P. Gregson, E.J.L. McInnes, R.E.P. Winpenny, Y.Z. Zheng, S.T. Liddle, D.P. Mills, N.F. Chilton, Studies of hysteresis and quantum tunnelling of the magnetisation in dysprosium(III) single molecule magnets, Dalton Trans. 48 (2019) 8541–8545, https://doi.org/10.1039/c9dt01655d.
[213] A. Chiesa, F. Cugini, R. Hussain, E. MacAluso, G. Allodi, E. Garlatti, M. Giansiracusa, C.A.P. Goodwin, F. Ortu, D. Reta, J.M. Skelton, T. Guidi, P. Santini, M. Solzi, R. De Renzi, D.P. Mills, N.F. Chilton, S. Carretta, Understanding magnetic relaxation in single-ion magnets with high blocking temperature, Phys. Rev. B. 101 (2020), https://doi.org/10.1103/PhysRevB.101.174402 174402.
[214] R.E.P. Winpenny, N.F. Chilton, M. Giansiracusa, D. Collison, A. Kostopoulos, Correlating blocking temperatures with relaxation mechanisms in monometallic single-molecule magnets with high energy barriers (Ueff > 600 K), Chem. Commun. (2019), https://doi.org/10.1039/C9CC02421B.
[215] G. Velkos, W. Yang, Y.R. Yao, S.M. Sudarkova, X. Liu, B. Büchner, S.M. Avdoshenko, N. Chen, A.A. Popov, Shape-adaptive single-molecule magnetism and hysteresis up to 14 K in oxide clusterfullerenes $Dy_2O@C_{72}$ and $Dy_2O@C_{74}$ with fused pentagon pairs and flexible Dy-(μ_2-O)-Dy angle, Chem. Sci. 11 (2020) 4766–4772, https://doi.org/10.1039/d0sc00624f.
[216] F. Liu, S. Wang, C.-L. Gao, Q. Deng, X. Zhu, A. Kostanyan, R. Westerström, F. Jin, S.-Y. Xie, A.A. Popov, T. Greber, S. Yang, Mononuclear clusterfullerene single-molecule magnet containing strained fused-pentagons stabilized by a nearly linear metal cyanide cluster, Angew. Chem. Int. Ed. 56 (2017) 1830–1834, https://doi.org/10.1002/anie.201611345.
[217] F. Liu, C.L. Gao, Q. Deng, X. Zhu, A. Kostanyan, R. Westerström, S. Wang, Y.Z. Tan, J. Tao, S.Y. Xie, A.A. Popov, T. Greber, S. Yang, Triangular monometallic cyanide cluster entrapped in carbon cage with geometry-dependent molecular magnetism, J. Am. Chem. Soc. 138 (2016) 14764–14771, https://doi.org/10.1021/jacs.6b09329.
[218] L. Spree, A.A. Popov, Recent advances in single molecule magnetism of dysprosium-metallofullerenes, Dalton Trans. 48 (2019) 2861–2871, https://doi.org/10.1039/c8dt05153d.
[219] D.S. Krylov, F. Liu, A. Brandenburg, L. Spree, V. Bon, S. Kaskel, A.U.B. Wolter, B. Büchner, S.M. Avdoshenko, A.A. Popov, Magnetization relaxation in the single-ion magnet $DySc_2N@C_{80}$: Quantum tunneling, magnetic dilution, and unconventional temperature dependence, Phys. Chem. Chem. Phys. 20 (2018) 11656–11672, https://doi.org/10.1039/c8cp01608a.
[220] C.H. Chen, D.S. Krylov, S.M. Avdoshenko, F. Liu, L. Spree, R. Westerström, C. Bulbucan, M. Studniarek, J. Dreiser, A.U.B. Wolter, B. Büchner, A.A. Popov, Magnetic hysteresis in self-assembled monolayers of Dy-fullerene single molecule magnets on gold, Nanoscale 10 (2018) 11287–11292, https://doi.org/10.1039/c8nr00511g.
[221] K. Chakarawet, M. Atanasov, J. Marbey, P.C. Bunting, F. Neese, S. Hill, J.R. Long, Strong electronic and magnetic coupling in M_4(M = Ni, Cu) clusters via direct orbital interactions between low-coordinate metal centers, J. Am. Chem. Soc. 142 (2020) 19161–19169, https://doi.org/10.1021/jacs.0c08460.
[222] J. Camacho-Bunquin, M.J. Ferguson, J.M. Stryker, Hydrocarbon-soluble nanocatalysts with no bulk phase: coplanar, two-coordinate arrays of the base metals, J. Am. Chem. Soc. 135 (2013) 5537–5540, https://doi.org/10.1021/ja401579x.
[223] P. Pyykkö, M. Atsumi, Molecular single-bond covalent radii for elements 1–118, Chem. - A Eur. J. 15 (2009) 186–197, https://doi.org/10.1002/chem.200800987.
[224] M.A. Palacios, J. Nehrkorn, E.A. Suturina, E. Ruiz, S. Gómez-Coca, K. Holldack, A. Schnegg, J. Krzystek, J.M. Moreno, E. Colacio, Analysis of magnetic anisotropy and the role of magnetic dilution in triggering single-molecule magnet (SMM) behavior in a family of $Co^{II}Y^{III}$ dinuclear complexes with easy-plane anisotropy, Chem. - A Eur. J. 23 (2017) 11649–11661, https://doi.org/10.1002/chem.201702099.
[225] A.K. Mondal, A. Mondal, B. Dey, S. Konar, Influence of the coordination environment on easy-plane magnetic anisotropy of pentagonal bipyramidal cobalt(II) complexes, Inorg. Chem. 57 (2018) 9999–10008, https://doi.org/10.1021/acs.inorgchem.8b01162.
[226] J.M. Zadrozny, J. Liu, N.A. Piro, C.J. Chang, S. Hill, J.R. Long, Slow magnetic relaxation in a pseudotetrahedral cobalt(II) complex with easy-plane anisotropy, Chem. Commun. 48 (2012) 3927–3929, https://doi.org/10.1039/c2cc16430b.
[227] K. Chakarawet, P.C. Bunting, J.R. Long, Large Anisotropy barrier in a tetranuclear single-molecule magnet featuring low-coordinate cobalt centers, J. Am. Chem. Soc. 140 (2018) 2058–2061, https://doi.org/10.1021/jacs.7b13394.
[228] A.W. Cook, J.D. Bocarsly, R.A. Lewis, A.J. Touchton, S. Morochnik, T.W. Hayton, An iron ketimide single-molecule magnet $[Fe_4(NCPh_2)_6]$ with suppressed through-barrier relaxation, Chem. Sci. 11 (2020) 4753–4757, https://doi.org/10.1039/d0sc01578d.
[229] P. Abbasi, K. Quinn, D.I. Alexandropoulos, M. Damjanović, W. Wernsdorfer, A. Escuer, J. Mayans, M. Pilkington, T.C. Stamatatos, Transition metal single-molecule magnets: a Mn_{31} nanosized cluster with a large energy barrier of ~60 K and magnetic hysteresis at ~5 K, J. Am. Chem. Soc. 139 (2017) 15644–15647, https://doi.org/10.1021/jacs.7b10130.
[230] N.E. Chakov, S.C. Lee, A.G. Harter, P.L. Kuhns, A.P. Reyes, S.O. Hill, N.S. Dalal, W. Wernsdorfer, K.A. Abboud, G. Christou, The properties of the $[Mn_{12}O_{12}(O_2CR)_{16}(H_2O)_4]$ single-molecule magnets in truly axial symmetry: $[Mn_{12}O_{12}(O_2CCH_2Br)_{16}(H_2O)_4]\cdot 4CH_2Cl_2$, J. Am. Chem. Soc. 128 (2006) 6975–6989, https://doi.org/10.1021/ja060796n.
[231] C.J. Milios, A. Vinslava, W. Wernsdorfer, S. Moggach, S. Parsons, S.P. Perlepes, G. Christou, E.K. Brechin, A record anisotropy barrier for a single-molecule magnet, J. Am. Chem. Soc. 129 (2007) 2754–2755, https://doi.org/10.1021/ja068961m.
[232] K. Uchida, G. Cosquer, K. Sugisaki, H. Matsuoka, K. Sato, B.K. Breedlove, M. Yamashita, Isostructural M(II) complexes (M = Mn, Fe, Co) with field-induced slow magnetic relaxation for Mn and Co complexes, Dalton Trans. 48 (2019) 12023–12030, https://doi.org/10.1039/c8dt02150c.
[233] C. Rajnák, J. Titiš, J. Moncol', F. Renz, R. Boča, Slow magnetic relaxation in a high-spin pentacoordinate Fe(III) complex, Chem. Commun. 55 (2019) 13868–13871, https://doi.org/10.1039/c9cc06610a.
[234] G. Handzlik, M. Magott, M. Arczyński, A.M. Sheveleva, F. Tuna, M. Sarewicz, A. Osyczka, M. Rams, V. Vieru, L.F. Chibotaru, D. Pinkowicz, Magnetization dynamics and coherent spin manipulation of a propeller Gd(III) complex with the smallest helicene ligand, J. Phys. Chem. Lett. 11 (2020) 1508–1515, https://doi.org/10.1021/acs.jpclett.9b03275.
[235] M.J. Martínez-Pérez, S. Cardona-Serra, C. Schlegel, F. Moro, P.J. Alonso, H. Prima-García, J.M. Clemente-Juan, M. Evangelisti, A. Gaita-Ariño, J. Sesé, J. Van Slageren, E. Coronado, F. Luis, Gd-based single-ion magnets with tunable magnetic anisotropy: Molecular design of spin qubits, Phys. Rev. Lett. 108 (2012), https://doi.org/10.1103/PhysRevLett.108.247213 247213.
[236] R.J. Holmberg, L.T.A. Ho, L. Ungur, I. Korobkov, L.F. Chibotaru, M. Murugesu, Observation of unusual slow-relaxation of the magnetisation in a Gd-EDTA chelate, Dalton Trans. 44 (2015) 20321–20325, https://doi.org/10.1039/c5dt04072h.

[237] D.C. Izuogu, T. Yoshida, H. Zhang, G. Cosquer, K. Katoh, S. Ogata, M. Hasegawa, H. Nojiri, M. Damjanović, W. Wernsdorfer, T. Uruga, T. Ina, B.K. Breedlove, M. Yamashita, Slow magnetic relaxation in a palladium-gadolinium complex induced by electron density donation from the palladium Ion, Chem. – A Eur. J. 24 (2018) 9285–9294, https://doi.org/10.1002/chem.201800699.
[238] J. Mayans, A. Escuer, Correlating the axial Zero Field Splitting with the slow magnetic relaxation in Gd^{III} SIMs, Chem. Commun. 57 (2021) 721–724, https://doi.org/10.1039/d0cc07474h.
[239] S.T. Liddle, J. van Slageren, Actinide Single-Molecule Magnets, in: Lanthanides Actinides Mol. Magn., Wiley-VCH Verlag GmbH & Co. KGaA, Weinheim, Germany, 2015, pp. 315–340, https://doi.org/10.1002/9783527673476.ch10.
[240] S.K. Singh, C.J. Cramer, L. Gagliardi, Correlating electronic structure and magnetic anisotropy in actinide complexes [$An(COT)_2$], $An^{III/IV}$ = U, Np, and Pu, Inorg. Chem. 59 (2020) 6815–6825, https://doi.org/10.1021/acs.inorgchem.0c00105.
[241] J.T. Coutinho, M. Perfetti, J.J. Baldoví, M.A. Antunes, P.P. Hallmen, H. Bamberger, I. Crassee, M. Orlita, M. Almeida, J. van Slageren, L.C.J. Pereira, Spectroscopic determination of the electronic structure of a uranium single-ion magnet, Chem. - A Eur. J. 25 (2019) 1758–1766, https://doi.org/10.1002/chem.201805090.
[242] K.R. Meihaus, S.G. Minasian, W.W. Lukens, S.A. Kozimor, D.K. Shuh, T. Tyliszczak, J.R. Long, Influence of pyrazolate vs N -heterocyclic carbene ligands on the slow magnetic relaxation of homoleptic trischelate lanthanide (III) and uranium(III) complexes, J. Am. Chem. Soc. 136 (2014) 6056–6058, https://doi.org/10.1021/ja501569t.
[243] J.J. Le Roy, S.I. Gorelsky, I. Korobkov, M. Murugesu, Slow magnetic relaxation in uranium(III) and neodymium(III) cyclooctatetraenyl complexes, Organometallics 34 (2015) 1415–1418, https://doi.org/10.1021/om501214c.
[244] N. Magnani, C. Apostolidis, A. Morgenstern, E. Colineau, J.-C. Griveau, H. Bolvin, O. Walter, R. Caciuffo, Magnetic memory effect in a transuranic mononuclear complex, Angew. Chem. Int. Ed. 50 (2011) 1696–1698, https://doi.org/10.1002/anie.201006619.